Charles University in Prague
Faculty of Mathematics and Physics

MASTER THESIS

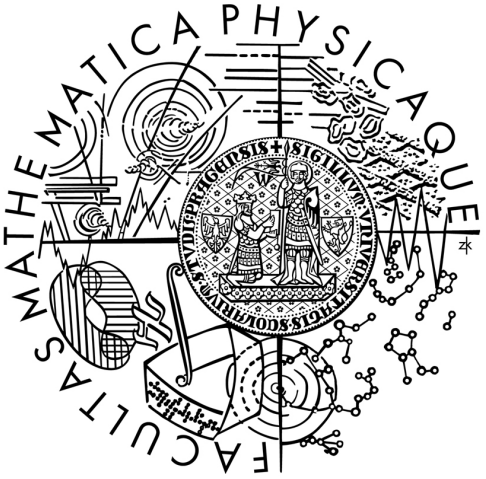

Ivana Ebrová

N-body simulations of shell galaxies

**Astronomical Institute
of the Charles University in Prague**

Supervisor: RNDr. Bruno Jungwiert, Ph.D.
Study program: Astronomy and Astrophysics

2007

In the first place I would like to thank to my supervisor Bruno Jungwiert for his great attitude towards the students. He always gave me much support, taught me a lot not only about the galaxies and the cooperation with him was always a pleasure and often fun. Further I would like to thank to Nicola Bennert for her useful and exhaustive help reviewing the thesis and to my colleagues, Jaroslava Schovancová and Miroslav Křížek, for many fruitful discussions and their persistent readiness to help. I am grateful to Dr. Gabriela Canalizo for supporting this project and kindly providing unpublished images. But most of all I have to thank to my partner, Jan Verfl, for his inexpressible help and support without which I would not be where I am.
This research was supported by the University of California – Riverside and was directly related to the Hubble Space Telescope program No. GO-10421 (PI: Dr. Gabriela Canalizo). Support for this HST program was provided by NASA through a grant from the Space Telescope Science Institute, which is operated by The Association of Universities for Research in Astronomy, Inc., under NASA contract No. NAS526555. Additional support was provided by the National Science Foundation, under grant No. AST 0507450. It was also supported by the Astronomical Institute of the Academy of Sciences of the Czech Republic through its Institutional Research Plan No. AV0Z10030501 and through the Center for Theoretical Astrophysics (Center of excellence No. LC06014 of the Czech Ministry of Education). This research has made use of NASA's Astrophysics Data System. Typeset in LyX, an open source document processor.

Prohlašuji, že jsem svou diplomovu práci napsala samostatně a výhradně s použtím citovaných pramenů. Souhlasím se zapůjčováním práce a jejím zveřejňováním.

V Praze dne 10. 8. 2007 Ivana Ebrová

Contents

Název práce: N-částicové simulace galaxií se slupkami (shell galaxies)
Autor: Ivana Ebrová
Katedra (ústav): Astronomický ústav UK
Vedoucí diplomové práce: RNDr. Bruno Jungwiert, Ph.D., Astronomický ústav AV ČR, v. v. i., a University of California – Riverside
e-mail vedoucího: bruno@ig.cas.cz

Abstrakt: Galaxie se slupkami jsou obvykle eliptické galaxie obsahující ve svém zářivém profilu jemnou strukturu v podobě koncentrických oblouků s ostrými vnějšími okraji. Tato práce obsahuje shrnutí našeho podrobného studia dosavadního výzkumu a publikací o tomto pozoruhodném fenoménu na poli pozorovacím i co se numerických simulací týče. Zároveň předkládáme výsledky vlastních simulací rozšiřující pohled na původ slupek v radiální kolizi hmotné eliptické galaxie s méně hmotnou. Do simulací je semianalytickým způsobem zavedeno dynamické tření vycházející z Chandrasekharovy formule. Hlavním výsledkem práce je, že dynamické tření spolu s postupným rozpadem menší galaxie, které je také diskutováno, může zásadně ovlivňovat proces vzniku slupek a musí se brát při jejich modelování v úvahu. Ukazuje se, že časové škály, na kterých se srážka odehrává jsou poměrně citlivé na zvolené parametry. Udáváme odhad jejich velikosti v různých případech. Úbytek hmoty malé galaxie v průběhu srážky sice účinek dynamického tření snižuje, ale nečiní jeho roli bezvýznamnou.

Klíčová slova: N-částicové simulace, galaxie: dynamika, galaxie: interakce, galaxie: vývoj

Title: N-body simulations of shell galaxies
Author: Ivana Ebrová
Department: Astronomical Institute of the Charles University
Supervisor: RNDr. Bruno Jungwiert, Ph.D., Astronomical Institute – Academy of Sciences of the Czech Republic and University of California – Riverside
Supervisor's e-mail address: bruno@ig.cas.cz

Abstract: Shell galaxies are ordinary elliptical galaxies that contain a fine structure in the form of concentric arcs with sharp edges in their luminous profile. This work contains a summary of our comprehensive study of the actual research and publications on this remarkable phenomenon, concerning both the observations as well as the numerical simulations. Along with it we present the results of our own simulations that broaden our view of the origin of the shells in a radial merger of a massive elliptical galaxy with a less massive one. We have introduced the dynamical friction into the simulation by semi-analytical means based on the Chandrasekhar formula. The main result is that the dynamical friction together with the gradual disintegration of the secondary galaxy that is also discussed can significantly affect the process of the shell formation and must be taken into consideration in their modelling. It turns out that the time scales on which the merger takes place are rather sensitive to the choice of the parameters. We present an estimate of their magnitude in different cases. The mass loss of the secondary galaxy during the merger mitigates the effect of the dynamical friction but does not make its role negligible.

Keywords: N-body simulations, galaxies: dynamics, galaxies: interactions, galaxies: evolution

Preface

Stellar shells, or ripples, are not only a nice and unique feature of elliptical galaxies, but their presence tells us that something notable is happening in the host galaxy. For the past almost thirty years they challenge the astronomers to extract some information from their appearance. So far they have resisted all the attempts to use them as a tool for accurate investigation of the potential of the underlying galaxy. Nevertheless, a better understanding of their formation can help us better understand the galaxies themselves.

The recent discovery of shells in the host galaxy of a quasar (see §8) has revived the interest in this phenomenon and its possible connection with the active galactic nuclei. What can we deduce from the observed structures about the processes that took place in the galaxy and what does it say about the presence of the quasar in its centre? The formation of shells can already be qualitatively reproduced in numerical simulations of galactic collisions with suitably chosen parameters. This gives us the hope to obtain more information about the undergone collision than in the case of the chaotic structures left behind by other types of violent galactic interactions. A better insight to one problem sheds more light on another, thus helping us to assemble another part of the mosaic of our understanding of the universe.

Before attempting to broaden the knowledge on the shell galaxies I had to first learn what has been already discovered. Considering the relative low general awareness of this topic, the amount of already published material is substantial. I try to share some of the information with the reader in Parts I (from the observational point of view) and II (concerning the numerical simulation), whereas in Part III I describe the model of the shell formation that I try to improve in the later chapters.

The dynamical friction has been long suspected to have a significant influence on the shell formation but this effect has not yet been thoroughly investigated. This thesis aims to improve this situation a little. Part IV presents a rather detailed discussion of the dynamical friction and its incorporation in the model. In Part V, the gradual disruption of the interacting galaxies is added to the effects of the dynamical friction. Part VI summarises the results of the preceding chapters, gives their further discussions and formulates topics I would like to deal with in the future.

Although I have tried to explain the idea of the shell formation in galactic mergers with the help of simple examples and illustrations, nothing can really replace the visualisation capabilities of a multiparticle numerical simulation, particularly when shown as a video sequence showing the process in its gradual course. To relieve this deficiency I have included a sub-frame of the sequence created by the MERGE 9 programme written by Bruno Jungwiert (2006, unpublished) showing approximately the central 50 kpc of the primary galaxy (with the primary galaxy's profile subtracted) during a merger with a small secondary galaxy simulated with 2,000,000 particles in the secondary galaxy[1] according to the strategy described in §11. The sequence starts on the last page and goes backwards so you can easily "play" it by quickly browsing the thesis. The complete sequence can be found in the AVI format (using the common LJPEG compression) on the CD accompanying the printed versions of the thesis.

[1]The parameters of the merger are the following: the mass of the primary is 3×10^{11} $M_\odot$, the secondary-to-primary mass ratio is 0.02, the Plummer radius of the primary is 7.6 kpc, of the secondary 0.76 kpc. The initial relative velocity of the galaxies was equal to the escape velocity of the secondary and the separation of their centres was 90 kpc. In the printed version, the sequence starts at 550 Myr and one page corresponds to the time step of 30 Myr.

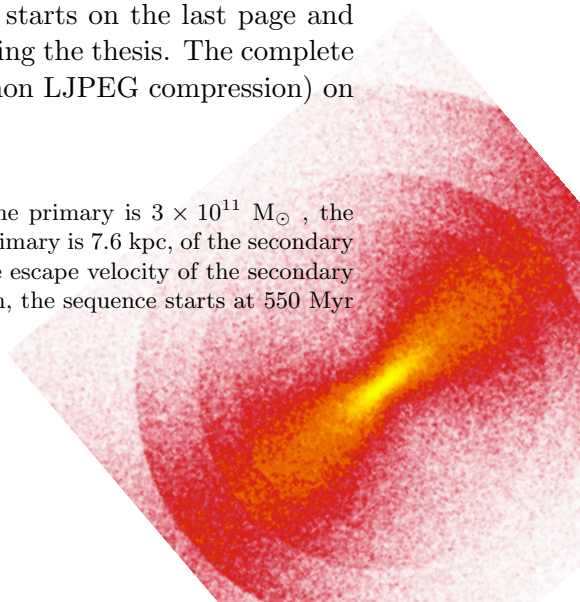

Part I
Shell Galaxies

1 Shell galaxies in brief

Shell galaxies, like e.g. the beautiful and renowned, NGC 3923 (see Fig. 1), are galaxies containing ring-like fine structures. These structures are made of stars and form open, (almost) concentric arcs which usually do not cross each other. The term "shells" has spread throughout the literature, gradually superseding the competing term "ripples". According to the knowledge gained over the past more than twenty years, their origin lies in the interactions between galaxies.

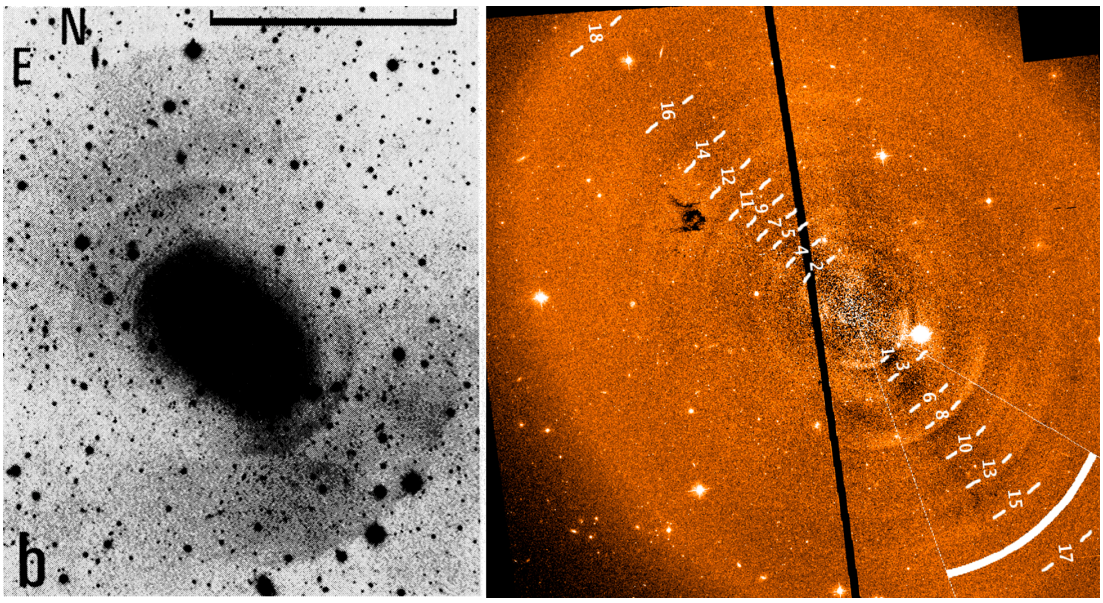

Figure 1: *Left: The shell galaxy NGC 3923 from Malin and Carter catalogue (1983). Scale bar is 5′. Right: Inner region of the same galaxy. The field of view is 202″× 202″(Sikkema et al., 2007). Both images were processed to emphasize the shell structure. Shells are in general not visible without special image processing.*

2 Shell galaxies in length

2.1 Observational history

"Forty years after the discovery that galaxies were independent stellar systems, we still have not penetrated very far into the mystery of how they maintain themselves or what physical forces are responsible for shaping their observed forms. The galaxies are the constituent units of mass and energy in the Universe, and yet we are still challenged by such questions as: What causes the characteristic shape of spiral galaxies? How are elliptical galaxies related to spirals? How are galaxies formed, and how do they evolve?" That's how the article Arp (1966b) about his Atlas of Peculiar Galaxies (Arp, 1966a) begins. We will now look at some aspects of galaxy structure and evolution as we understand it today, another forty years later.

The Hubble Classification, developed in the thirties, divides galaxies in a few categories (Fig. 2). But not only the dedicated group of "Irregular galaxies" (containing

all the galaxies that cannot be put into any other group shown in Fig. 2) is by itself a huge one – in fact, quoting from Arp (1966b), "... when looked at closely enough, every galaxy is peculiar."

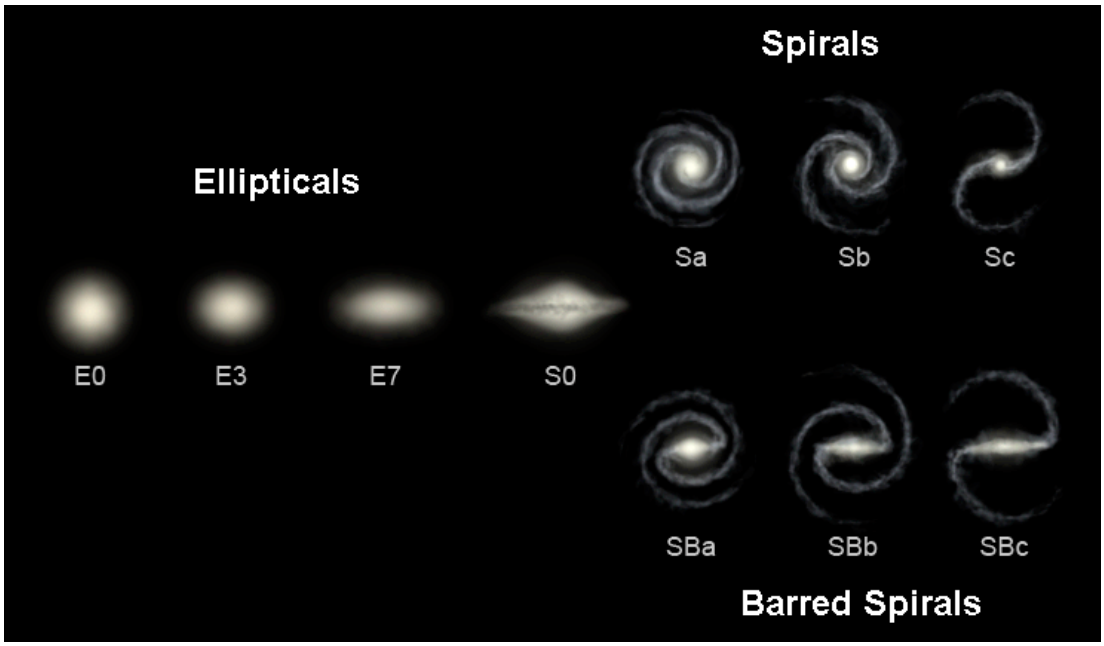

Figure 2: *The Hubble sequence (Ville Koistinen, tr.wikipedia.org)*

And it was also Halton Arp, who first noticed the shell galaxies in his Atlas of Peculiar Galaxies. (He used the term "shells" to describe the structures associated with galaxy Arp 230). That is why almost every article about shell galaxies includes a reference to this Atlas, or the accompanying article. The Atlas contains 338 objects, divided into several subgroups. Shell galaxies are found under "concentric rings" (Arp numbers 227 to 231), but also Arp 223 is in fact a shell galaxy. All above mentioned galaxies can bee seen in Fig. 3, their more common names are listed in Table 1. Furthermore, for example Arp 153–155 (a nice triplet of galaxies seen in Fig. 12 in §2.6) or Arp 226 (NGC 7252) were also recognized as members of this privileged group.

Arp 223	NGC 7585
Arp 227	NGC 470+474
Arp 228	IC 162
Arp 229	NGC 507+08
Arp 230	IC 51
Arp 231	IC 1575

Table 1: *Numbers of Arp's shell galaxies (from Fig. 3) in New General Catalogue (NGC) or Index Catalogue (IC).*

To date, the only (at least partial) list of shell galaxies is "A catalogue of elliptical galaxies with shells" from Malin and Carter (1983). The authors present a catalogue of 137 galaxies (with declination south of $-17°$) that exhibit shell or ripple features at large distances from the galaxy or in the outer envelope. Some further work has been done on this set of galaxies: Wilkinson et al. (1987a,b) examined these shell galaxies to find radio and infrared sources, Wilkinson et al. (1987c) carried out two-colour CCD photometry of 66 Malin-Carter galaxies, Carter et al. (1988) obtained nuclear spectra for 100 of the

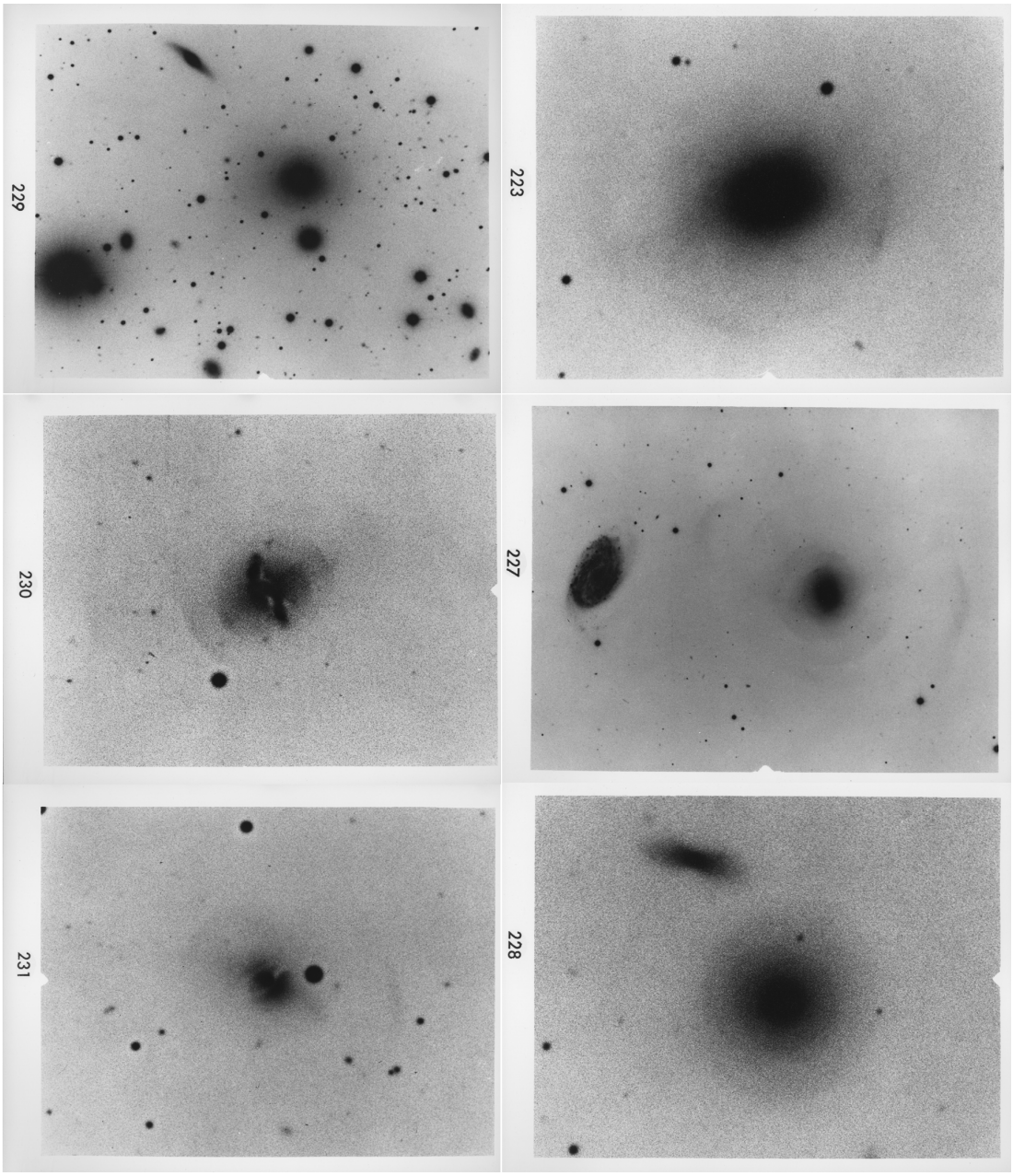

Figure 3: *Shell galaxies in "Atlas of Peculiar Galaxies", Arp (1966a).*

galaxies in the catalogue. In a series of articles, Longhetti et al. (1998a,b); Rampazzo et al. (1999); Longhetti et al. (2000, 1999) (the fifth part surprisingly preceding the fourth) examined star formation history in 21 catalogued shell galaxies. Forbes et al. (1994) were searching for secondary nuclei in 29 shell galaxies. Larger samples of shell galaxies were studied for example by Schweizer 1983, Thronson et al. (1989), Forbes and Thomson (1992) or Colbert et al. (2001). Their results will be mentioned in the following chapters.

Unsurprisingly, many observational studies have been carried out over decades for many individual shell galaxies. Here, I present their long, but surely not complete list, in a chronological order:

- Wright (1974): NGC 5128 = Cen A
- Malin (1979): M 89 = NGC 4552
- Schweizer (1980): NGC 1316 = Fornax A
- Malin and Carter, 1980 NGC 1344 and 3923
- Schweizer (1982): NGC 7252
- Carter et al. (1982): NGC 1344
- Malin et al. (1983): NGC 5128
- Bosma et al. (1985): NGC 1316
- Fort et al. (1986): NGC 2865, 3923, and 5018
- Pence (1986): NGC 3923 and 3051
- Wilkinson et al. (1986a): NGC 5128
- Schombert and Wallin (1987): Arp 227 = NGC 474
- Prieur (1988): NGC 3923
- McGaugh and Bothun (1990): Arp 230, NGC 7010, and Arp 223 = NGC 7585
- Balcells and Carter (1993): NGC 7626
- Schiminovich et al. (1995): NGC 2865
- Forbes et al. (1995): IC 1459
- Sahu et al. (1996): NGC 7562
- Balcells and Sancisi (1996) and Balcells (1997): NGC 3656
- Reduzzi et al. (1997): NGC 7019
- Petric et al. (1997): NGC 1210
- Carter et al. (1998): NGC 3923
- Hau et al. (1999): NGC 2865
- Turnbull et al. (1999): NGC 474 and 7600
- Pellegrini (1999): NGC 3923
- Wilkinson et al. (2000): 0422-476[2]
- Charmandaris et al. (2000): NGC 5128
- Balcells et al. (2001): NGC 3656
- Goudfrooij et al. (2001): NGC 1316
- Horellou et al. (2001): NGC 1316
- Hibbard and Sansom (2003): NGC 3610, 3640, and 7626
- Rampazzo et al. (2003): ESO 2400100, IC 5328, NGC 1553, 7070A, and 7135
- Stickel et al. (2004): NGC 5128
- Pierfederici and Rampazzo (2004): IC 1575, NGC 474, 6776, 7010, and 7585
- Rampazzo et al. (2006): NGC 474
- Serra et al. (2006): IC 4200
- Sikkema et al. (2007): NGC 1344, 3923, 5982, 474, 2865, and 7626
- Rampazzo et al. (2007): NGC 2685, 5018, and 7135
- Canalizo et al. (2007): MC2 1635+119.

2.2 Image processing

The detection of shells in galaxies is not a simple matter. Even the famous NGC 3923 (Fig. 1) was known as a "normal" bright elliptical until the end of the 1970s. In some cases, shells can be seen directly on high-resolution images. But to resolve

[2] The reference name of object derived from the 1950 coordinates. The last digit is a decimal fraction of degree, truncated. Notation used in Malin and Carter (1983) catalogue.

possible further (inner) shells, or reveal other galaxies as shell galaxies, some more or less sophisticated techniques have to be used.

Unsharp masking seems to have been first used in Germany in the 1930s as a way of increasing the acutance, or apparent sharpness, of photographic images. In the photographic process, a large-format glass plate negative is contact-copied onto a low contrast film or plate to create a positive. However, the positive copy is made with the copy material in contact with the back of the original, rather than emulsion-to-emulsion, so it is blurred. After processing this blurred positive is placed in contact with the back of the original negative. When light is passed through both negative and in-register positive (in an enlarger for example), the positive partially cancels some of the information in the negative. Because the positive has been intentionally blurred, only the low frequency (blurred) information is canceled. In addition, the mask effectively reduces the dynamic range of the original negative. Thus, if the resulting enlarged image is recorded on contrasty photographic paper, the partial cancellation emphasizes the high frequency (fine detail) information in the original, without loss of highlight or shadow detail. The resulting print appears sharper than the one made without the unsharp mask; the apparent acutance is increased. Malin 1977 (cited in Prieur, 1988) developed unsharp masking for use in astronomy.

When Malin and Carter (1983) compiled their catalogue, they used a **method described by Malin (1978)** to make extremely faint structure on astronomical plates visible. Malin wrote: "The procedure which avoids the imaging of fog grains, can be applied to photographic images that are not apparent on visual inspection and which can not be detected by conventional macrodensitometry. Faint images tend to be located in the uppermost layers of the developed emulsion while grains due to chemical fog are distributed at random throughout the total thickness of the emulsion coating." Forbes and Thomson (1992) used a method described in their article to examine their modest sample of galaxies and found eight new.

Today there is a broad range of digital methods that can be used to reveal and highlight the details. To search for the shells we can imitate the smooth profile of the galaxy by a function of virtually any complexity and simply subtract it from the image ("**host galaxy subtraction**") or divide the image by it, just as Fig. 4 demonstrates. A similar method has been used by Turnbull et al. (1999) during their observations of NGC 474 and 7600, see Fig. 8 and 9 in §2.4.

To detect fine structure in ellipticals and related merger galaxies, Schweizer and Ford (1985) use a **digital masking** – a filtering algorithm similar to the photographic unsharp masking. Figure 5 illustrates the procedure with an image of Arp 230. First they suppressed the brightest star by interpolating the surrounding sky across it, then all fainter stars were cleaned by running a filter (a circularly shaped median filter of $6''$ diameter across the whole image), and finally they smeared the image by convolution with a 2-D Gaussian weighting function (with $\sigma = 5''$ and a circular boundary at r = 2σ). Clearly, the difference image shows the ripples, inner ring, and dust lanes of the galaxy much better, at the price of increased visibility of the photographic plate noise.

An alternative approach to improving the visibility of faint structures in an image is to create a **structure map**. This method, based on the probabilistic image-restoration method of Richardson and Lucy (Richardson, 1972) has been used e.g. to process HST images of Seyfert galaxies (Pogge and Martini, 2002) as this method is especially suitable to deal with overexposed galactic nuclei. As for unsharp masking, the image is divided with a suitably smoothed copy of itself, in this process however the "suitability" of the smoothing filter is greatly increased by using the appropriate Point Spread Function (PSF) of the specific imaging device. The Point Spread Function is defined

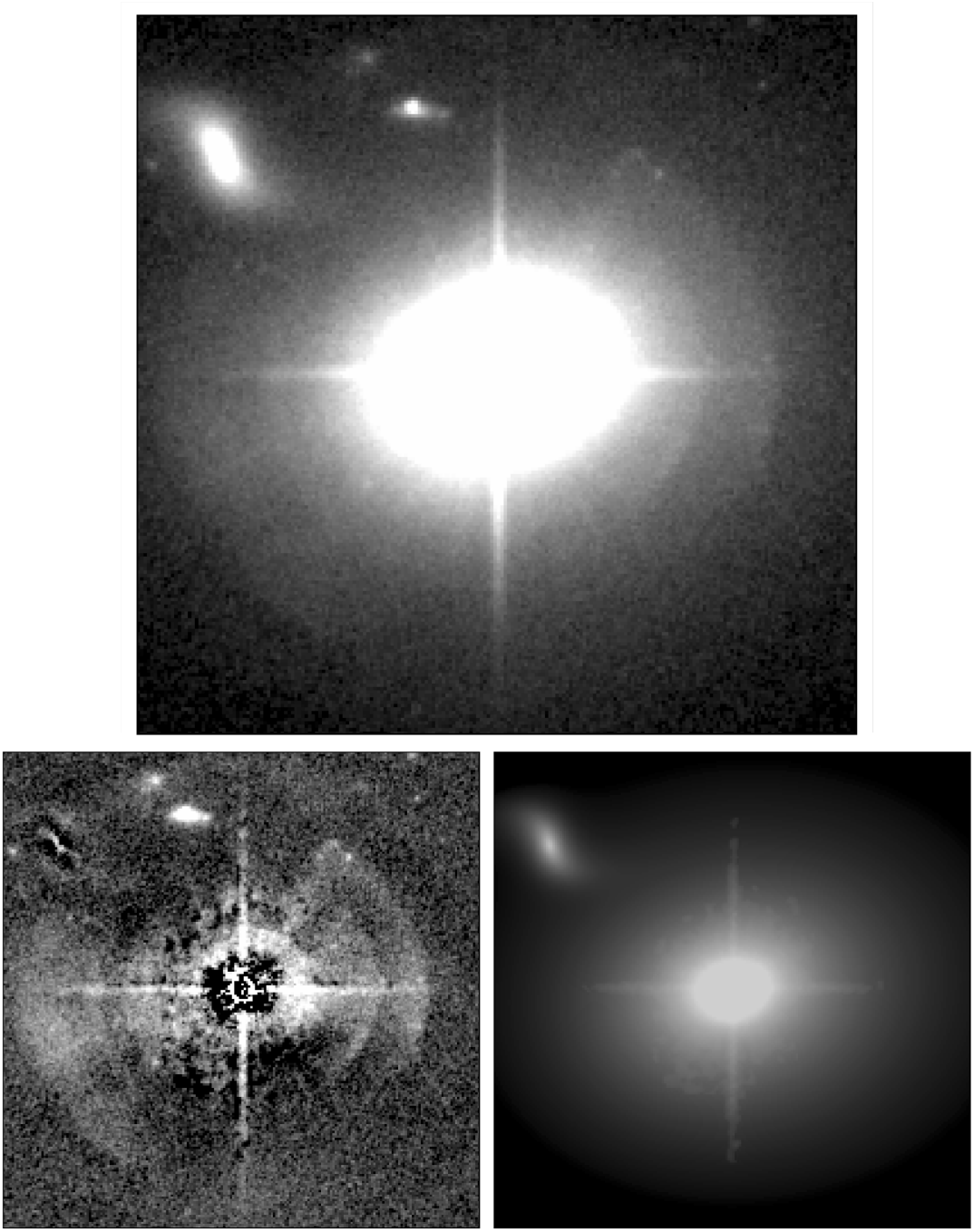

Figure 4: *Top: Very deep ACS/WFC image (total integration time of 11432 s) of a formerly unknown shell galaxy, the host galaxy of the QSO MC2 1635+119 (Canalizo et al., 2007; Bennert et al., 2007, the three images shown here are unpublished and were kindly provided by G. Canalizo and N. Bennert). The shell structure is already visible in this final reduced but otherwise unaltered image. The image size is 10″×10″. The residual image is shown in the bottom left panel and was obtained by subtracting a model – fitted using GALFIT (Peng et al., 2002) – for the host galaxy light (bottom right) from the original data (top).*

as the response of the imaging system (camera and telescope) to a point source – thus any image can be viewed as a convolution of the true optical signal and the PSF.

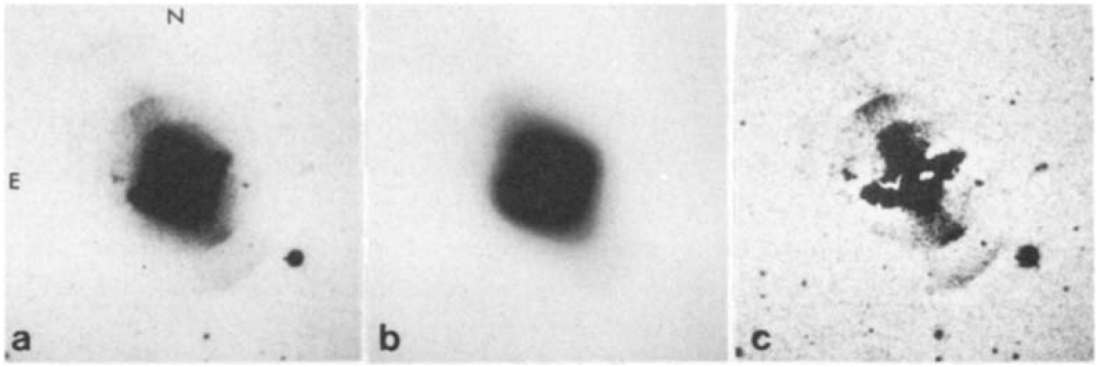

Figure 5: *(a) A scanned plate of Arp 230 shell galaxy (see also Fig. 3) obtained at the Cerro Tololo Inter-American Observatory 4-m telescope, (b) an unsharp digital mask produced from the original image as described in the text, (c) a masked image obtained by subtracting the unsharp mask (multiplied by 0.8, from the original image and increasing the contrast of the display by a factor of four), Schweizer and Ford (1985).*

While the complete Richardson-Lucy procedure iteratively proceeds towards the reconstruction of the original optical signal from the convolution, repetitively applying sophisticated theorems from the theory of probability, the structure map is effectively just the first correction calculated in this process (with some suitable amendment) and thus represents the difference between the smooth profile of the image and its enhanced version, showing only the fine structure. As this procedure can be entirely formulated in terms of convolutions, effective algorithms that use the fast Fourier transform exist to carry out the job in the Fourier domain.

Because the method is based on reconstructive analysis, it usually produces better results than simple unsharp masking (for comparison see Fig. 6). On the other hand, it is exquisitely sensitive to noise and artifacts in the images, so sometimes several iterations including manual removal of problematic features are needed for satisfactory results.

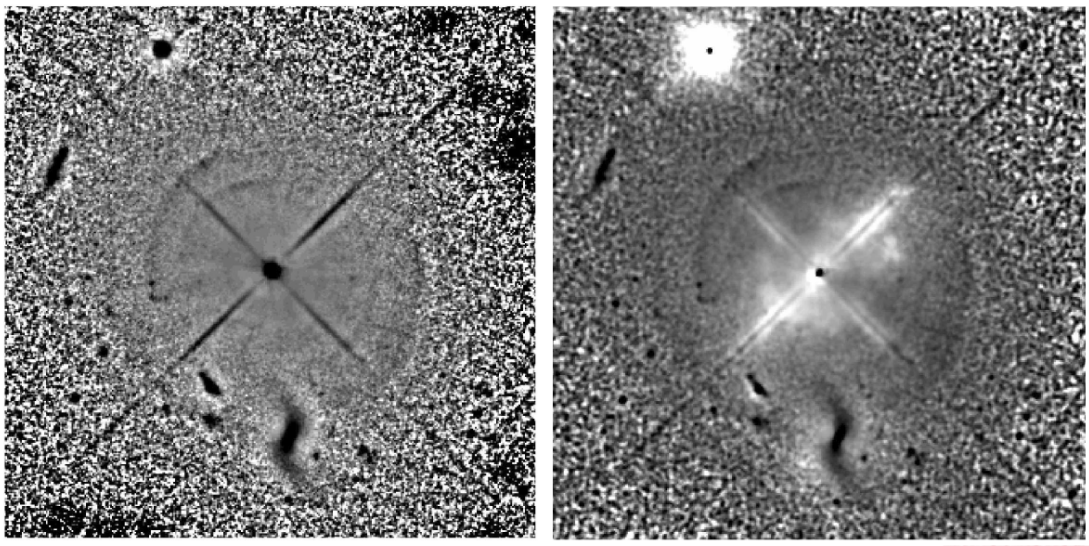

Figure 6: *Different methods used to detect fine structure in the galaxy from Fig. 4. Left: An unsharp-masked image, right: a structure map, Canalizo et al. (2007); Bennert et al. (2007).*

2.3 Occurrence of shell galaxies

Originally (Arp, 1966b; Malin and Carter, 1983), shells were discovered basically in galaxies of E, E/S0 or S0 **morphological type** (according to the Hubble classification, Fig. 2). Schweizer and Seitzer (1988) discovered that they can be found also in S0/Sa and Sa galaxies and even one Sbc galaxy (NGC 3310) was found likely to contain a shell. In fact, Schweizer and Seitzer were against the term "shells", supporting the term "ripples" being more descriptive and not forcing a particular geometric interpretation. NGC 2782 (Arp 215) is probably a spiral galaxy with shells which Arp misclassified as spiral arms rather than as shells, see Fig. 7.

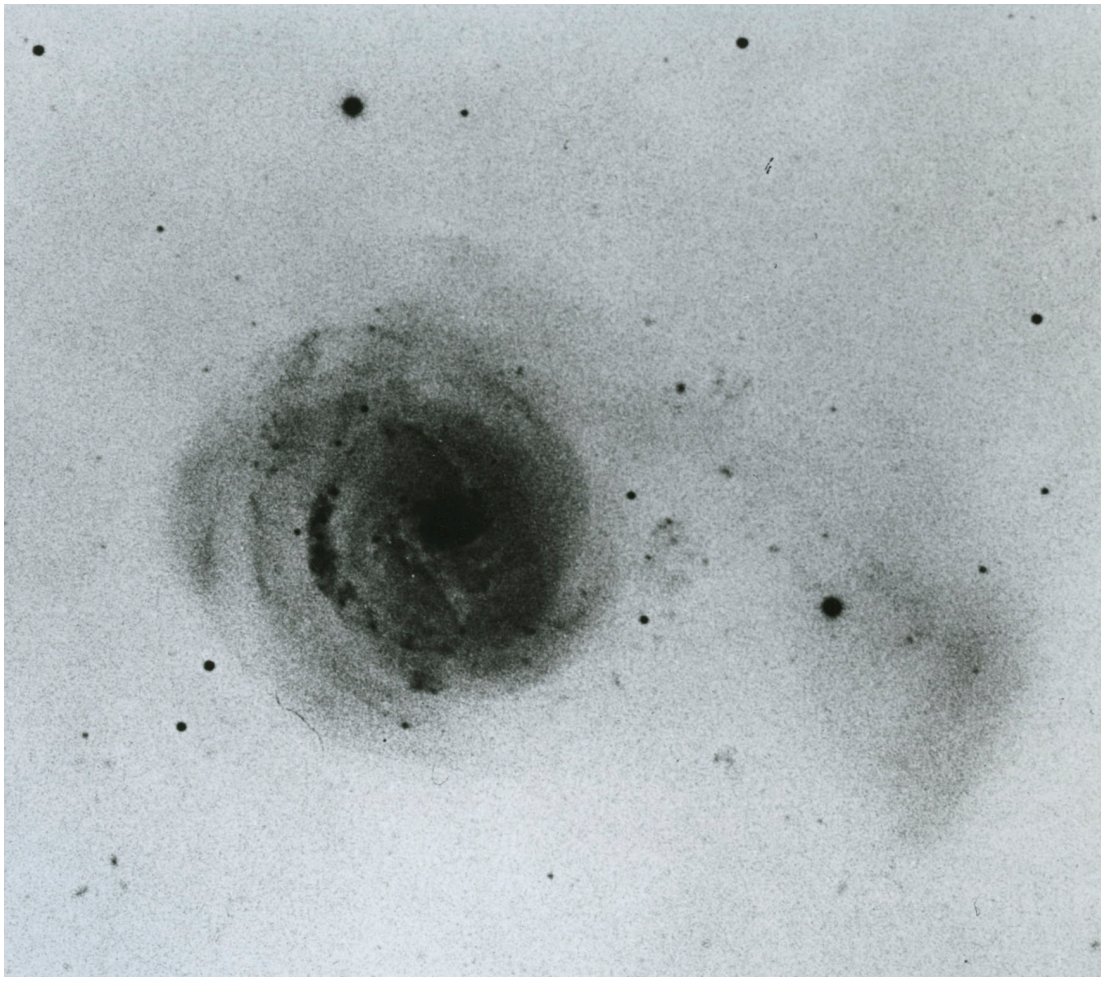

Figure 7: *A spiral galaxy probably containing shells, Arp 215 (NGC 2782), Arp (1966a).*

The realistic estimate of the **relative abundance** of shell galaxies (Malin and Carter, 1983 and Schweizer, 1983; Schweizer and Ford, 1985 both cited in Hernquist and Quinn, 1988) is about 10% in early-type galaxies. I use the term "early-type galaxies" to denote commonly the Hubble types E, E/S0, and S0, because many galaxies gradually wander between these classes according to different classifications or simply during time (not physically, of course, e.g. because of better observations). Hubble originally believed that elliptical galaxies were an early form which might have later evolved into spirals. This is no longer true, but this early belief left its imprint in the astronomers' jargon, who still speak of "early type" or "late type" galaxies according to whether a galaxy's type appears to the left or to the right in the diagram (Fig. 2). Schweizer and Seitzer (1988) quoted similar results for their sample of more than a

hundred of galaxies, with the abundance of 6% for S0 and 10% for E type galaxies, but with significantly lower number among spirals (around 1%).

Another important piece of information from the above mentioned studies is the **environmental dependence** of occurrence of shell structures. They are seen about five times more often in isolated galaxies than in galaxies in clusters. Malin and Carter (1983) explored 137 shell galaxies – 65 (47.5%) are isolated, 42 (30.9%) occur in loose groups (of these 13% have one or two close companions), only 5 (3.6%) occur in clusters or rich groups, and the remaining 25 (18%) occur in groups of two to five galaxies. Taking into account only isolated galaxies, the relative abundance of shell galaxies increases to 17%. Similar result was reached more recently by Colbert et al. (2001) – they detected shell/tidal features in nine of the 22 isolated galaxies (41%), but only one of the twelve (8%) group early-type galaxies shows evidence for shells. Reduzzi et al. (1996) presented their result that 4% of 54 pairs of galaxies (pairs are located in low-density environments) and 16% of 61 isolated early-type galaxies exhibit shells. Schweizer and Ford (1985) have investigated an unbiased sample of 36 isolated giant ellipticals, in order to study their fine morphology. They found that 16 of them (44%) possess ripples (some of them very weak, as Schweizer and Ford note). In contrast to this, Marcum et al. (2004) did not find a single shell galaxy in their sample of nine early-type galaxies previously verified to exist in extremely isolated environments, even though, according to the prognosis, at least four shell galaxies should have been present. The probability of this (a sample of nine early-type galaxies from regions of low galaxy density with no shell) is about 1% if we assume that 40% of galaxies in low-density environments have shells.

However, the true abundance of shell galaxies can still be different from what has been summarized here. It crucially depends on which galaxies we classify as shell galaxies and on our ability to detect faint shell in otherwise innocent looking galaxies.

2.4 Appearance of the shells

Shells have been detected in various **numbers**, appearance and distributions. Rich systems like NGC 3923 (Fig. 1) or NGC 5982 (Sikkema et al., 2007) show about 30 shells, but it is rather an exception among shell galaxies. A large fraction of the Malin-Carter catalogue (1983) consists of galaxies with less then 4 shells. It is in fact difficult to make statements about numbers of shells in galaxies, because the detection of all of them (sometimes even the proof of their existence) is a delicate matter. Shells actually contain only a **fraction of total luminosity** of the host galaxy, mostly between 3 to 6% and their **surface brightness contrast** is very low, about 0.1–0.2 mag.

Shells are **stellar** structures that form arcs in galaxies (circular or slightly elliptical) that either lie within a specific double cone on opposite sides of the galaxy, or encircle the galaxy almost all around. In general, they are sharp-edged features. They tend to have sharp outer boundaries, but many of them are faint and diffuse. Prieur (1990) and Wilkinson et al. (1987c) recognized three different **morphological categories** of shell galaxies.

- Type I (Cone) – shells are interleaved in radius. That is, the next outermost shell is usually on the opposite side of the nucleus. They are well-aligned with the major axis of the galaxy. Shell separation increases with radius. Prominent examples are NGC 3923 (Fig. 1), NGC 5982, NGC 1344 but also NGC 7600 in Fig. 8.

- Type II (Randomly distributed arcs) – shell systems that exhibit arcs which are

randomly distributed all around a rather circular galaxy. A typical example of this kind is NGC 474 in Fig. 9.

- Type III (Irregular) – shell systems that have more complex structure or have too few shells to be classified.

Prieur (1990) has found all three types in approximately the same fraction.

Dupraz and Combes (1986) state that the **angular distribution** of the shells is strongly related to the eccentricity of the galaxy. When the elliptical is nearly E0, the structures are randomly spread around the galactic center. On the contrary, when the galaxy appears clearly flattened ($>$ E3), the shell system tends to be aligned with its major axis. In this case, shells are also interleaved on both sides of the center. Their **ellipticity** is in general low, but neatly correlated to the eccentricity of the elliptical. Nearly E0 galaxies are surrounded by circular shells, while the ellipticity of the shells is of about 0.15 for E3–E4 galaxies.

When we define the **radial range** of the shell system as the ratio between the distance from the galactic centre to the outermost and the innermost shells, then this range of radii, over which shells are found, is large. The value reaches over 60 for type I galaxy NGC 3923 (the innermost shell is less than 2 kpc from centre and the outermost one $\sim$100 kpc, Prieur 1988), but in most systems, a ratio of 10 or less would be more typical. The range is lower than 5 for systems where only a few shells are detected.

Figure 8: *R-band galaxy-subtracted image of the type I galaxy NGC 7600, Turnbull et al. (1999). North is up and east is to the left. The dark oval shape is an artifact of the subtraction process. The easternmost shell lies 215″ away from the galaxy centre. The field of view is 9′.*

Figure 9: *R-band galaxy-subtracted image of the type II galaxy NGC 474, Turnbull et al. (1999). North is up and east is to the left. The easternmost shell is 202″ from the galaxy centre. NGC 470 is located just off the frame, ∼300″ west. The field of view is 9′.*

In their sample of three shell galaxies, Fort et al. (1986) found that the characteristic **thicknesses** of shells are of the order of 10% or less of their distance from the centre of the galaxy.

Wilkinson et al. (1987c) probed 66 of the 74 galaxies in the range from 01h 40m to 13h 46m in the Malin and Carter (1983) catalogue. They found that shells commonly occur **close to the nucleus**. In roughly 20% of the systems these innermost shells have **spiral morphology**.

2.5 Colours

At the beginning of the research on shell galaxies, it was widely believed that shells are rather bluer than the underlying galaxy (Athanassoula and Bosma, 1985). But it was rather difficult to obtain relevant data for shells with only several percent of galaxy's luminosity and the uncertainty was probably huge.

Carter et al. (1982) presented broad-band optical and near-IR photometry of NGC 1344. The colour indices derived suggest that the shell comprises a stellar population, perhaps bluer than the main body of the galaxy. The first CCD photometric observations of shell galaxies were made in April 1983 at the CFHT (Canada-France-Hawaii Telescope) by Fort et al. (1986) for their three objects (NGC 2865, NGC 5018, and NGC 3923). Unlike the shells of NGC 2865 and NGC 5018 which were found bluer than the galaxy itself, the shells of NGC 3923 had similar colour indices to those of the galaxy. The results were obtained from the outer shells of the galaxies.

Pence (1986) got the same result for NGC 3923 and in addition for NGC 3051 as well. On the other hand, McGaugh and Bothun (1990) found both redder and slightly bluer systems of shells among their three shell galaxies (Arp 230, NGC 7010, and Arp 223 = NGC 7585). Multicolour photometry of NGC 7010 shows a colour trend between the centre and the galaxy periphery, red in the centre and blue further out.

Recent observations, using the ever-improving observational capabilities may turn the old myth of blue shells over. Sikkema et al. (2007) wrote: "To date, observations give a confusing picture on shell colours. Examples are found of shells that are redder, similar, or bluer, than the underlying galaxy. In some cases, different authors report opposite colour differences (shell minus galaxy) for the same shell. Colour even seems to change along some shells; examples are NGC 2865 (Fort et al., 1986), NGC 474 (Prieur, 1990), and NGC 3656 (Balcells, 1997). Errors in shell colours are very sensitive to the correct modeling of the underlying light distribution. HST images allow for a detailed modeling of the galaxy light distribution, especially near the centres, and should provide increased accuracy in the determination of shell colours." In their sample of six galaxies (NGC 1344, NGC 3923, NGC 5982, NGC 474, NGC 2865, NGC 7626) they find only one shell (in NGC 474) with blue colour. All other shells have similar or redder colours – what is just contrary to the results of Fort et al. in 80's for NGC 2865 and Carter et al. (1982) for NGC 1344. Sikkema et al. attribute the red colour to dust which is physically connected to the shell (see §2.6).

Forbes et al. (1995) measured shell colours of shell galaxy IC 1459 (they have classified this shell system as type II) and found them to be similar to the underlying galaxy. In their study of the shell galaxies NGC 474 and NGC 7600, Turnbull et al. (1999) found inner shells redder than the outer ones. For the first shells, colours seem to follow those of the galaxy, for NGC 7600 three outermost shells are bluer than the galaxy. In Liu et al. (1999) it is said that a preliminary reduction of the shell sample shows that most of the shells have colours that are similar to the elliptical. The shell colours in the shell galaxy 0422-476 are scattered around the underlying galaxy value (Wilkinson et al., 2000). Pierfederici and Rampazzo (2004) inspected another sample of five galaxies with shells (NGC 474, NGC 6776, NGC 7010, NGC 7585, IC 1575) and found the colour of the shells being similar to or slightly redder than that of the host galaxy with the exception of one of the outer shells in NGC 474, the only interacting galaxy in the sample.

2.6 Gas and dust

Sikkema et al. (2007) detected central **dust** features out of dynamical equilibrium in all of their six shell galaxies. Using HST archival data, about half of all elliptical galaxies exhibit visible dust features (Lauer et al. 2005: 47% of 177 in field galaxies). On the other hand, Colbert et al. (2001) found evidence for dust features in approximately 75% of both the isolated and group galaxies (17 of 22 and 9 of 12, respectively). But in their sample also all of the galaxies that display shell/tidal features contain dust. Also Rampazzo et al. (2007) found all of their three shell galaxies to show evidence of dust features in their centre.

Moreover, Sikkema et al. (2007) discovered that the shells contain more dust per unit stellar mass than the main body of the galaxy. This could explain redder colour of shells which is observed in many cases (§2.5). Observational evidence for significant amounts of dust residing in a shell was also found (Stickel et al., 2004) in NGC 5128 (Fig. 12).

In general, both the ionized and neutral gas contents of shell galaxies are thus comparable to those of normal early-type galaxies. However, arcs of **H I** have been

Galaxy	M_{HI} ($10^9 M_\odot$)	L_B ($10^9 L_\odot$)	M_{HI}/L_B	R_{HI} (kpc)	Environment
Unsettled HI					
NGC 0474	1.8	57.0	0.032	110	NGC 470 (5′)
NGC 5018	3.1	135.0	0.023	98	Group
NGC 7135	1.6	54.4	0.029	206	Sp (6′), Irr (12′)
Settled HI w/o ring or disk					
NGC 1210	5.5	36.2	0.152	58	Isolated
NGC 2865	2.4	28.4	0.085	60	Two Dwarfs
Settled HI w/ ring or disk					
Arp 230	2.3	19.3	0.119	20	Isolated
MCG -5-7-1	5.6	20.0	0.280	56	Isolated
NGC 5128	0.6	22.9	0.026	17	Group

$H_0 = 50$ km s^{-1} Mpc^{-1}; R_{HI} = extent of HI from galaxy center. Enviroment radius ∼500 kpc.

Figure 10: *HI properties in shell galaxies, Schiminovich et al. (1997).*

discovered (Schiminovich et al., 1994, 1995) lying parallel to but outside of the outer stellar arcs in a few shell systems (Cen A = NGC 5128, NGC 2865, NGC 474). In Centaurus A, gas has the same arc-like curvature but is displaced $1'$ to the outside of the stellar shells. A similar discovery has been made by Balcells et al. (2001) in NGC 3656. The shell, at 9 kpc from the centre, has traces of H I with velocities bracketing the stellar velocities, providing evidence for a dynamical association of H I and stars at the shell. Petric et al. (1997) found an off-centred H I ring in NGC 1210. A short report about H I in shell galaxies can been found in Fig. 10.

Rampazzo et al. (2003) analyzed the **warm gas** kinematics in five shell galaxies. They found that stars and gas appear to be decoupled in most cases.

Pellegrini (1999) found that the softer X-ray component which likely comes from hot gas, is not as large as expected for a global inflow, in a galaxy of an optical luminosity as high as that of NGC 3923.

Charmandaris et al. (2000) reveal the presence of dense **molecular gas** in the shells of NGC 5128 (Cen A). Cen A is a giant elliptical galaxy with strong radio lobes on either side of a prominent dust lane situated along its minor axis. Observations show a warped gaseous disk which has been accreted along the minor axis and the presence of a bisymmetric bar-like distribution of hot dust in the inner disk. Charmandaris et al. detected CO emission from two of the fully mapped optical shells with associated H I emission, indicating the presence of 4.3×10^7 $M_\odot$ of H_2, assuming the standard CO to H_2 conversion ratio. All structures can be seen in Fig. 11.

About 5×10^8 $M_\odot$ of molecular gas is located in the inner $2'$ of the NGC 1316 (Fornax A, Fig. 12) and is mainly associated with the dust patches along the minor axis (Horellou et al., 2001). In addition, the four H I detections in the outer regions are all far outside the main body of NGC 1316 and lie at or close to the edge of the faint optical shells and X-ray emission of NGC 1316. Each clump contains 1 to 2×10^7 $M_\odot$ of H I. The location and velocity structure of the H I are reminiscent of other shell galaxies such as Cen A.

Around 8×10^7 $M_\odot$ of neutral hydrogen, and some 10^9 $M_\odot$ of molecular hydrogen

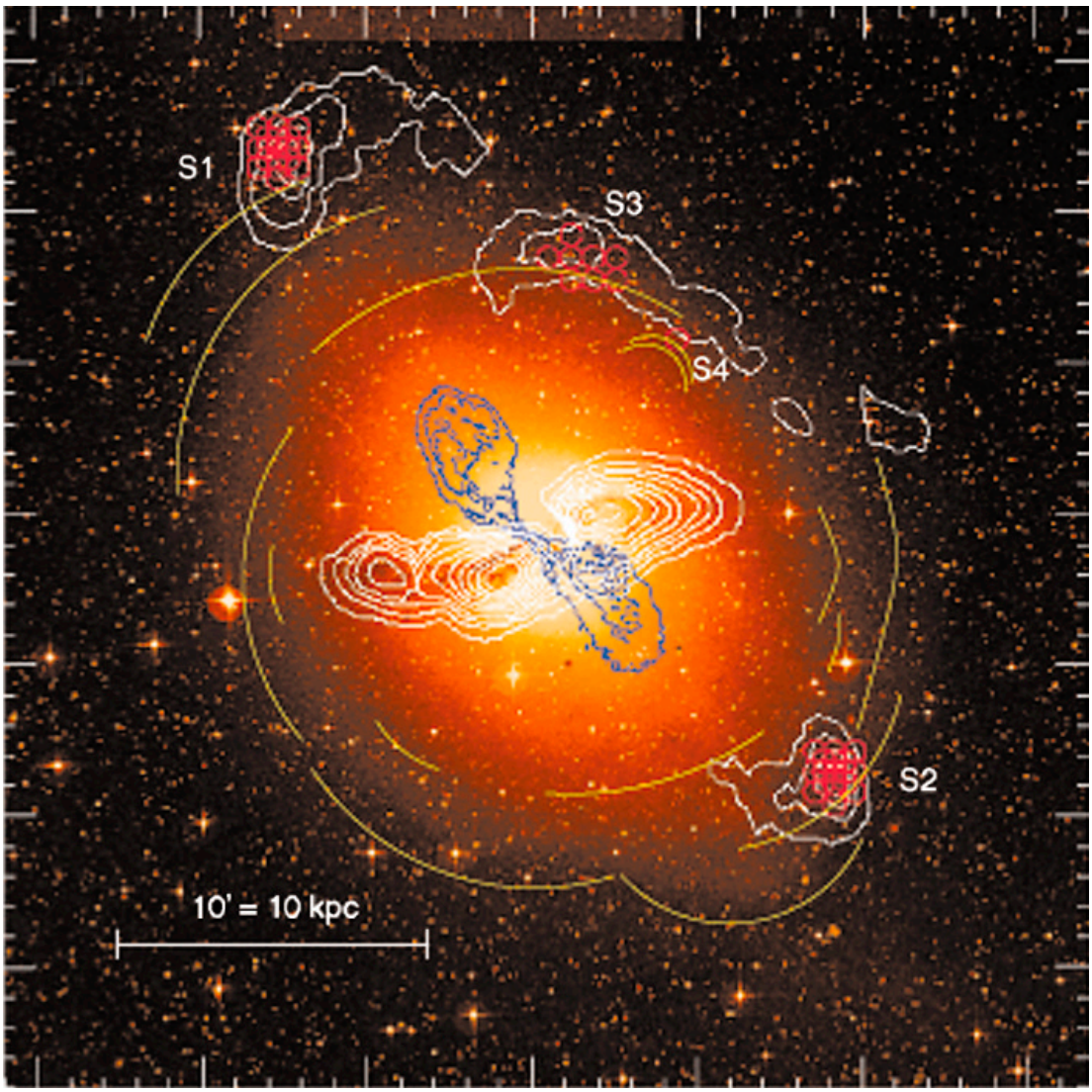

Figure 11: *A Digitized Sky Survey optical image of Cen A with the contours of H I gas superimposed in white. The positions observed in CO are marked with the red circles. The locations of the outer stellar shells are underlined by the yellow solid lines. The inner 6cm radio continuum lobes are depicted by the blue contours. Note the jet alignment with the location of the CO detections. The outer radio lobes are far more extended. Charmandaris et al. (2000).*

have been previously found in NGC 3656 (in Fig. 12) by Balcells and Sancisi (1996). Roughly 10% of the total gas content, one third of the neutral hydrogen, lies in an extension to the south, what is also similar to Cen A.

The shell galaxy IC 1575 (Pierfederici and Rampazzo, 2004) has an interesting similarity with Cen A, once again and for the last time. It shows a strong central dust-lane structure and two radio lobes symmetric to the optical position and orthogonal to the dust-lane. An active nucleus in the centre drives the jet orthogonally to the dust-lane, producing the two radio lobes. It is more than 1000 times weaker in absolute flux than Cen A.

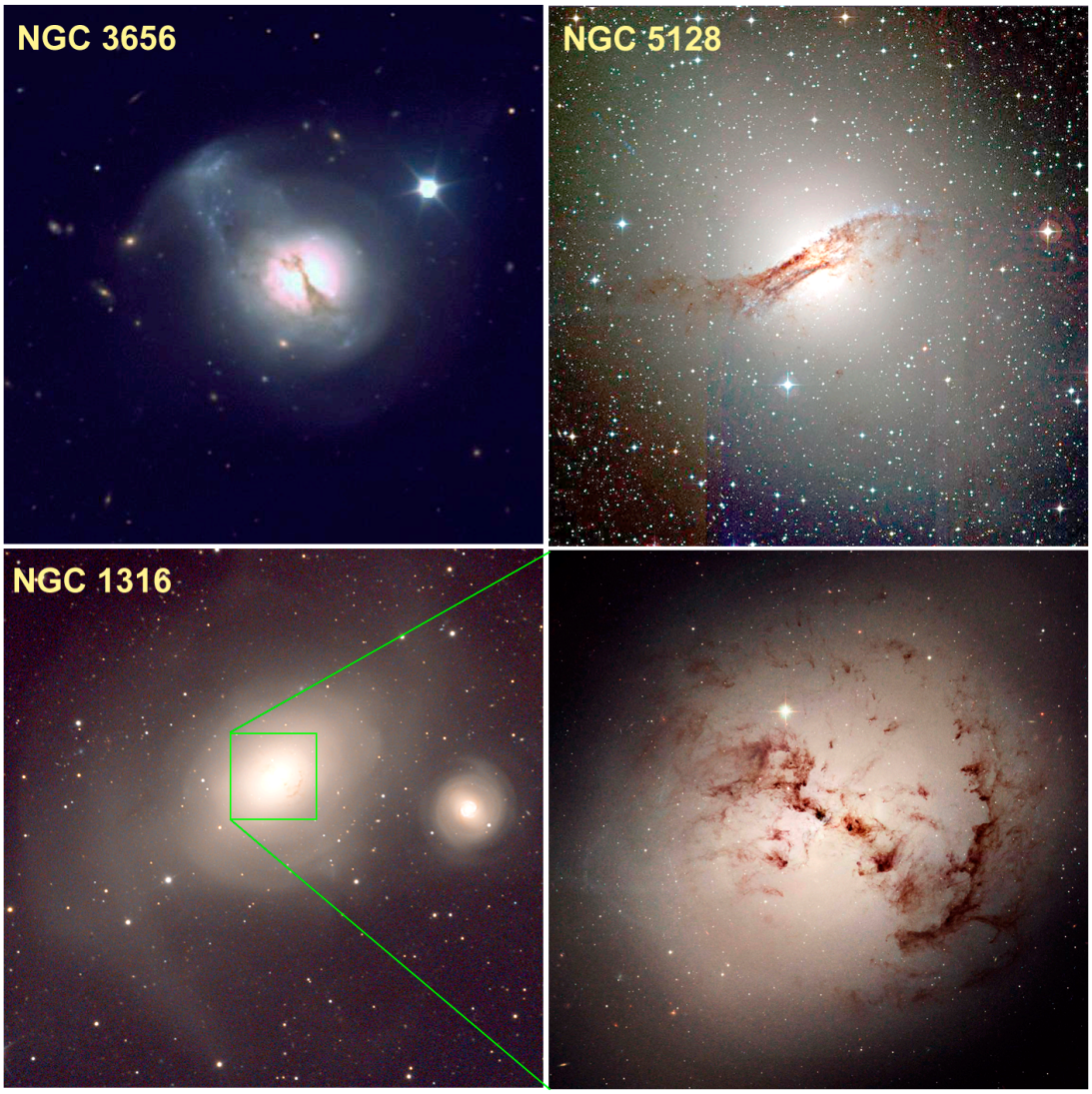

Figure 12: *Three shell galaxies containing similar dust features. Top left: NGC 3656 from LRIS spectrometer at Keck observatory, Hawaii, by Dr. Kurtis A. Williams. Top right: NGC 5128 (Centaurus A, Arp 153) from the ESO 2.2-m telescope taken with the WFI camera. Bottom left: NGC 1316 (Fornax A, Arp 154) by Daniel Verschatse – Santiago de Chile. Bottom right: Detail of central regions of NGC 1316 (Arp 155) from the HST.*

2.7 Radio and infrared emission

Wilkinson et al. (1987a) surveyed a subset of 64 galaxies of the Malin & Carter catalogue at 20 and 6 cm with the VLA. Apart from Fornax A, only two galaxies of their set contained obvious extended **radio sources**. Forty-two per cent of the galaxies were detected, down to a 6-cm flux density limit of about 0.6 mJy. This detection rate does not differ significantly from a normal population of mixed elliptical and S0 galaxies. In addition, Wilkinson et al. found that the sample contains objects with a wide variety of optical appearances, suggesting that shell galaxies are not a homogeneous class with uniform physical characteristics.

A more interesting discovery was made by Wilkinson et al. (1987b). Eight of the previous sample of 64 shell galaxies plus two from Sadler (1984) sample of E and S0

galaxies were **detected by IRAS**. And here comes the discovery: All of these galaxies are also radio sources with 6-cm flux densities $\geq$0.6 mJy. They noted that according to the binomial distribution, the probability of finding all 10 galaxies at both wavelengths by chance would be 0.1 per cent. From non-shell galaxies which are detected in the IRAS survey, only 58% are radio sources. So, there is a strong **radio-infrared correlation**. In the tree-dimensional radio-infrared-shell space, no significant correlation is seen in any two dimensions, but a correlation is apparently found if all three are taken together.

Thronson et al. (1989) investigated infrared colour-colour diagram of early-type galaxies. On average, shell galaxies appear to have broadband **mid- and far-infrared** energy distributions very similar to those of normal S0 galaxies, although many of them were classified as ellipticals.

2.8 Other features of host galaxies

From their sample of 100 shell galaxies, Carter et al. (1988) derived that about 15–20% of shell galaxies have **nuclear post-starburst spectra**.

Longhetti et al. (2000) have studied star formation history in a sample of 21 shell galaxies and 30 early-type galaxies that are members of pairs, located in very low density environments. The last star formation event (which involved different percentages of mass) that happened in the nuclear region of the shell galaxies is statistically old (age of burst from 0.1 to several Gyr) with respect to the corresponding one in the sub-sample of the interacting galaxies (age of burst $<$ 0.1 Gyr or ongoing). This distinction has been possible only using diagrams involving newly calibrated "blue" indices.

There is an obvious strong association between **kinematically distinct/decoupled cores** (marked with pleasure "KDC" or "KDCs") and shell galaxies. First example of an elliptical galaxy with a **KDC** was NGC 5813 (Efstathiou et al., 1982). These galaxies are characterized by a rotation curve that shows a decoupling in rotation between the outer and inner parts of the galaxy. In some spectacular cases, the core can be spinning rapidly in the opposite direction to the outer part of the galaxy (e.g. IC 1459). It was found by Forbes, 1992 (cited in Hau et al., 1999) that all of the nine well-established KDCs and a further four out of the six "possible KDCs" possess shells.

Some galaxies are known to contain multiple nuclei (e.g. NGC 7135, 0632-629, 1152-374). Forbes et al. (1994) conducted the first systematic search for **secondary nuclei** in a sample of 29 known shell galaxies. They find six (20%) galaxies with a possible secondary nucleus, what they concluded to be a probable upper limit to the true fraction of secondary nuclei. On the other hand, Longhetti et al. (1999) in their sample of 21 shell galaxies found only one (ESO 240-100) to be characterised by the presence of a double nucleus.

The shell galaxies have an enormous **diversity of central surface brightness** (Wilkinson et al., 1987c).

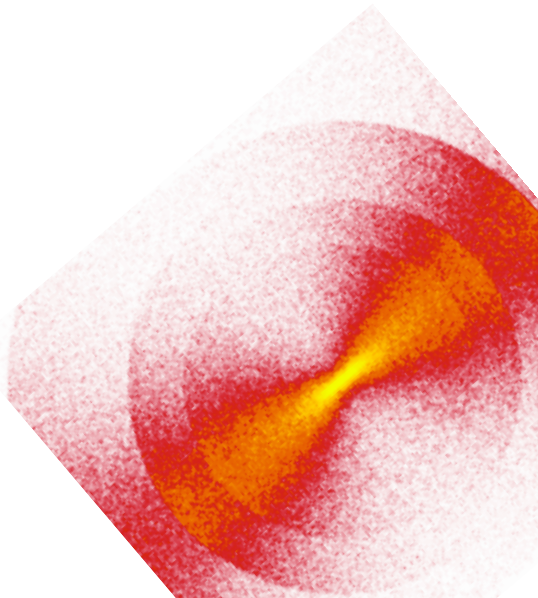

3 A brief summary of shell characteristics

This section contains a summary of §§2.3 to 2.8.

1. Shells are observed in ∼10% of early-type galaxies (E and S0) and ∼1% of spirals.
2. Shell galaxies occur markedly most often in regions of low galaxy density.
3. The number of shells in a galaxy ranges from 1 to ∼30.
4. The shells contain at most a few per cent of the overall brightness of the galaxy.
5. Surface brightness contrast of the shells is very low, about 0.1–0.2 mag.
6. Shells are of stellar nature.
7. Shells are interleaved in radius for type I shell galaxies (see in §2.4), and their separation increases with radius.
8. They are aligned with the galaxy's major axis and slightly elliptical for flattened galaxies, and randomly spread around the galactic centre for nearly E0 galaxies.
9. The range of shells' radii is typically less then 10 but can reach over 60.
10. Shells commonly occur close to the nucleus.
11. In roughly 20% of the systems, the innermost shells have spiral morphology.
12. Shells can have any colour, perhaps they are rather similar to or slightly redder than the host galaxy.
13. The colours of shells are different even in the same galaxy, tend to be red in the centre and bluer further out.
14. It seems that galaxies with shells also contain central dust features.
15. An increased amount of dust has been observed in shells.
16. There is a question of the connection between the shells and the cold gas that has been discovered in some shell galaxies.
17. The detection rate of radio emission of shell galaxies is similar to other early-type galaxies.
18. There is probably a strong radio-infrared correlation for galaxies which possess shells.
19. 15–20% of shell galaxies have nuclear post-starburst spectra.
20. There is a strong association between kinematically distinct/decoupled cores and shells in galaxies.
21. The shell galaxies have an enormous diversity of central surface brightness.

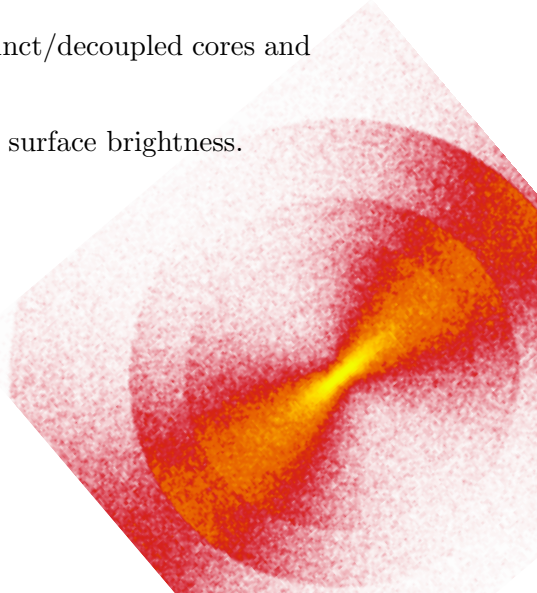

Part II
Scenarios of Origin

During all the time (roughly from 1980) that shells have been discussed, about six more or less different scenarios of their origin have been proposed. Some of them were not much successful (§4), others are still lively debated. The most viable of them are probably the Weak Interaction Model (§5) and the Merger Model (§6) that struggle for the favour of observational data, for they are both well able to explain many of the shell characteristics, still they have rather different grounds.

4 Gas dynamical theories

The first theory of shell formation has been proposed by Fabian et al. (1980), who suggested that shells are regions of recent star formation in a shocked galactic wind. Gas produced by the evolution of stars in an elliptical galaxy and driven out of the galaxy in a wind powered by supernovae would be heated and compressed as it passes through a shock. As the gas cools, star formation can occur. This scenario was expanded by Bertschinger (1985) and Williams and Christiansen (1985). Kundt and Krause (1985) suggested that several gaseous shells are ejected by the active nucleus but remain gaseous, each of these filamentary structures being in pressure equilibrium with the intergalactic medium.

4.1 Williams and Christiansen model

In the Williams and Christiansen (1985) model, shells are initiated in a blast wave expelled during an active nucleus phase early in the history of the galaxy, sweeping the interstellar medium in a gas shell, in which successive bursts of star formation occur, leading to the formation of several stellar shells. These bursts occur when the gas is cooled enough by radiative cooling, and stop when the gaseous medium is reheated by supernovae explosions. The stars formed in that way follow similar, highly radial, bound orbits, moving in phase with each other and spending much of their time near apogalacticon, thus taking on the appearance of a shell. Multiple shells may be produced when conditions allow repeated episodes of shell cooling and supernovae heating to occur in the blast wave.

This scenario was inspired by the supposedly bluer colour of the shells, but as time and the measurements have shown, it is not that hot with the blue colour (see in §2.5), and there are many more arguments against these internal origin theories. As Williams and Christiansen mention, star formation is a subject only to local conditions and is a stochastic process. This is in conflict with the observed interleaving of shells in many shell galaxies. Further, there is the failure to detect either ionized or neutral gas associated with the shells except in a very few cases. In their article, Dupraz and Combes (1986) have given arguments against this model: "First, the mechanism of star formation in such a galactic wind is not known. But given the usual efficiency of star formation in the interstellar medium of actual galaxies, the galaxy should have possessed a very large amount of interstellar matter (at least 10^{11} $M_\odot$), in order to produce 10^{10} $M_\odot$ of stars (typical shell system mass). Also, the swept-up medium could be too diluted for massive stars, and then supernovae, to form. Finally, even if such shells form, the supernovae explosions might rapidly dispel the wind which would exclude that as much as 20–25 shells form around a single galaxy, as is observed for

NGC 3923 and NGC 1344." Today, we know that the gas content in early-type galaxies is not that small, but many other facts remain valid.

4.2 Reconciliation

Loewenstein et al. (1987) reconciled previous models of internal origin of shells with the last observations at that time. An outward-moving disturbance from the galactic core or nucleus, leads to a period of enhanced star formation as it propagates through the hot interstellar medium. Only a modest outburst is demanded by the authors to cause a period of disturbed star-formation. An initial mass function will be skewed to low masses due to much higher pressure and the lack of dust. The newly-formed stars have a low velocity dispersion, since the gas out of which they form is nearly in hydrostatic equilibrium, so they will occupy a small volume in the orbital phase-space of the underlying galaxy. The shells were produced in the same phase-wrapping mechanism as in the merger model (§6.2) as you can see in Fig. 13 – an example of a simple numerical simulation, where stars are created behind a constant-velocity wave and then continue in their orbits through a galactic (stellar plus halo) background potential. One-sided or highly asymmetric disturbance in the nuclear or core region is needed for interleaving of shells.

To produce shells with the observed wide range of radii, such a disturbance must

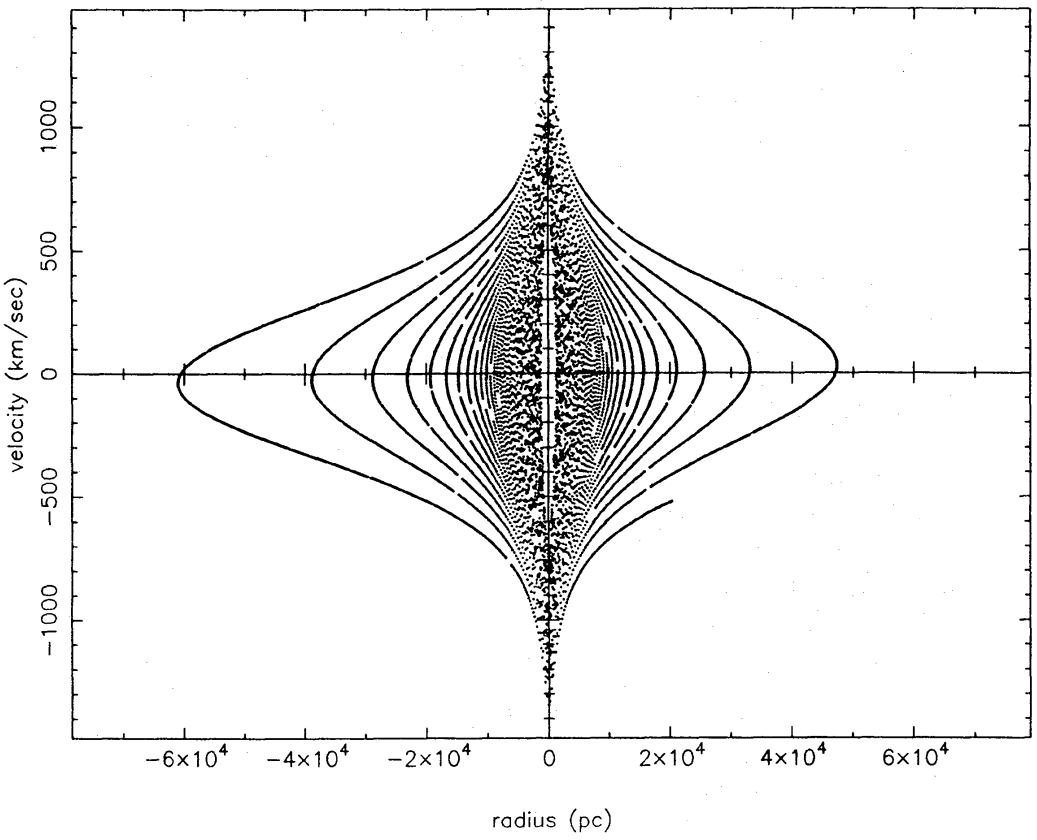

Figure 13: *Phase-space diagram after 1.5×10^9 yr for stars forming behind a disturbance of 10^{49} J. The simulation follows the motion of 10,000 particles orbiting in a galactic potential starting with velocities equal to the velocity amplitude of the disturbance at the appropriate radius, Loewenstein et al. (1987).*

create an observable population of stars on a time-scale shorter than the time of the free-fall across the galaxy (10^8–10^9 yr). Loewenstein et al. note that the sound crossing time in a gas at 10^7 K is comparable with the free-fall time.

The initial outburst could be due to activity in the nucleus fueled by the cooling inflow. But the model does not exclude the merger hypothesis, since a merger can lead to a burst of star formation in the galactic core that is the precursor of the initial blast wave. That is why the numerous observed characteristics of a recent merger in shell galaxies do not exclude this hypothesis.

The inner shells are older than the outer ones in this scenario. This could lead to the colour gradient which seems to be observed in some cases (point 13 in §3) and which was not known at the time.

All these arguments are sound, but other observed aspects of shell galaxies seem to exclude the model of Loewenstein et al. anyway. Aside from the already mentioned points, Colbert et al. (2001) discovered a consistency of the colours of the isolated galaxies with and without shells and it argues against the picture in which shells are caused by asymmetric star formation. Also, the failure to detect either ionized or neutral gas associated with the shells except in a very few cases argues against this scenario (see §2.6). Finally, the lack of signs of recent star formation in the shells is the most fatal reality for the model discussed here.

4.3 Stellar shells and hot coronae creation

A rather different scenario was proposed by Umemura and Ikeuchi (1987), and was quickly forgotten for its clumsiness and only a little agreement with observations. They tentatively considered a hot supernova-driven galactic wind as a process which produces both extended multiple stellar shells and hot X-ray coronae which have been detected around a number of early-type galaxies. Few of them also have shells (NGC 1316, NGC 1395, NGC 3923, and NGC 5128). Sequential stellar shell formation is due to successive collisions of the galactic wind with accreting ambient matter which is left over in the process of the galaxy formation. Sweeping up the accreting gas to create a cooled thin shell which is disrupted by gravitational instability to trigger star formation, is similar to the foregoing scenarios. Subsequently the wind blows through this stellar shell and interacts again with the accreting external gas to generate another dense gaseous shell which results in the next stellar shell by fragmentation (Fig 14). Furthermore, the hot winds may produce X-ray emitting coronae, because the temperature of supernova-driven winds is expected to be 10^7 K.

The theory of Umemura and Ikeuchi explains nicely why shell galaxies are found mostly in the region of low galaxy density. They found that if the wind luminosity (power) is below a critical luminosity, the ram pressure of accreting gas suppresses the outflow of the wind, so that there will be no extended stellar shells formed by their mechanism. The critical luminosity becomes larger if the ambient gas density is higher, and the ambient gas density is higher in clusters. Moreover, the younger shells tend to be located in outer region.

Nevertheless, this scenario suffers from much the same diseases as the former ones. Moreover, it gives no explanation for the increasing separation of shells with radius, since the distribution of shells is variable with the lapse of time in this scenario. However, this theory seems to be primarily out of game because of the observed systematic interleaving of shells.

All the models mentioned above (§§4.1–4.3) more or less fell in condemnation and oblivion before they even started to try explaining more detailed characteristics observed in shell galaxies.

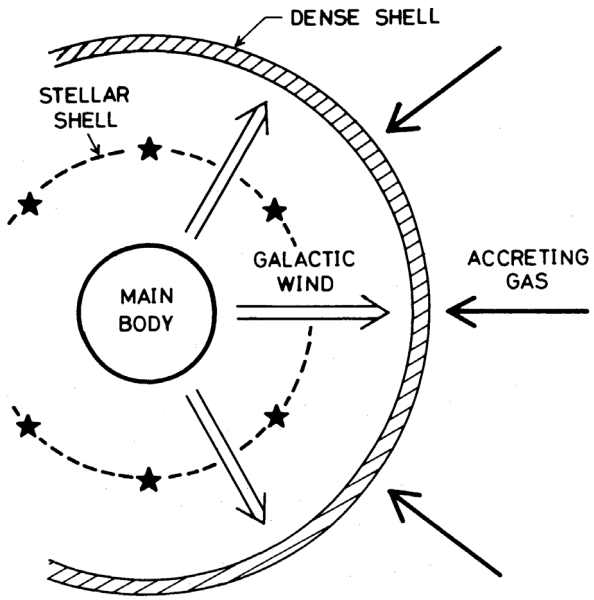

Figure 14: *Schematic illustration of the sequential stellar shell formation by interactions of galactic wind with accreting ambient gas, Umemura and Ikeuchi (1987).*

5 Weak Interaction Model

Thomson and Wright (1990) came up with an elegant and revolutionary model of shell formation in elliptical/S0 galaxies which is still in the game today. According to them, shells are density waves induced in a thick disc population of dynamically cold stars by a weak interaction with another galaxy – whence the name, the Weak Interaction Model (WIM). A year later, this hypothesis was further developed and supported by new simulations of Thomson (1991).

5.1 Thick disc

Thomson and Wright state that already Toomre and Toomre (1972) and Wright (1972) modelled encounters between cold-disc systems of comparable mass to produce tails and bridges. When the mass of the secondary is reduced, a predominantly bisymmetric spiral density wave is induced in the cold primary. Now, we have to imagine a similar, but thick, disk included in an early-type galaxy. This notion is not that easy, because elliptical galaxies are known to be dynamically hot systems, what is a weakness of this model.

To support their theory, the authors state that Thronson et al. (1989) pointed out that most of the elliptical galaxies with shells catalogued by Malin and Carter (1983) are classified elsewhere as S0s. As such, a significant population of dynamically cold stars moving on nearly circular orbits would not be unexpected in these systems. They also note that faint thick discs could be present in many elliptical galaxies without detection. Only when resonant features are induced in this cold population would such subsystems become visible.

Thomson and Wright computed models for several values of the "heat parameter" σ/v, where σ is the root mean square random component and v is the circular component of the velocity. They showed that only a dynamically cool population of stars in nearly circular orbits ($\sigma/v < 0.05$) contributes to the shell-forming process. Thus the

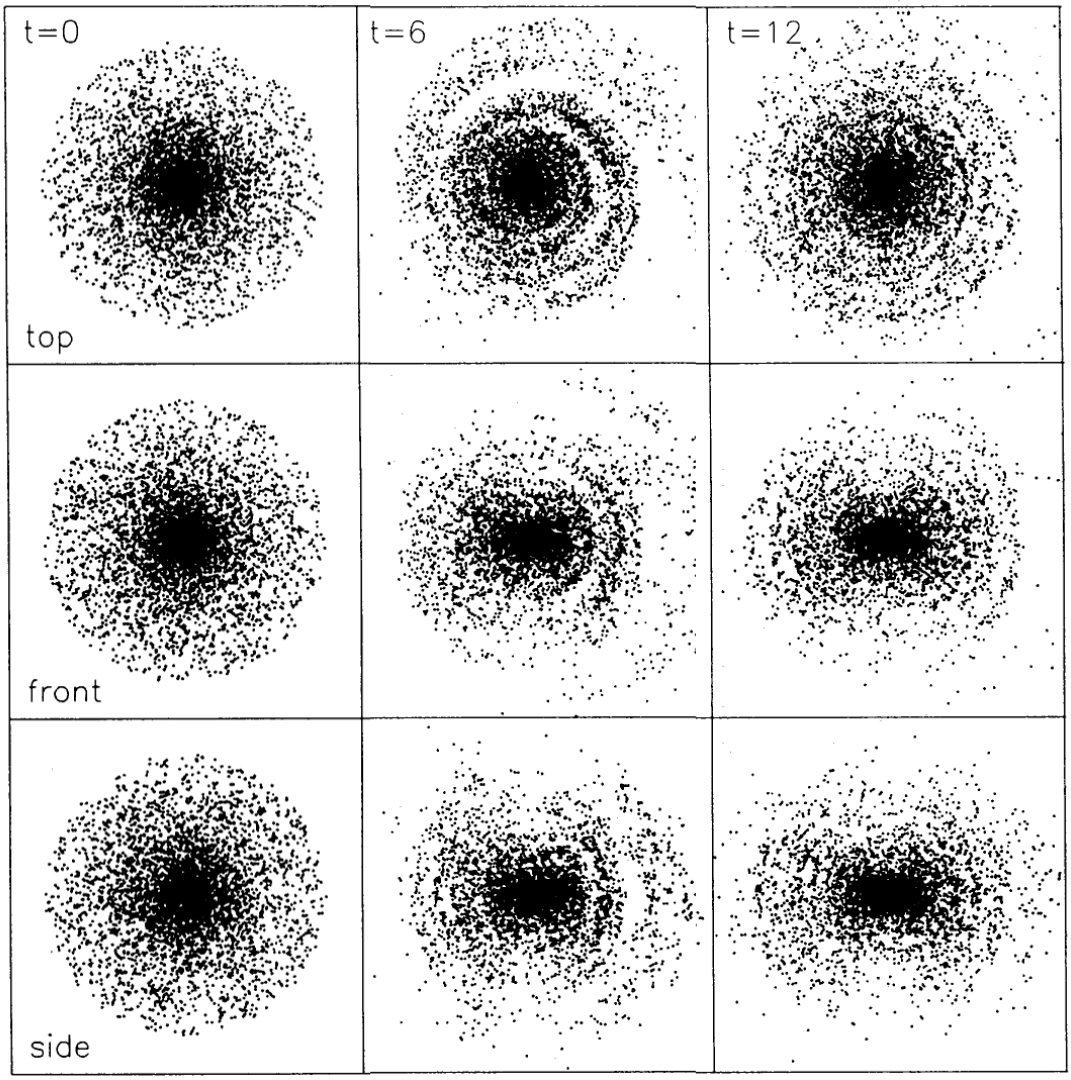

Figure 15: *The evolution of the encounter with a secondary galaxy having 0.05 of the primary mass, viewed from three different angles, Thomson and Wright (1990). The secondary galaxy passes the perigalacticon at time t = 3, through the middle of the simulated thick disc. One time unit is approximately 10^9 yr.*

thick disc population is always cold (i.e. no random motions are added to the calculated initial velocities) in their simulations (Thomson and Wright, 1990; Thomson, 1991). In all cases, the cold thick disc was simulated by 10^4– 10^5 massless test particles under the influence of the combined time-varying potential of the primary and secondary galaxies.

The authors noted that a thick-disc population which makes up only a few per cent of the total mass of a galaxy is required to explain the faint features seen in most shell galaxies. But the disc must by heavy enough to produce shells which form a few per cent of the overall brightness of the galaxy (point 4 in §3). Wilkinson et al. (2000) looked for such a disc in the shell galaxy 0422-476 and found no sign of an exponential disc, or any thick disc additional to the short-axis tube orbits already expected within an oblate ellipsoidal potential.

5.2 Encounter

The WIM has always been simulated with the parabolic encounter of the secondary galaxy, since more circular orbits would decay rapidly during a close encounter, resulting in a merger scenario, while more hyperbolic orbits would result in encounters too quick to be effective. Wright (1972) also concluded that fast, hyperbolic orbits were not important due to the high relative velocity and therefore small impulse given to the primary. This fact can also account for the less frequent occurrence of shell galaxies in clusters than in the field (point 2 in §3, more detailed in §2.3).

Thomson and Wright derived that secondary masses of about 0.05–0.2 of the primary mass are the most likely candidates to form well-defined shell structures in thick-disc systems. For a secondary galaxy with a relative mass of 0.2, stronger features are induced, but the definition of the shells is subsequently lost due to the increased random motion (heat) of the particles. Even larger secondary masses would disrupt the thick disc to form tails and bridges well outside the initial boundary of the primary galaxy. On the other hand, reducing the mass still further produces a correspondingly smaller response in the cold disc, such that relative masses of $\sim$0.01 are not capable of inducing significant effects during an encounter at this distance.

Most of the simulations are run with an encounter when the plane of the secondary's orbit is in the plane of rotation of the primary thick-disc population. But it is shown that shells are still formed preferentially along and perpendicular to the effective plane of rotation of the primary galaxy, and not along the plane of the secondary's orbit, during an encounter which has an orbital inclination of 45°.

The total time of the shell structure's visibility is typically around 10 Gyr in Thomson and Wright (1990). But in Thomson (1991), simulations the shells are visible for only about 3 Gyr.

The question is, whether the requirement of a parabolic encounter is not as peculiar as the much criticised requirement of a predominantly radial encounter in a merger model (§6). The non-effectiveness of hyperbolic encounters is required to explain the rareness of shell galaxies in clusters, on the other hand probably no one has checked, what would happen to the weak-interaction structure after another pass of the secondary, but it will not be anything nice, I guess. Neither the effects of the dynamical friction nor tidal stripping have ever been investigated in the WIM framework.

Possibly, the age of the shell system can be deduced from its appearance and thus the presence of a suitable secondary galaxy at an appropriate distance could be checked. But e.g. around NGC 3610 no surrounding galaxies were found (Silva and Bothun, 1998).

The effect of the perigalactic distance of the secondary galaxy is described in §5.4.

5.3 Projection effects

Prieur (1990) has sorted shells in galaxies into three morphological types that he found to occur in roughly the same number (see §2.4), and he was probably the first who guessed this could be a projection effect. In WIM, the host galaxy is an oblate[3] spheroid, and shells are readily formed as spiral density waves in the thick disc which is symmetric about the plane of symmetry of the galaxy. Naturally, the system viewed from above (face-on) appears as a type II shell galaxy (randomly distributed arcs, see in §2.4) and also rounded. When the system is viewed from the front or side (edge-on), shells look like type I (§2.4) – aligned with the major axis and interleaved, since our view is a cut

[3] An *oblate* ellipsoid is rotationally symmetric around its shortest axis, whereas for a *prolate* ellipsoid the axis of symmetry is the longest one. A *triaxial* ellipsoid has no rotational symmetry at all.

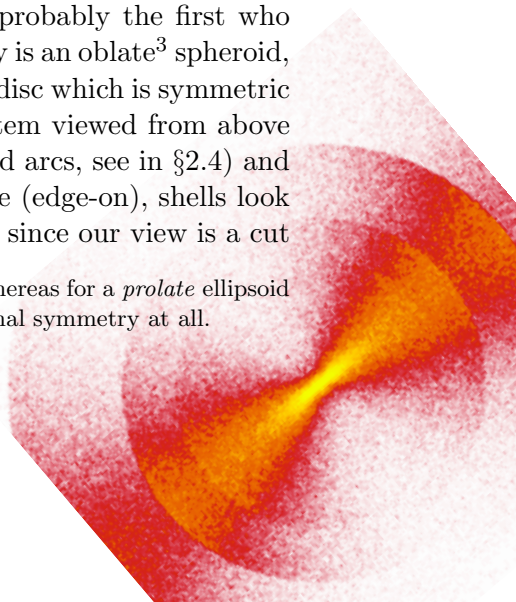

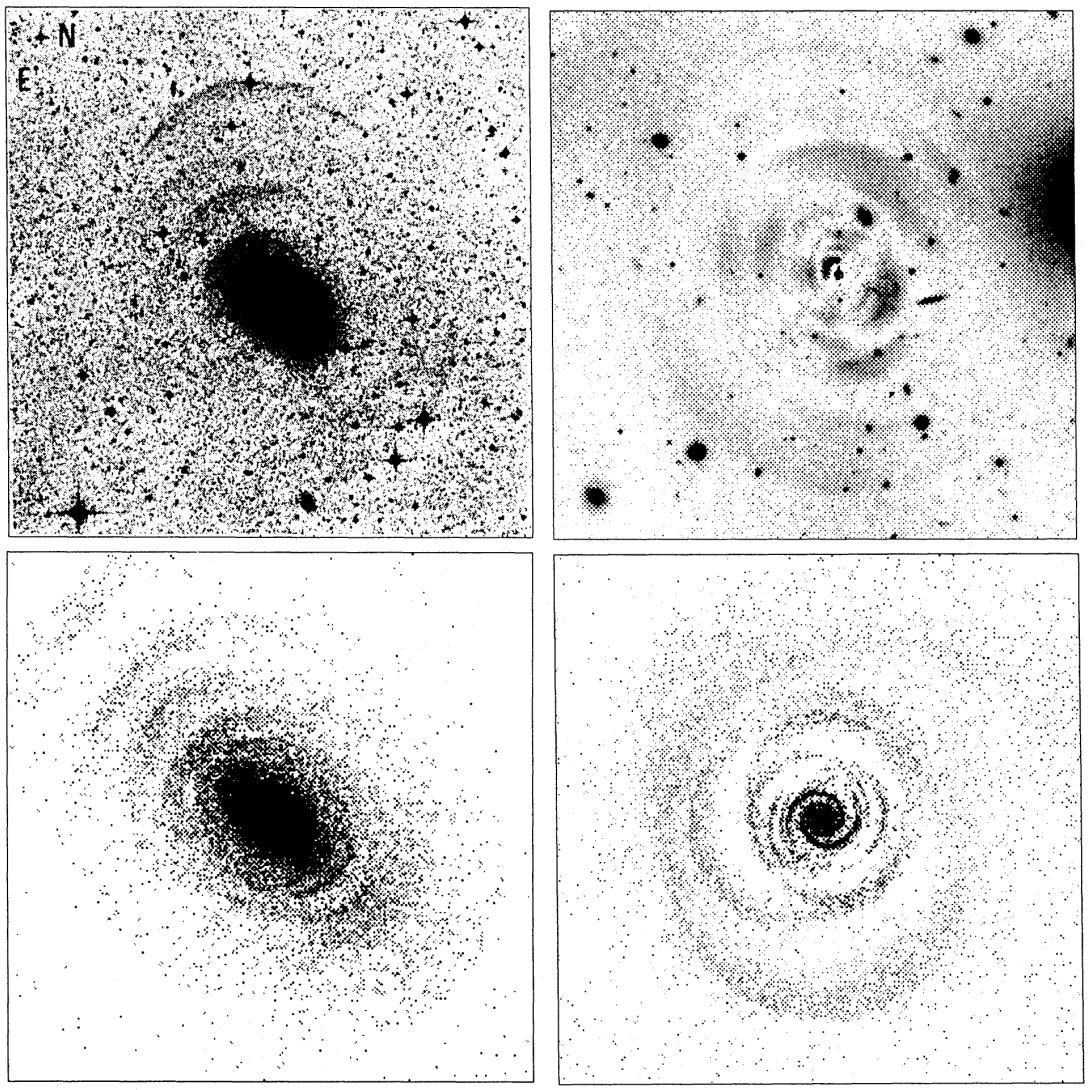

Figure 16: *Top left: Type I shell galaxy NGC 3923 (reproduced from Malin and Carter 1980). Bottom left: Simulated weak interaction model viewed edge-on. Top right: Type II shell galaxy 0422-476 (reproduced from Wilkinson et al. 1986b). Bottom right: Simulated weak interaction model viewed face-on. Thomson (1991).*

through a spiral (this satisfies points 7 and 8 in §3). The results of the simulations compared to the observed galaxies can be seen on the (suggestive) Fig. 16.

The model also gives the correct relative frequency of these two types (i.e. 1:1), since the systems appear as type II shell galaxies when viewed at inclination angles less than approximately 60° (0° is face-on). At inclination angles larger than 60°, the systems appear as type I. The authors also explain the absence of shells in late-type galaxies: "It is important to note that shells form only in thick disc systems. The corresponding features in thin disc systems are the more familiar spiral arms. Indeed it is just because spiral galaxies have predominantly thin discs that shells are not observed around these galaxies."

This model does not suffer from the loss of shell structure when viewed under an unfavourable angle and thus does not require the true abundance of shell systems to be even larger than we see, as opposed to the the Merger model (§6). The shells can be seen from every possible angle (they only look different), what can explain their

high abundance in early-type galaxies (point 1 in §3, more detailed in §2.3). As we change the viewing angle, the observed ellipticity changes from E0 (for 0°) to E4 (90°), where E4 may be the true ellipticity of the galaxy, since Prieur 1990 (cited in Thomson 1991) found a strong peak at this value in the type I ellipticity histogram. However, implications of this would be somewhat strange – either all elliptical are E4 type oblate spheroids seen from different angles, or shells do occur only in E4 galaxies, what would be probably in contradiction to their relatively frequent occurrence.

Prieur (1988) pointed out that the shells in NGC 3923 are much rounder than the underlying galaxy and have an ellipticity which is similar to the inferred equipotential surfaces. This idea was originally put forward by Dupraz and Combes (1986) who found such a relationship for their merger simulations (§6). The same effect can be seen in the simulations presented by Thomson (1991).

5.4 Radial distribution

Another advantage of the WIM lies in its ability to explain the occurrence of the shells over a broad range of radii (point 9 in §3) and close to the nucleus (point 10), since shells are formed in the thick disc that is already present in the galaxy. No further energy loss is required.

In the simulations, the density wave occurs outside the perigalactic distance of the secondary galaxy in the form of an one-armed spiral. Looking from the side, we see interleaved shells and their separation increases with radius (point 7 in §3), see Fig. 17.

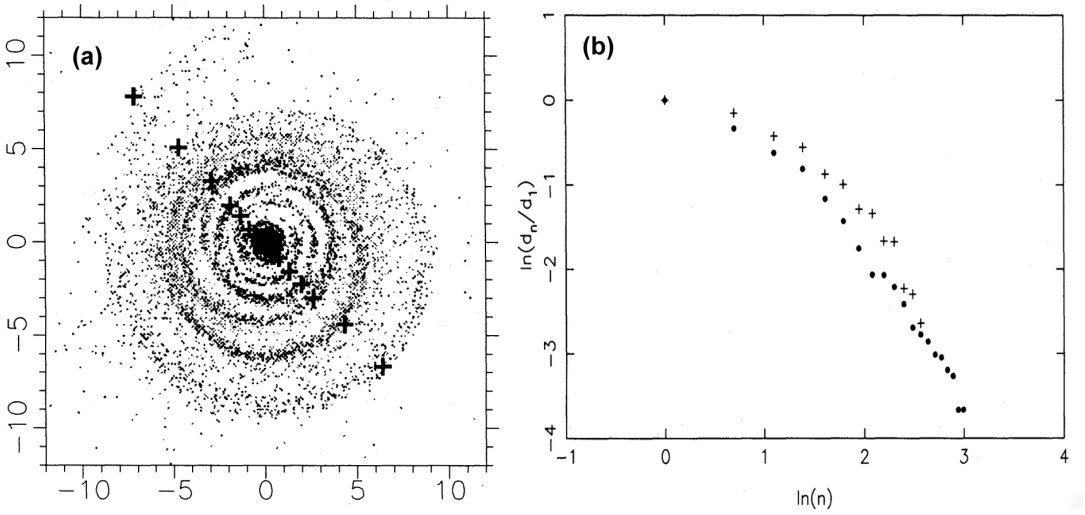

Figure 17: *(a) Simulated shell galaxy showing only particles from the equatorial band. The shell radii are determined from the marked (+) shell positions. (b) Radial distribution of shells in NGC 3923 by Prieur (1988) (•), and the radial distribution of simulated shells (+) as determined from (a). The author (Thomson, 1991) follows the convention of numbering the shells from outside, as it was introduced by the competing merger model (see §6) according to the order of shell formation that this model expects.*

In his study of the shell galaxy NGC 3923, Prieur (1988) discussed varying distribution of the shells – interleaved in outer region and roughly symmetric in inner parts. According to this model, in the outer region of the galaxy, the simulations show a predominantly one-armed trailing spiral density wave which, when viewed edge-on, gives rise to the interleaving of the outer shells, naturally aligned with the major axis. Inside

the perigalactic radius of the path of the intruder, the tidal forces produced during the encounter induce a bi-symmetric kinematic density wave in the thick disc.

Thomson has achieved an almost breathtaking agreement with the observation of radial shell distribution (Fig. 17), except for the innermost shells that have not appeared at all in his simulations. But he believes it could be remedied by shrinking the core radius of primary galaxy.

5.5 Kinematically distinct cores

The WIM for shells does not predict the existence of a kinematically distinct nucleus (KDC, point 20 in §3). Since the shells are produced as a reaction to a grazing incidence passage, the presence of the rapidly rotating nuclear system in a shell galaxy is purely coincidental in this framework, unless the core is formed by mass transfer.

Hau and Thomson (1994) further investigated whether a weak interaction could explain the existence of KDCs, and proposed a mechanism whereby a counter-rotating core could be formed by the retrograde passage of a massive galaxy past a slowly rotating elliptical with a pre-existing rapidly rotating central disc. In this picture, it is the outer regions of the galaxy that are anomalous, the direction of rotation there is changed or reversed, whereas the central disc is relatively unaffected.

In their study of the shell galaxy NGC 2865, Hau et al. (1999) state that the requirement of the WIM for the nuclear disc to be primordial is in conflict with the observed absorption line indices. It is also unlikely that a passing galaxy can transfer a large amount of orbital angular momentum over a period longer than 0.5 Gyr without being captured or substantially disrupted, as NGC 2865 has an extended massive dark halo (Schiminovich et al., 1995). Thus a purely interaction induced origin for the shells and KDC in NGC 2865 is ruled out.

5.6 Observational confrontation

The observation by Pence (1986) that the surface brightness of shells in NGC 3923 is a "surprisingly constant" fraction (∼3–5%) of the surface brightness of the underlying galaxy means that the shell surface brightness profile must follow the same $R^{1/4}$ profile[4] as the underlying galaxy. The WIM produces shells with the correct surface brightness, since they are formed in a thick disc which has the same surface brightness profile as the underlying galaxy. It is however necessary to note against it that neither Pence (1986) nor even Prieur 1988 did know all of the currently identified shells in NGC 3923 (Sikkema et al., 2007). Moreover, e.g. Turnbull et al. (1999) found that the two outermost shells of NGC 474 have a higher surface brightness than most of the inner shells, though not significantly so. This means that the shell surface brightness does not follow that of the galaxy as well as in shell galaxies NGC 474 and NGC 7600 (Turnbull et al., 1999) and 0422-476 (Wilkinson et al., 2000). Similarly for NGC 2865, the WIM origin is in conflict with the existence of bright outer shells, their blue colours, and their chaotic distribution (Fort et al., 1986), Fig. 18.

Furthermore, Carter et al. (1998) revealed a minor axis rotation of the famous NGC 3923 what suggests a prolate or triaxial potential, and challenges the requirement of an oblate potential by the WIM. They noted that it is difficult to induce minor axis rotation in an oblate potential without inducing any corresponding major axis rotation that has not been observed.

[4]The $R^{1/4}$ profile (the so-called de Vaucouleurs' law) stands for a luminosity profile corresponding to the function $const \times exp(-kR^{1/4})$, where k is another constant.

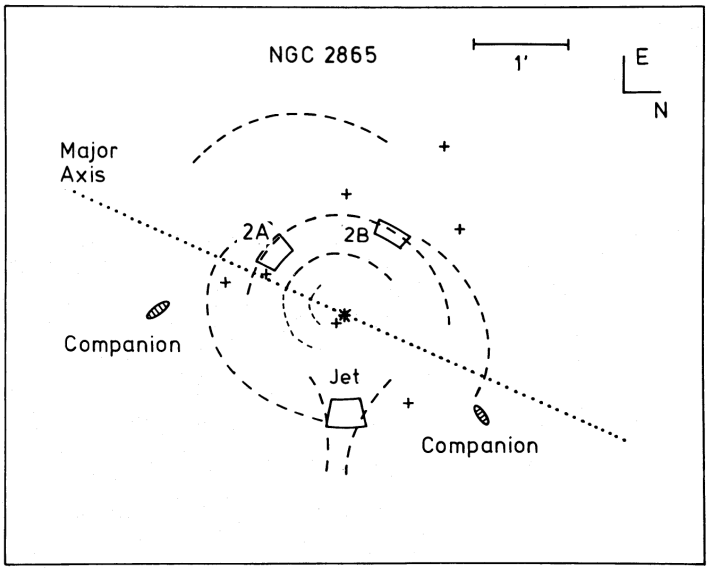

Figure 18: *Schematic diagram of the distribution of shells around NGC 2865. The shells are represented by the dashed lines; the lighter dashed lines represent very faint shells whose existence is uncertain, Fort et al. (1986).*

In Silva and Bothun (1998), a work with a poetic title "The Ages of Disturbed Field Elliptical Galaxies", one of the examined galaxies was the shell galaxy NGC 3610. The authors note that the spectacular morphological fine structure of this galaxy leads to the natural conclusion that this galaxy has undergone a recent merger event. This scenario is supported by the existence of a centrally concentrated intermediate-age stellar population which is a prediction of the dissipative gas infall models. Furthermore, the central stellar structure could have been formed by this infalling gas. It seems unlikely that the structures were formed by a nonmerging tidal interaction since there is no nearby galaxy.

It is interesting that nobody has ever noticed any general one-armed spiral in the outer shells of type II shell galaxies nor any bisymmetric spiral in inner regions. Only Wilkinson et al. (1987c) probed 66 shell galaxies and found that in roughly 20% of the systems these innermost shells have spiral morphology. But they did not specify which galaxies they were nor what spiral morphology has been found. Thomson (1991) explains: "The broken appearance of the shells is actually an interference pattern formed by the leading and trailing density waves induced during the encounter", and he adds that the faint residual one-armed leading spiral feature seen at the end of some of the simulations is probably an m = 1 kinematic density wave[5]. The relative importance

[5]Here a common method of decomposition of a 2D density or potential to Fourier modes in the azimuthal direction (that is, Fourier transforming in the angle separately for every radius) is used. The potential is decomposed as

$$\Phi(R,\theta) = \Phi_0(R) + \sum_{m=1}^{\infty} \Phi_m(R)\cos[m(\theta - \theta_{0m}(R))],$$

what means a sum of harmonics with different amplitudes and phase shifts for every R. The Φ_0 ($m = 0$) mode is the axisymmetric part of the potential, the $m = 1$ mode has an azimuthal period of 360°, the $m = 2$ mode has 180° and so on. It is most frequently used for spiral galaxies. The $m = 1$ mode corresponds to one spiral arm (θ_{01} is dependent on R) or a closed structure (an ellipse when $\theta_{01}$is a constant) not concentric with the galaxy. The $m = 2$ mode is the most common, being either a bar (constant θ_{02}) or two spiral arms. In the WIM case, the $m = 2$ mode (bi-symmetric spiral density wave) is important for the inner parts of the disk.

of this mode for the shell forming process is not fully understood, but it does play an important role in determining the shell morphology produced by the more massive encounters. An interference pattern is set up between this leading spiral arm and the trailing spiral arms which gives rise to the broken arc-like appearance of the shells seen soon after the encounter (approximately 2 Gyr after the beginning of the encounter).

Wilkinson et al. (2000) found many arguments for and against the WIM in their study of the shell galaxy 0422-476.

Longhetti et al. (1999) favour the WIM, since they derived that in shell galaxies, the age of the last star forming event ranges from 0.1 to several Gyr. If the last burst of stellar activity that affects the absorption line strength indices, correlates with the dynamical mechanism forming the shell features, these shells are long lasting phenomena. The WIM predicts such a long life for the shells (§5.2), whereas for the merger model (§6) Quinn (1984) guessed a shorter lifetime due to the initial dispersion of velocities that the stars of the shell inherited. But for example, Dupraz and Combes (1986) happily simulated their systems for 10 Gyr, as can be seen in Fig. 24 in §6.3.

A consequence of the WIM is that the stars which make up the shells must be in nearly circular orbits. That is almost opposite to the conclusions of the merger model (§6). It could be thus decided from measurements of shell velocity fields which model is favoured, but this is indeed a formidable task, as the shells contain at most a few per cent of the overall brightness of the host galaxy. Some attempts have been already carried out (Balcells and Sancisi, 1996), but as far as I know, the results are inconclusive.

5.7 Showdown

To conclude, the WIM has nice explanations for many phenomena related to the shells (§§5.3 and 5.4), for which the competing merger model (§6) seeks explanations with difficulties or has none at all. On the other side, the WIM suffers from some deficiencies and obscurities (§§5.1, 5.2, and 5.5), but primarily, it seems not to be confirmed by the observations (§5.6).

6 Merger Model

6.1 Introduction

The pioneering work of Toomre and Toomre (1972) demonstrated that many of the spectacular filamentary structures associated with peculiar galaxies (for example Arp 1966b) are probably the result of a close encounter between disclike systems. The restricted three-body analysis they employed was, however, not capable of following the encounter to its steady state conclusion in a self-consistent manner.

The idea of a connection between mergers and shells was first published by Schweizer (1980) in his study of the shell galaxy NGC 1316 (Fornax A). The presence of shells (or "ripples" as Schweizer calls them) deep within NGC 1316 and a surprising number of galaxies with ripples but no companions fosters his belief that Fornax A, too, has been shaken by a recent intruder rather than by any of the present neighbours. Schweizer imagined that the ripples represent a milder version of the strong response that occurs in the disc of a galaxy when an intruder of comparable mass free-falls through the centre: A circular density wave runs outward, followed sometimes by minor waves, and give the galaxy the appearance of a ring (Lynds and Toomre, 1976; Toomre, 1978), as e.g. in the "Cartwheel" galaxy (ESO 350-40, Fig. 19).

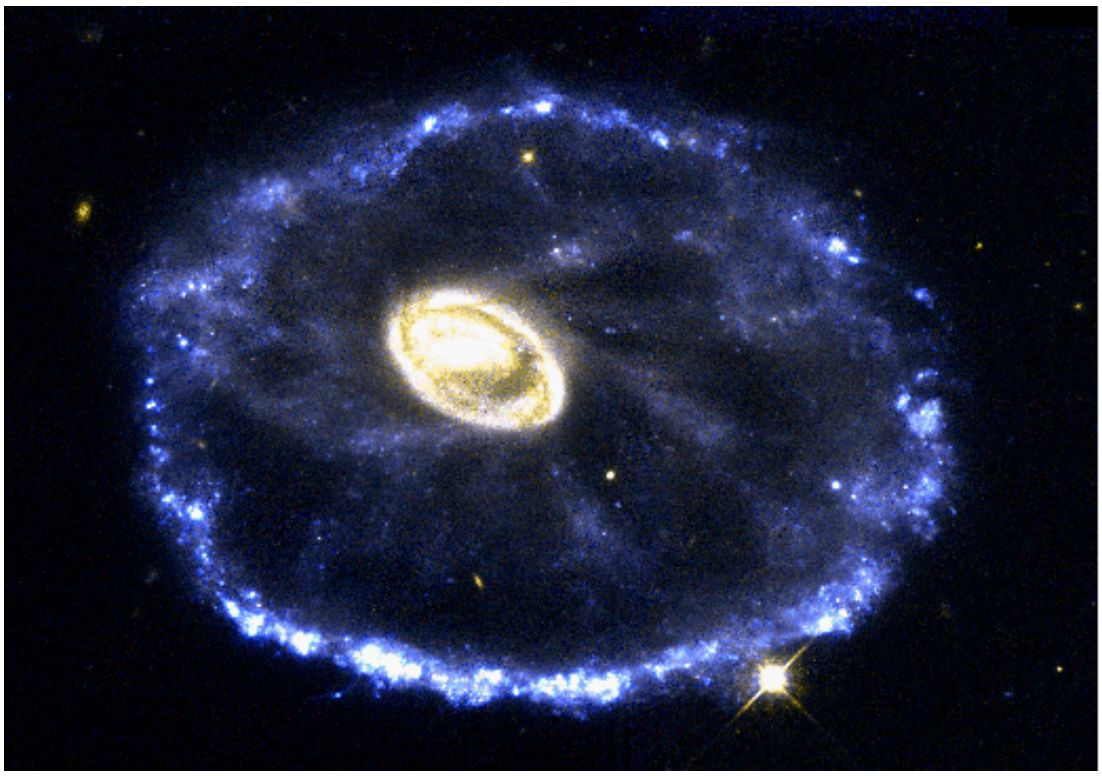

Figure 19: *The "Cartwheel" galaxy from HST.*

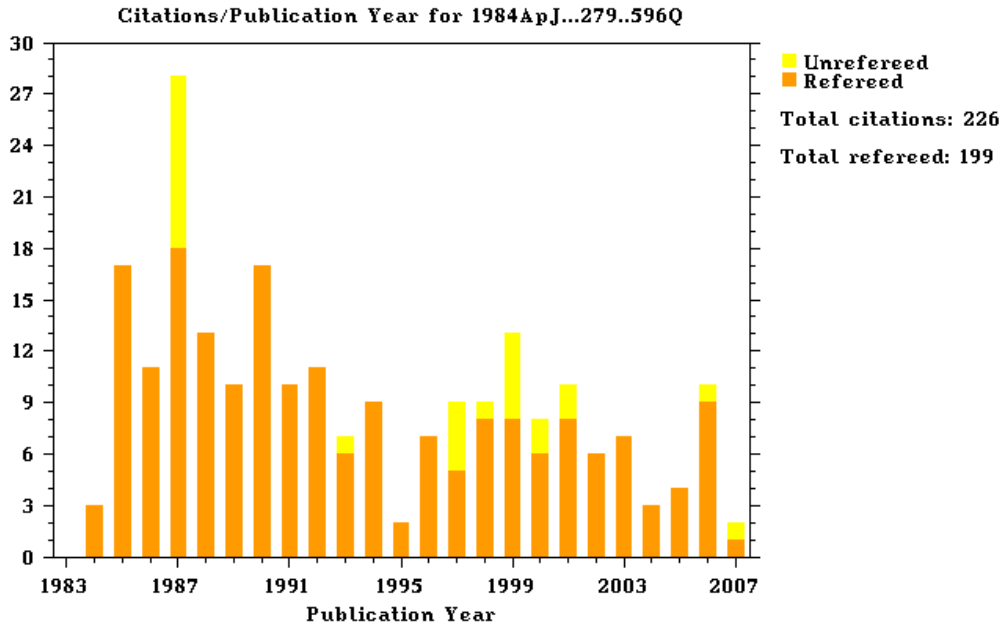

Figure 20: *Citations history for Quinn (1984) from the ADS (The Astrophysics Data System) Database.*

Quinn (1983, 1984) took up the idea of a merger origin of shells, but showed it in a slightly different spirit. The work rightly rose interest and its liveliness is proved also by its citations history in Fig. 20. Many other articles followed this direction: Dupraz and Combes (1986) examined shells in prolate and oblate systems, Hernquist and Quinn (1987b) tried to find out more about the galaxy's potential using shells, Hernquist and

Quinn (1987a) used shells to study the modified Newtonian dynamics, Dupraz and Combes (1987) thought about effects of dynamical friction on the radial distribution of a shell system, James and Wilkinson (1987) made their point on initial tidal effects of shell formation, Piran and Villumsen (1987) carried out an attempt of a self-consistent simulations of shell formation, Hernquist and Quinn (1988, 1989) explored parameters of such a collision, Heisler and White (1990) successfully self-consistently simulated the secondary galaxy. The dynamics of the gas during shell formation was studied by Hernquist and Weil (1992); Weil and Hernquist (1993a,b), Kojima and Noguchi (1997) and Combes and Charmandaris (1999, 2000); Charmandaris and Combes (2000).

6.2 Phase wrapping

In this paragraph I will briefly describe the idea of the merger origin of shells. The interested reader is however referred to Part III for a deeper understanding. It should be also noted that already Lynden-Bell (1967) described something like a pig-trough dynamics in violent relaxation in stellar systems.

When a small galaxy enters the scope of influence of a big elliptical galaxy on a radial or close to a radial trajectory, it splits up and its stars begin to oscillate in the potential of the big galaxy which itself remains unaffected. In their turning points, the stars have the slowest speed and thus tend to spend most of the time there, they pile up and produce arc-like structures in the luminosity profile of the host galaxy.

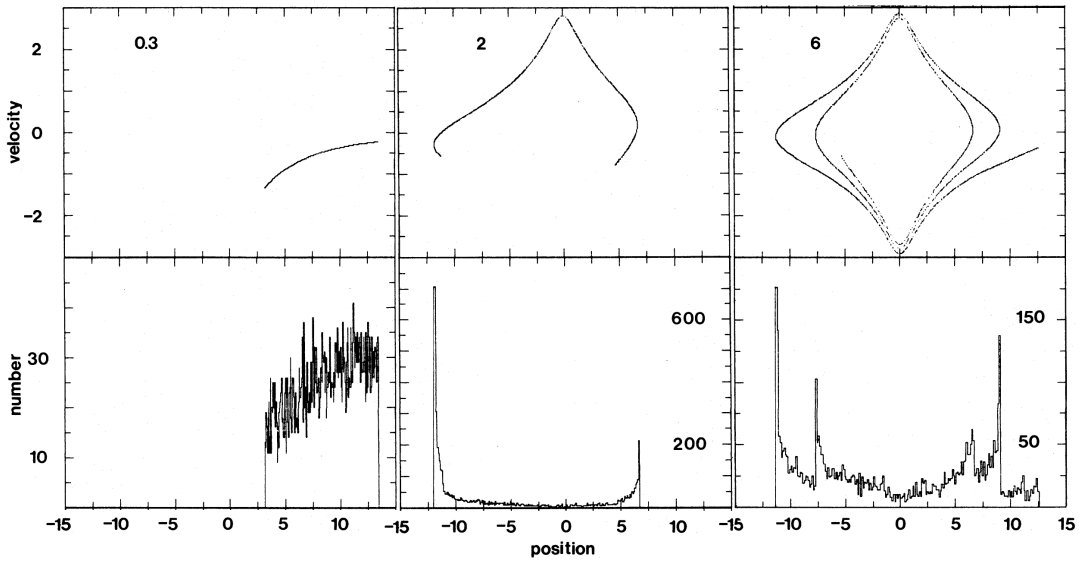

Figure 21: *Time evolution of 5,000 test particles falling from rest into an isochrone potential in phase space (upper row) and configuration space (lower row), Quinn (1984). The numbers in the top left of each phase plane plot shows the time passed in units of the radial period of the most tightly bound particle. The configuration space distribution of the particles at each time is shown directly below the corresponding phase plot. Positions are in units of the isochrone scale length, and velocities are in units of* $(GM/10a)^{1/2}$*, where M is the total mass and a the scale length.*

This mechanism can be illustrated in a simplified one-dimensional case (more in §10). In Fig. 21, we can see how the particles falling from rest oscillate in the isochrone potential[6]. The density maxima occur near the turnaround points of the particle or-

[6]The isochrone potential is a spherical potential that is often used a simple model potential for

bits. The maximal radial position of the orbit is first reached by the most tightly bound particles, but as more distant particles stop and turn around, the density wave propagates slowly in radius to the outermost turning point set by the least bound particle. Meanwhile, in Fig. 21 (first row) we can see the particles' behaviour in the phase space (velocity-position diagram). The particles in phase space form a characteristic structure, for which this mechanism of shell formation is often called "phase wrapping".

The reader who did not fully comprehend this description can read §10 first. The reader who did, can however read it and still improve his/her understanding.

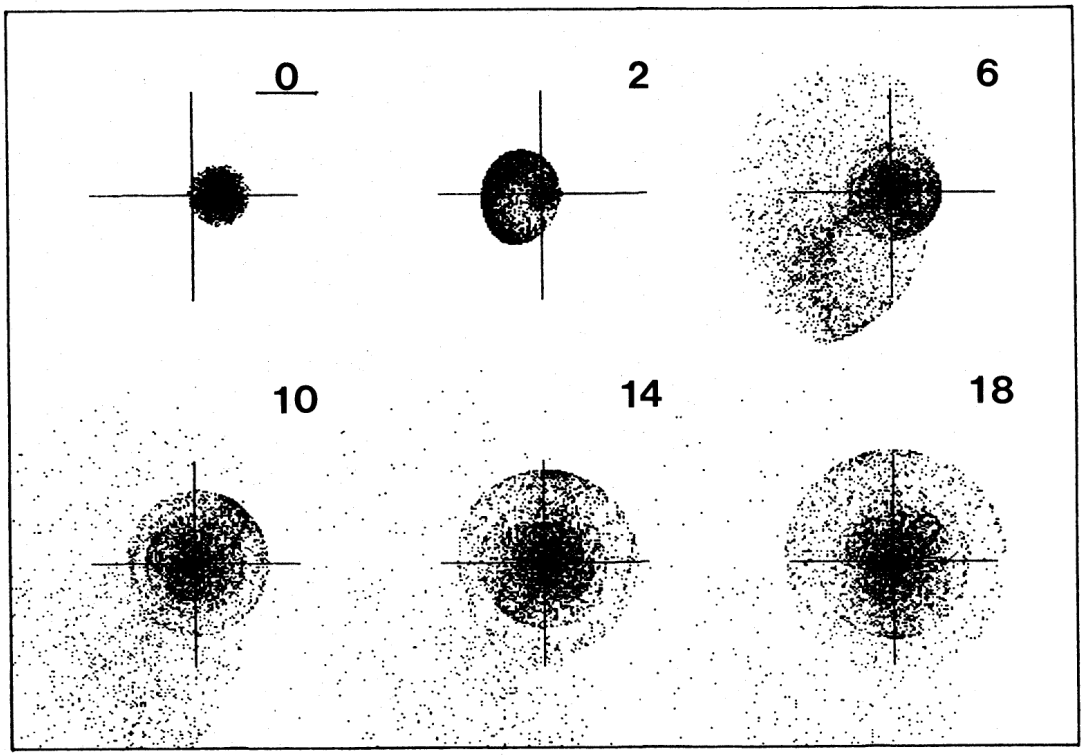

Figure 22: *Time evolution of the radial, planar encounter between an exponential surface density disk and a 100 times more massive fixed and rigid isochrone potential, Quinn (1984). The cross denotes the centre of the isochrone potential, and the disk is initially moving to the left. The evolution is viewed from above the orbit plane (X–Y plane), and the times indicated are in units of the circular period at a radius of one scale length in the isochrone potential. The bar under the initial time is 10 scale lengths long. The disk is rotating in a counterclockwise sense.*

A two-dimensional view of a 3D simulation of shell origin by Quinn (1984) is depicted in Fig. 22 and the corresponding phase diagram in Fig. 23. Quinn (1984) used 5000 test particles initially distributed according to a fictitious potential of the secondary galaxy with an exponential surface density. No random velocities are initially present in the disk. The disks are released from a point corresponding to the tidal radius (see §16) in the target field at a mass ratio of 10:1 which is 4.2 scale lengths. The disks are assumed to disrupt instantaneously and completely at the tidal point and to have no significant internal disturbance before reaching this point. The centre of mass of the disk is infalling along the X-axis at two-thirds of the escape velocity, and the disk is in the X-Y plane. The primary galaxy is represented by a fixed isochrone potential.

galaxies. Its dependence on the radial coordinate r can be written as $GM/(a+\sqrt{a^2+r^2})$, where a is the scale length, M is the total mass of the system and G is gravitational constant.

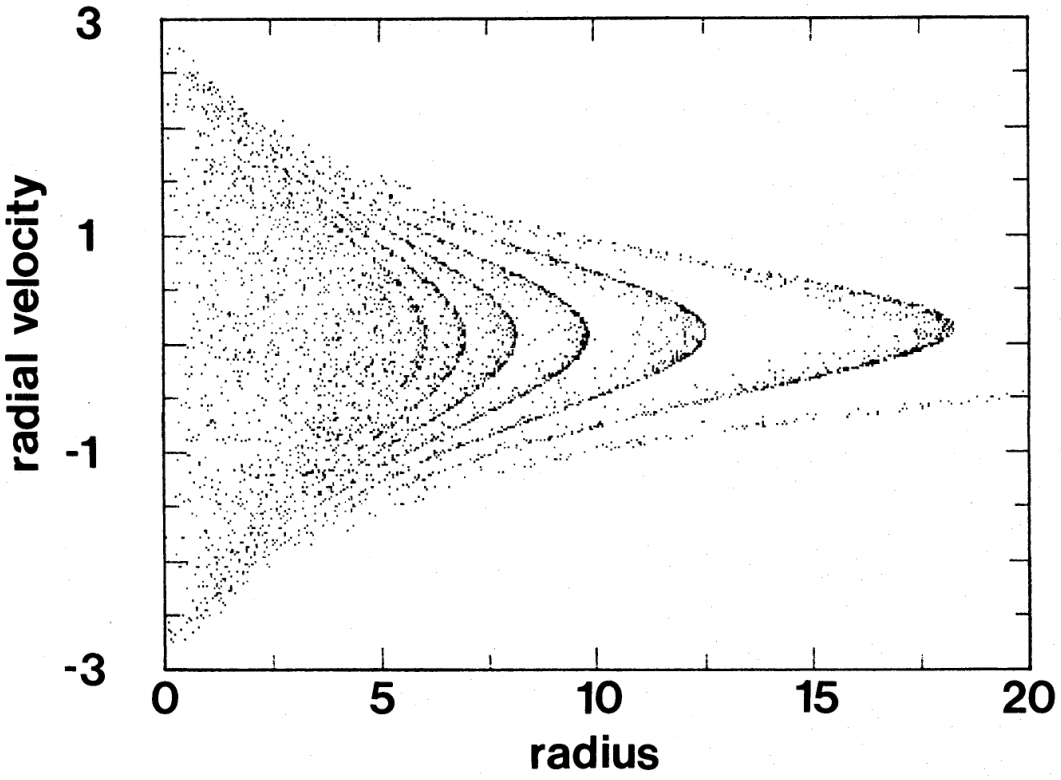

Figure 23: *The radial velocity-radius plane for particles in the model shown in Fig. 22 at time 18, Quinn (1984). Radii are in units of the isochrone scale length, and velocities are in units of* $(GM/10a)^{1/2}$.

Already beforehand, Quinn 1982 (cited in Quinn 1984) carried out more realistic encounters involving N = 1,000 self-gravitating N-body disks with velocity dispersion and freely moving rigid potentials and was also able to produce shell structures of the type described above.

The edges in density are technically the caustics of the mapping of the phase density of particles into physical space. As a natural consequence, the shells are **interleaved** in radius and their separation increases with radius (point 7 in §3). Furthermore, the range of the number of shells present around ellipticals is a simple consequence of the age of the event. More shells will imply that a longer time has passed since the merger event. A more detailed explanation can again be found in §10.

6.3 Ellipticity of host galaxy

Dupraz and Combes (1986) used the same strategy for their simulations as Quinn 1984 (fixed potential of primary, launching test particles of secondary from tidal point, see §6.2), this time with the number of particles tripled (15,000) and an ellipsoidal potential of the host galaxy. They tried to explain the observed characteristics of shell morphology (point 8 in §3) with the encounter of the secondary galaxy with a **prolate or oblate** primary galaxy.

Fig. 24 shows the result of such a merger of a disc galaxy and an E-galaxy. The secondary galaxy falls into the prolate galaxy around its symmetry axis and into the oblate galaxy perpendicularly to its symmetry axis (the symmetry axis is the major axis when the E-galaxy is prolate, minor axis when oblate). The disc of the secondary

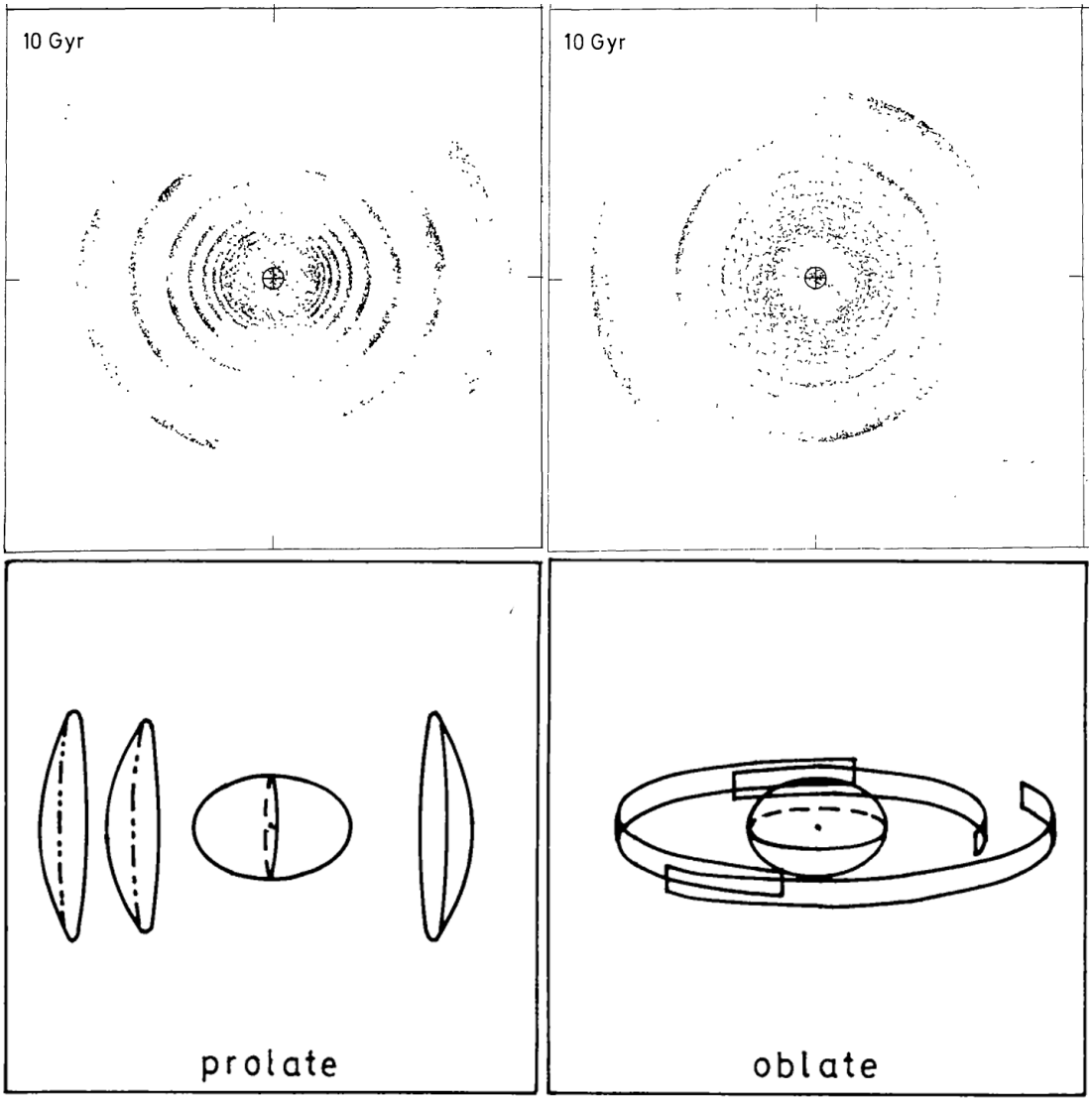

Figure 24: *Shell formation in prolate (left, viewed edge-on) and oblate (right, viewed face-on) galaxy. In the top row, the result of the simulation is shown, in the bottom a corresponding sketch of the situation, Dupraz and Combes (1986).*

galaxy is always oriented in the direction of the collision. In the prolate case, the companion stars achieve pendular motion along the major axis of the E-galaxy. The shells form consequently along this axis, alternatively on one side and the other (type I shell galaxy, see §2.4). On the contrary, in the oblate case, the shell system does not possess any symmetry, since there is no privileged major axis here. The shells appear randomly spread around the centre of the E-galaxy (type II shell galaxy).

Dupraz and Combes (1986) state that a shell system is found aligned with the major axis of an elliptical galaxy, only when the E-galaxy is prolate and the impact angle is likely to be lower than 60°. A shell system is found aligned with the minor axis of an E-galaxy, only when the latter is oblate and the impact angle is lower than ∼30°. It is interesting to note that no such system, with the shell aligned with the minor axis, is known.

However, all this results were **negated** by Hernquist and Quinn (1989), who also simulated an ellipsoidal potentials of the primary galaxy. Their result is that if the

potential well maintains the same shape at all radii as in the simulations of Dupraz and Combes, then the shape of the dark matter halo, as well as that of the central galaxy, is responsible for aligning and confining the shells. If, on the other hand, the potential is allowed to become spherical at large radii, the shell alignment and angular extent are less sensitive to the properties of the potential at small radii. This means that two primaries, one oblate and the other prolate, can have similar projected shapes and similar outer shells if the outer isopotentials in each case become spherical. Hence the shape of the potential at large as well as small radii needs to be considered when examining shell extent and alignment.

Even the same authors formerly tried to get some information about the potential of several chosen shell galaxies (Hernquist and Quinn, 1987b), but for those reasons and the reasons stated in §§6.4 and 6.5, they were left with nothing to say but: "The shell morphology is sensitive to the shape of the primary at large and small radii as well as to the detailed structure of the companion. This would imply that it is difficult, if not impossible, to infer the form of the primary from the shell geometry alone. In this conclusion, we disagree with Dupraz and Combes (1986)." This resulted in a fading interest for the shells, and after the great boom in the 1980's, a period of silence started.

6.4 Companion

The choice of the **type of the secondary** galaxy initially felt on a disc galaxy. The authors were probably led to it by two aspects. Firstly, dynamically cold systems promised to be better in shell formations, since they occupy smaller phase volume than comparably massive velocity dispersion supported galaxies. In such a process of non-colliding stars we can assume phase volume conservation according to Liouville's theorem. This means that a system with an initially small phase volume keeps this property and forms sharper shells. So, the visibility of the shell system is expected to be lower for an elliptical companion than for a spiral companion of the same mass, since the velocity dispersion is greater for the elliptical. Secondly, the observations seemed to suggest that the stars in shells have the colour indices of late-type galaxies (see §2.5). Later observations have shown that the shells are not that blue (see also §2.5), but yet before the simulation showed that the shell systems can be formed by a disc as well as an elliptical companion (Dupraz and Combes, 1986; Hernquist and Quinn, 1988).

Hernquist and Quinn (1988, 1989) themselves call their code "hybrid test particle/restricted three-body scheme". In their simulations, the gravitational influence of the secondary galaxy is modelled through a smooth potential. The secondary and the primary galaxy attract each other up to the moment when a defined tidal point is reached by companion at which the potential of the secondary is suddenly switched off. Along all this, 20,000 test particles of the secondary move.

In the first of the above-mentioned articles, Hernquist and Quinn (1988) examined among others the influence of the **phase volume** and **velocity dispersion** of spherical companion on shell formation. As was already mentioned above, higher dispersion means higher blur of resulting shells through the increase of the phase volume (velocity dispersion is proportional to the square root of mass of the accreted companion). Another effect brought in by higher dispersion is that the material can be captured into more tightly bound orbits, so shells are produced more rapidly, since the shell production rate is indirectly proportional to the shortest period of stellar oscillations (see §10.2, equation 9). This effect is clearly seen in Fig. 25, where phase diagrams for 4 different phase volume vs. velocity dispersion combinations are depicted. This means that for the same potential of the primary galaxy we can easily get different shell systems by changing some parameters of the accreted galaxy, what constituted one of

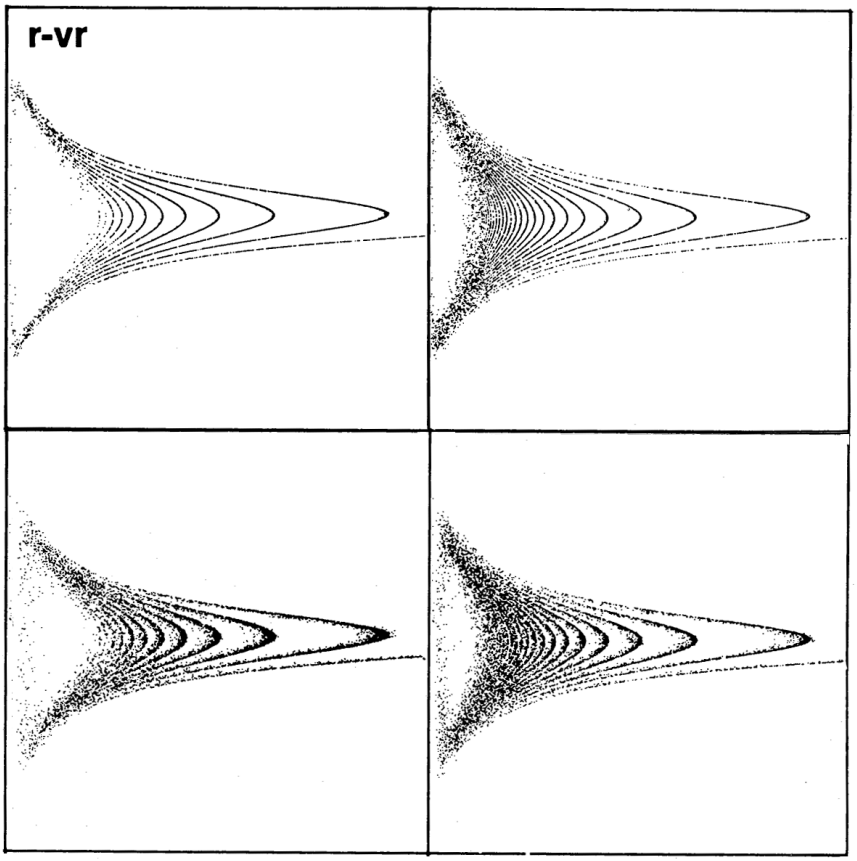

Figure 25: *Radial velocity versus radial position diagrams of 4 different shell systems at the same time, Hernquist and Quinn (1988). Systems in the same column have the same velocity dispersion, systems in the same row have the same phase volume. The first row has smaller phase volume, the left column has larger velocity dispersion. To keep the phase volume with increased velocity dispersion, the galaxy is made more spatially compact.*

several serious problems of the idea to explore the potential of host galaxy through its shell system (see §6.3).

The disc-like secondary galaxy has some extra options that the spherical one lacks. By accreting differently inclined discs we can get different peculiar structures. The resulting configuration of sharp-edged features is considerably more complex and disordered than for a spherical companion. For a very flat system, where is also the possibility of forming caustics through **spatial wrapping**. That is to say, as the sheet of particles moves and folds in three-dimensional space, sharp edges can be formed in its two-dimensional projection onto the plane of the sky. Projection effects become critical in this context, as evidenced by the different viewing angles, see Fig. 26. This effect was evident already in the simulations by Quinn (1984).

6.5 Radial distribution of shells

The radial distribution of shells was always probably the most watched aspect of the merger model. From §6.2 we already know how easily the merger model reproduces the interleaving in radii. The shell formation is closely connected to the period of radial oscillation in the host galaxy potential (see §10.2), what is in any case an increasing

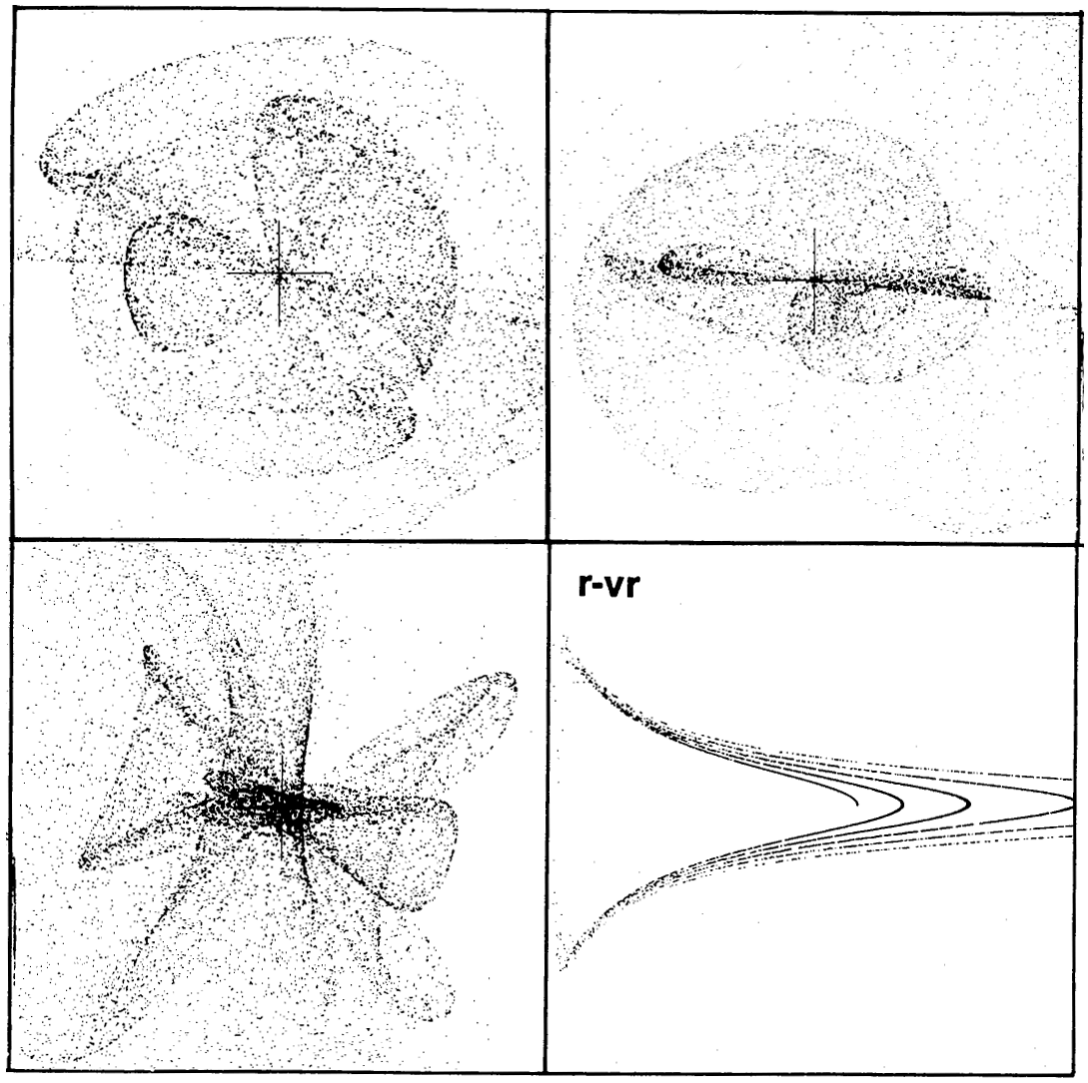

Figure 26: *Radial encounter of an inclined disk companion with a spherical Plummer primary (mass ratio 1:100). The inclination of the disk was 45° with respect to the direction of the encounter. Four frames show the three spatial projections and the phase space density (radial velocity vs. radius) at the same time, Hernquist and Quinn (1988).*

function of radius (see §9.3). The shells as density waves receding from the centre, composed in every moment of different stars, are the older the further from the centre they are. With time, the frequency of the shells increases, thus the distances between shells decrease towards the centre, what is also in agreement with observations (see §2.4). This mechanism is more thoroughly explained in §10.

The above-mentioned facts suggest a connection of shell distribution and the potential of the underlying galaxy. But already Quinn (1984) discovered that the radial distribution of shells derived from the potential inferred from the observed luminous matter distribution cannot agree with the observed reality.

Quinn (1984) derived that the potential of the shell galaxy NGC 3923 must be less centrally condensed at radii $1 < r/r_e < 4$ (where r_e is the half-mass radius) than the luminous matter observations predict. This discovery was reflected by Dupraz and Combes (1986); Hernquist and Quinn (1987b) as they added an extensive dark matter

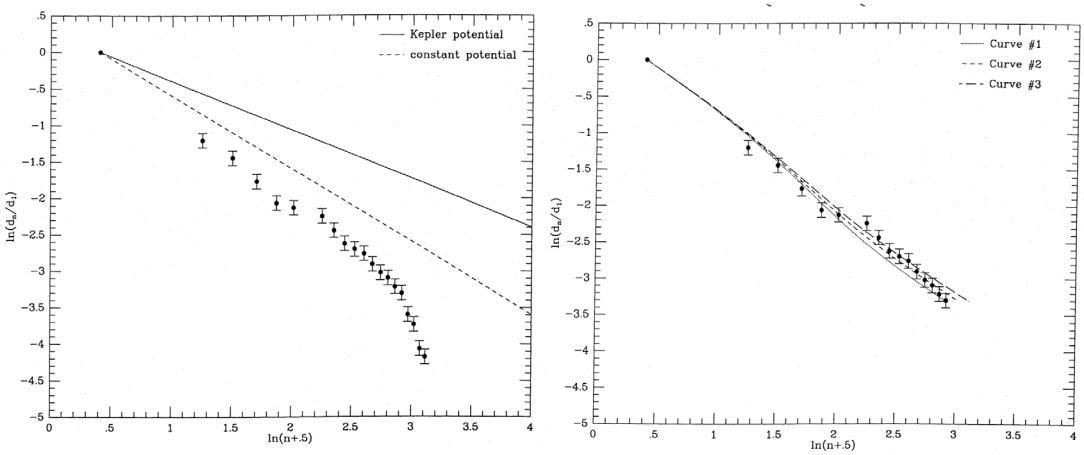

Figure 27: *Left: Observed shell distribution for NGC 3923, with error bars, and the expected shell distributions for a Kepler field (solid line) and a constant potential (dashed line). (The constant potential represents an approximation to the logarithmic behaviour expected for an isothermal halo.)*
Right: Representative shell distributions predicted for the sum of an $r^{1/4}$ law potential and a truncated, nonsingular isothermal halo, compared with the observations of NGC 3923. The ratio of the dark halo to luminous matter is 49:1, 38:1, and 31:1 in favour of the halo for lines 1, 2, and 3 respectively.
The shells are traditionally numbered from the outermost inwards, according to their suspected age, Hernquist and Quinn (1987b).

halo in their simulations and then they were able to better reproduce the observed **shape of the shell distribution**, as it can be seen in Fig. 27. But immediately after that, Dupraz and Combes (1987) synthesised successfully a similar radial distribution taking into account the dynamical friction (see Part IV) instead of dark matter. Moreover, in spite of the simplicity of their model, they synthesised a wide variety of shapes for the shell distribution by varying only the two parameters: mass ratio of primary and secondary and impact parameter. It all lead to the conclusion that the shell system is not suitable to study the host galaxy's potential.

The cornerstone of the merger theory is also the huge **range of radii** in which the shells occur. A simple merger simulation, as of Quinn 1984 (see §6.2), is not able to produce shells simultaneously on large and small radii. The presence of shells deep within the host galaxy (and thus the presence of deeply bound stars that once were part of the secondary galaxy) was mysterious from the very beginning. But because at that time the merger model had no direct competition, it was felt more as a challenge than a flaw. However, the advent of the WIM (§5) that does not have any problems explaining this phenomenon, challenges the merger model more seriously.

Quinn (1984) suggested three possible explanations: First, the infall velocity of the disk may have been small and hence the disk was initially strongly bound to the elliptical. Second, the mass ratio may have been closer to unity, and hence energy could have been transferred from orbital motion to internal velocity dispersion. But as the most probable explanation he promoted the idea that the disruption process is a gradual one and that the centre-of-mass motion of the disk is subject to dynamical friction.

Another effect that no one predicted was found by Heisler and White (1990). They self-consistently simulated the secondary galaxy by 5,000 particles and left the primary

as a rigid potential. During the disruption event there is a substantial transfer of energy between the various parts of the satellite. Stars which lead the main body through the encounter are braked and later form the inner shell system. Stars which lag the main body are accelerated and turn into an escaping tail, see Fig. 28. This transfer is asymmetric and, for the encounters they have studied, the surviving core suffers a net **loss of orbital energy** which can shrink the apocentre of its orbit by a large factor. All these transfer effects increase with the mass of the satellite.

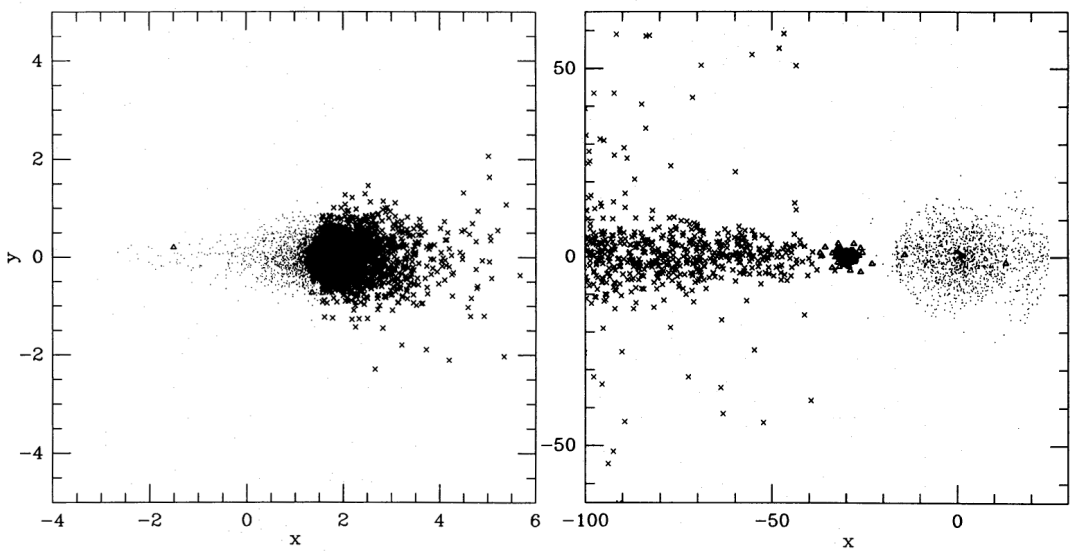

Figure 28: *Projection on to the x-y plane for the fiducial encounter, using the self-consistent method, Heisler and White (1990). Particles that (will) make up the surviving bound satellite core are represented by a triangle, those that are (will be) closely bound to the giant are represented by a dot and those that are (will be) on less bound or escape orbits are plotted with a cross. The situation is shown in the time equals 390 (left) and 800 (right) of their time units.*

In the case of Heisler and White, the satellite is dropped from 50 distance units (corresponding perhaps to about 100 kpc) and reaches the apocentre in the distance of 38 space units. If the secondary galaxy were not to be modelled self-consistently, it could not stop sooner than again at the distance of 50. It should be emphasised that this energy transfer happens only within the original secondary galaxy and no dynamical friction from the stars of the primary galaxy is accounted for in this case.

This scenario also allows the shell formation in a larger spread of radii. In another passage and disruption of the companion, a new set of more tightly bound shells is created. Further, the combination of the loss of orbital energy in this way and the dynamical friction could bring new results, if properly modelled. Unfortunately, no self-consistent simulation allowing this has been done to date.

The idea that shells are useless as a direct probe to the potential of the underlying galaxy is considered generally valid, but Merrifield and Kuijken (1998) proposed an **alternative method** for using shells to constrain the form of the gravitational potential in the case of validity of the Quinn (1984) model (described in §6.2). Their method only uses the fact that phase wrapping is an efficient mechanism for concentrating stars of very nearly equal energies. The stars in the shell are close to their turning point and thus their kinetic energy is close to zero. The velocity they have on radii inside the

shell indicates their kinetic energy that is equal to the difference of the potential there and in the position of the shell.

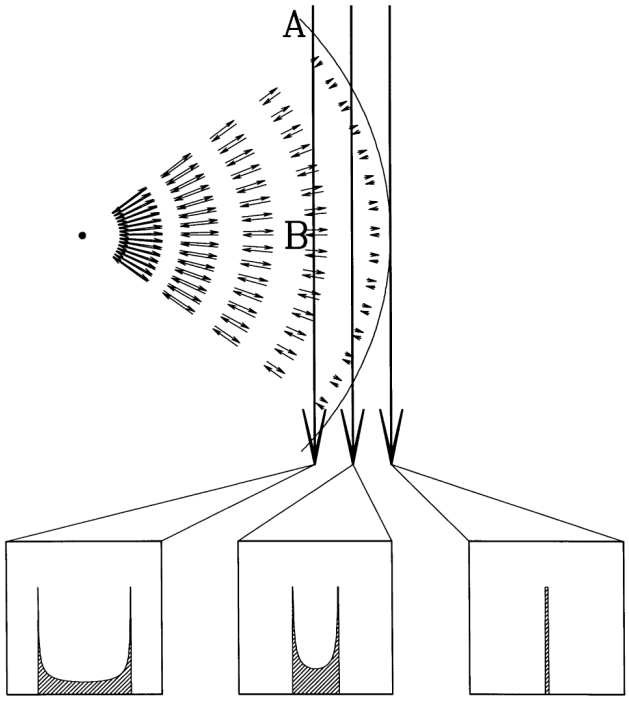

Figure 29: *Schematic diagram showing the velocities of stars in a spherical shell system. The top part of the diagram shows a monoenergetic system of stars moving on radial orbits, and the inset figures show the distributions of the line-of-sight velocities of these stars down three lines of sight, Merrifield and Kuijken (1998).*

Merrifield and Kuijken explain the principle of the measurement with the help of a simple case of one spherical shell: Clearly, the line-of-sight velocity of a star depends on its location with respect to the shell edge. Near the outer edge of the shell (point A in Fig. 29), stars are close to turning around in their orbits, and so their velocities will lie near the systemic velocity of the host galaxy. Similarly, stars near the tangent point (point B) move mostly transverse to the line-of-sight velocities, also resulting in near-systematic observed velocities. At intermediate positions, stars do have finite line-of-sight velocities, however; moreover, on lines of sight further in from the shell edge, orbital speeds are larger, resulting in larger line-of-sight velocities. The resulting distributions of velocity are sketched schematically in the lower panels of Fig. 29.

In practice the situation is far more complex and the shells themselves are faint structures in a bright galaxy, so the fulfilment of this program seems almost impossible. However, the authors state that they have carried out signal-to-noise ratio calculations for some of the brighter shell galaxies such as NGC 3923, and have ascertained that data of the requisite quality could be obtained with a couple of nights' integration using a 4-m telescope. As far as I know, no one has even attempted something like this, but with the technological progress the observation capabilities are gradually increasing.

6.6 Radiality of the merger

The assumption of a radial merger is the most awkward and criticised point of Quinn's model of shell formation. In his work, Quinn (1984) has shown that if the centre-of-mass

motion of the infalling disk is predominantly nonradial, the merger produces confused, often overlapping shells which appear enclosing. This does not correspond to what we see in real shell galaxies.

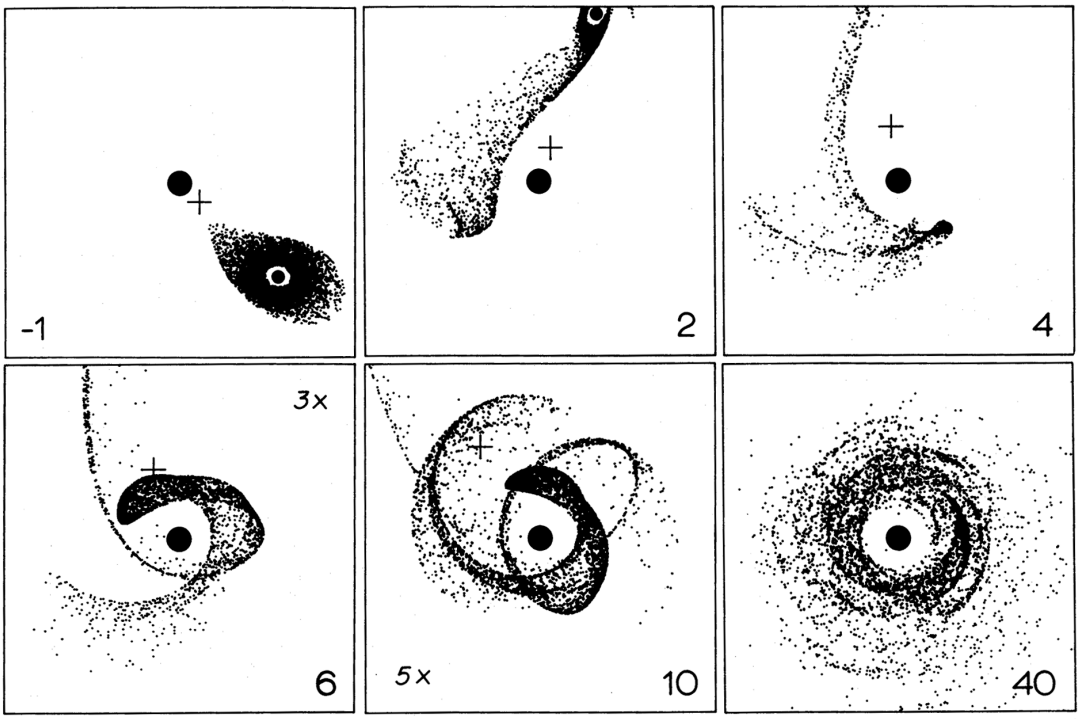

Figure 30: *Nonradial, prograde encounter (contributed by A. Toomre, taken from Hernquist and Quinn 1988) between an uninclined (in respect to the plane of encounter) disk companion and a spherical Plummer primary (mass ratio 1:40). Time t = 0 corresponds to closest approach. The cross locates the centre of mass. To enhance contrast, three times the initial number of random particles was plotted in frame t = 6, and 5 times in t = 10.*

On the other hand, A. Toomre modelled an off-axis release of a nonrotating, inclined disk into a fixed spherical force field (shown in Schweizer 1983) and his results resemble the observed shapes, see Fig. 30. The model was similar to that of Quinn in that the disk was released as a set of test particles with identical subparabolic velocities. The shells are created via the **mass transfer** from the secondary galaxy flying by on a parabolic trajectory to the right from the centre of the primary galaxy which is in the centre of the frames in Fig. 30. A big portion of the companion ends off paper, probably to other diploma theses. The captured part forms a complex structure around the primary galaxy.

In this case, a complete merger is not necessary to produce the shells, so this does not actually fit in the "Merger model" chapter, but it is logically connected, so we leave it here. Hernquist and Quinn (1988) present examples of objects from the Arp atlas (Arp, 1966a) that may well have resulted from such nonmerging encounters. Galaxies in Fig. 31 – Arp 92 (NGC 7603), 103, 104 (NGC 5216 + NGC 5218), and 171 (NGC 5718 + IC 1042) all show evidence of interactions as well as diffuse shell-like features surrounding the more luminous galaxy. Hernquist and Quinn (1988) also note that, as in the strictly planar case (Fig. 30), the term " shell " can occasionally be a misnomer since the stars near the vicinity of a sharp edge are not necessarily distributed on a three-dimensional surface in space.

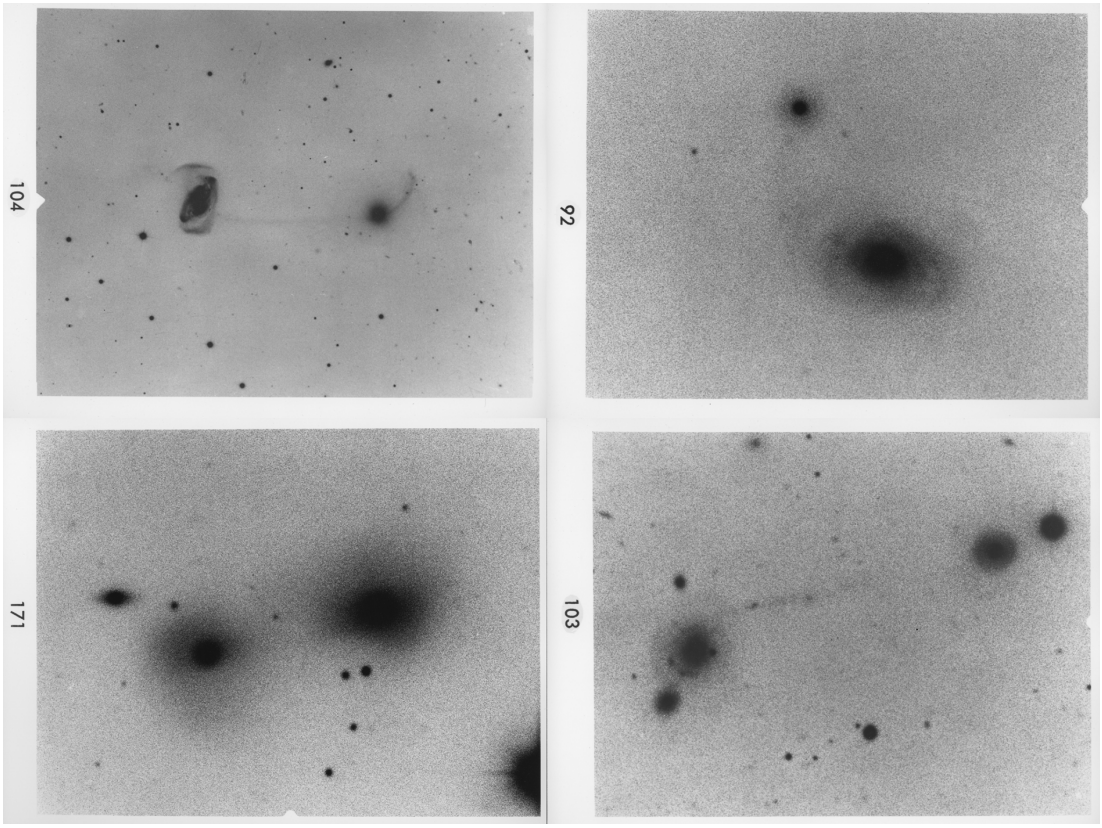

Figure 31: *Possible shell galaxies produced by mass transfer, Arp (1966a).*

However, the requirement of a fairly radial encounter stays valid to produce type I shell galaxies (see §2.4) as NGC 3923 or NGC 7600 that we have already seen in Figs. 1 and 8, respectively.

Dupraz and Combes (1987) considered that the shell distribution from the parabolic encounter with friction remains unchanged for a (small but) significant range of **impact parameters.** The more massive the secondary galaxy is (compared with the primary), the larger range is allowed. González-García and van Albada (2005a,b) carried out N-body simulations of encounters between spherical galaxies with and without a dark halo with $\sim 10^4$ particles. Shells are rather a byproduct of their work, but they were able to get them even for impact parameters enclosing 95% of the total mass of the primary. Even earlier, Barnes (1989) examined the evolution of a compact group of six disk galaxies in a self-consistent simulation of 65,536 particles. The result was a giant elliptical galaxy containing the shells. The shells were created during the final infall of the last galaxy into the merged body of all other galaxies. The initial distribution of the disc galaxies and their inclinations were by no means special, and Barnes did not specifically try to get the shells. This simulation may mean that during the evolution of a compact group, the shell galaxies are indeed formed in the final stage of the merger. Furthermore, it is supported by the observed high occurrence of shells in isolated giant galaxies (see §2.3).

6.7 Major mergers

Hernquist and Spergel (1992) published results of their simulation of a major merger which creates shells, see Fig. 32. Two identical galaxies with self-gravitating disks and halos (total number of particles was 163,840) merged following a close collision from a

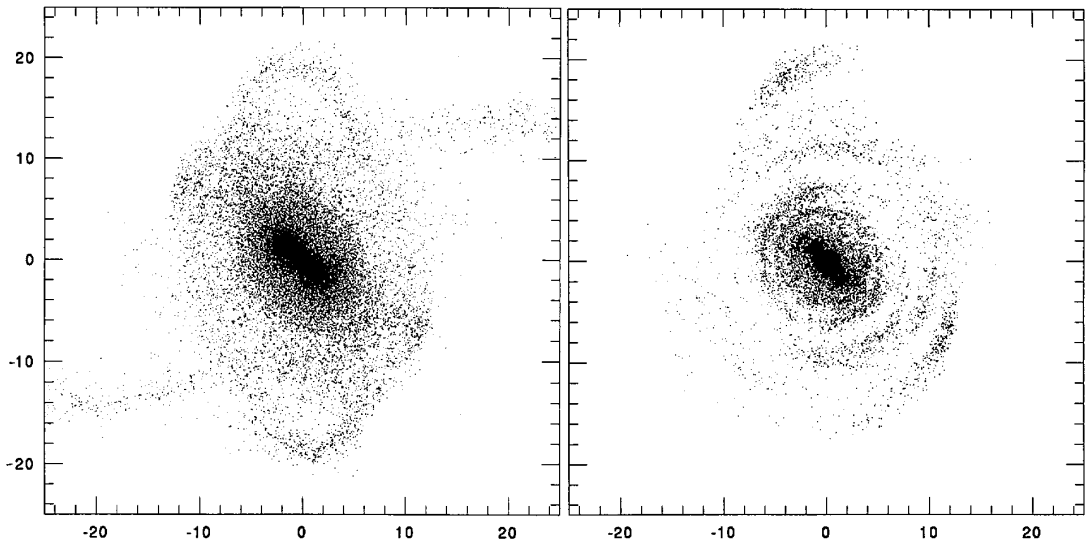

Figure 32: *Left: A luminous remnant of a merger between two equal-mass disk-halo galaxies. Right: Subsets of particles from one progenitor disk having relatively small radial velocity. Each panel measures 25 length units per edge where unit length corresponds to the exponential scale length of each progenitor disk. Scaled to the Milky Way, each edge measures roughly 75 kpc, Hernquist and Spergel (1992).*

parabolic orbit. The plane of each disk initially coincides with the orbital plane and the pericentre separation for the ideal parabolic orbit is 2.5 scale length. When plotted in phase space, the remnant in Fig. 32 (right panel) exhibits more than 10 clearly defined phase-wraps which can be identified with shells. Shells also occur near the nucleus and appear to be aligned with the major axis of the resulting galaxies.

González-García and Balcells (2005) examined the creation of elliptical galaxies from mergers of discs with $\sim 10^4$ particles. They used disc-bulge-halo or bulge-less, disc-halo models with mass ratios of the participants of 1:1, 1:2, and 1:3 and various impact parameters. As a result of those mergers, shells which could be identified in phase space occurred sometimes. They found out that models without bulges with the mass ratio of 1:2 or 1:3 lead to more prominent shells. But these were always shell systems of type II (all-round) or type III (irregular), see §2.4. González-García and Balcells note the lack of shells in remnants of equal-mass mergers and on all prograde mergers. This contrasts with the shell system presented by Hernquist and Spergel (1992), a prograde merger of two equal-mass, bulge-less discs. The perfect alignment of the disc spins with the orbital angular momentum may have favoured the formation of shells in their model.

González-García and van Albada (2005a,b) have also carried out simulations of encounters between spherical galaxies (see §6.6): In their first paper without a dark halo and in the second one with a dark halo (with mass ratios of 1:1, 1:2, and 1:4). The sharpness of the occurring shells was higher in models with a halo. A head-on collision for a run with mass a ratio 4:1 showed the shells even after 5 Gyr from the first encounter of the galaxy centres. But the shells showed up also in the merger with 1:2 mass ratio and a nonzero impact parameter. In any case, the shells are formed from particles of the less massive galaxy through the same phase wrapping that was established by Quinn (1984) as can be seen in Fig. 33.

To summarise, shells can be formed via a merger even in the cases when the mass ratios are not as dramatic as it has been simulated in the 80s (the big mass of the

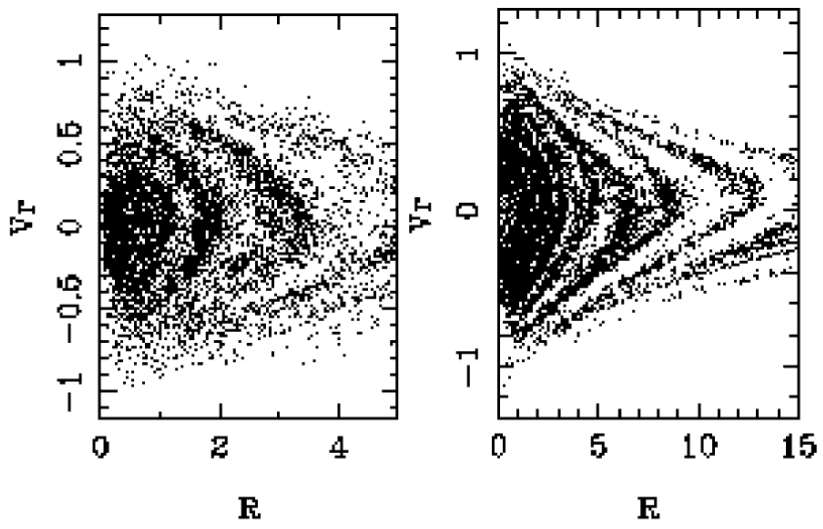

Figure 33: *Phase-space diagrams of the simulations of the remnant after the merger of spherical galaxies with a dark halo, González-García and van Albada (2005b). Left: mass ratio 1:2 and impact parameter equal to half mass radius of luminous component of the bigger system. Right: mass ratio 1:4, head-on collision (impact parameter equal zero).*

secondary galaxy could influence the alignment of shells with the major axis of the host galaxy, but no one has so far explored it). It is probably not common to have shells when two disc galaxies of comparable masses merge. Hernquist and Spergel (1992) got shells in their model maybe only thanks to the very special conditions of the collision they have chosen. Furthermore, the interleaving structure and more generally the distribution of shells is not known for such cases. Also, Fig. 32 (right panel) shows a peculiar display of only the particles with a radial velocity close to zero which obviously cannot be directly obtained from observations.

Some authors have guessed a major-merger origin for the shell galaxies in their observational studies (Schiminovich et al., 1995; Balcells et al., 2001; Goudfrooij et al., 2001; Serra et al., 2006).

6.8 Pros and cons

Merger models can well explain the interleaving of shells and their increasing separation with radius (point 7 in §3) and the number of shells increases with time. The observed brightness of shells puts a lower limit to the mass of the original secondary galaxy that is usually several per cent of the primary (point 4 in §3). The question of an alignment of shells with the major axis of the host galaxy and the correlation between the type of the shell galaxy and ellipticity (point 8 in §3) remains unsettled for the merger model. The merger model has also problems explaining the large range of radii where the shells are found and their occurrence at low radii (point 9 and 10 in §3). Mergers of different secondary galaxies can explain different colours of shells and their possible difference from the colour of the underlying galaxy (point 12 in §3).

A merger origin of shell systems is supported by many observations, a list of which would be lengthy, so we merely state that it is a majority of works listed at the end of §2.1. It seems that all the shell galaxies that have been so far examined in detail contain dust close to the nucleus (point 14 in §3). These dust features are often found to be out of dynamical equilibrium (see §2.6), what clearly points to their external

origin. Shell galaxies contain even more characteristics believed to be the results of a merger, including tidal tails, multiple nuclei or nuclear post-starburst spectra.

When double nuclei are concerned, according to Forbes et al. (1994) it seems, that fewer than 20% of shell galaxies do contain a second nucleus (see §2.8) – a characteristic that one would expect in a galaxy after a merger event. The authors calculate that this could be an expected frequency due to the short lifetime of the nucleus of the secondary galaxy as opposed to the long-living shells. They note that it is also the expected frequency for the WIM origin of shell galaxies – the galaxies with the double nuclei would be those we see at the moment when the secondary galaxy just passes through the primary.

A large support for merger theories comes from the kinematically distinct cores (KDCs). Even before it was recognized that all known galaxies with KDCs are shell galaxies, (point 20 in §3, see also §2.8), the origin of KDCs from mergers of galaxies has been independently anticipated. Already Kormendy 1984 proposed this mechanism for the formation of counterrotating cores in elliptical galaxies and Balcells and Quinn (1990) investigated this using self-consistent numerical simulations of mergers between elliptical galaxies of unequal mass, and found that the core kinematics in the remnant depend mostly upon the orbital angular momentum at a late stage of the merger, whereas the kinematics of the outer regions is largely the original kinematics of the primary. Thus, in retrograde encounters a counter-rotating core can form. Hernquist and Barnes 1991 (cited in Turnbull et al. 1999) demonstrated the formation of a counterrotating central gas disk in a merger of two gas-rich disk galaxies of equal mass. But this model is less widely accepted than the previous one. Hau and Thomson (1994) suggested a model that would comply with the WIM, but it is probably even less popular.

Enormous diversity of central surface brightness (point 21 in §3) and other characteristic show that shell galaxies are otherwise not a compact or privileged group of galaxies – so to say, the secondary cannot choose on what it falls. Still some selection effect seems to be there, because shell galaxies are much more often seen in regions with low galactic density (point 2 in §3). That can be explained with velocities in galaxy clusters being too high for one galaxy to be captured by another, or the influence of the surrounding galaxies breaks the shells structure or even prevents it from forming; or both.

As the observations show, shells in galaxies are fairly common (point 1 in §3, see also §2.3). It means that in fact they occur even more frequently because from the three-dimensional shape of the shells as introduced by Quinn 1984 (§6.2), we can easily understand that we see shells only when looking from angles close to the plane perpendicular to the line of the collision. But it is not that improbable as the shells in mergers are formed in a much larger range of impact parameters than it was originally believed (see §§6.6 and 6.7) and interactions between galaxies are quite a common matter.

7 Conclusions of Part II

It is possible that different mechanisms work together to form the shell galaxies we observe today. It cannot be even excluded that more than one mechanism was present in one particular galaxy. But according to all the knowledge summarised in this part, it is the interactions between galaxies that have the fundamental influence on the mechanisms forming the shell galaxies.

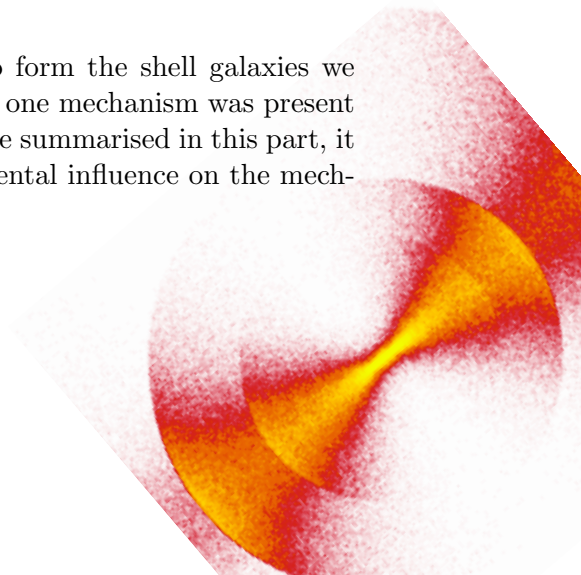

Part III
Our model

In the whole Part III and the following we assume the merger origin of the shells. An overview of the units used here and their conversion to some more traditional systems of units can be found in Appendix A.

8 Motivation

One of the great open questions in the galactic astronomy is why do the active galactic nuclei[7] (AGN) exist in some galaxies. The extremely bright of them, usually distant, are quasars (quasi-stellar objects, QSO). The AGNs are generally believed to be a result of accretion onto a supermassive black hole at the centre of the host galaxy. No other mechanism is known that would be able to produce so much energy in such a little area, which the AGNs occupy. But why does a galaxy boast an AGN and another one, which looks otherwise the same, does not? Probably the most discussed triggering mechanism is a merger event.

Dunlop et al. (2003) thoroughly studied 33 galaxies containing an AGN (13 radio-quiet quasars, 10 radio-loud quasars and 10 radio galaxies) and, among other things, they found out that the quasar host galaxies are not a recent outcome of violent mergers. But Canalizo et al. (2007) presented very deep images of five of these seemingly undisturbed galaxies. Four of them contain obvious signs of galactic interaction. One of them is the host galaxy of the QSO MC2 1635+119, which was discovered to contain shells. This in fact gave rise to this thesis. In order to say anything about the connection between the merger that created the shell system of of this galaxy and its quasar, we have to better understand the mechanism of the shell formation, what is the topic this thesis aims to contribute to.

We had the opportunity to see the host galaxy already if Figs. 4 and 6, but given its importance to this work, we present another portrait of it, see Fig. 34. As a brand new study by Canalizo et al. (2007) shows, the galaxy hosting MC2 1635+119 has five interleaved shells (2 on one side and 3 on the other) between the radii 6.6 and 12.5 kpc (labelled a to e). The shells are centred on the galaxy, closely aligned with its major axis and shape roughly a biconical structure. Apart from this polished shell system the galaxy contains other arc-like features extending as far as ∼65 kpc.

9 Plummer sphere

9.1 Potential and density

All the simulations in this part are for the sake of simplicity carried out for spherical galaxies, i.e. elliptical galaxies with zero ellipticity. The gravitational potential of each of the galaxies is modelled with the Plummer profile with varying parameters in different simulations :

$$\Phi(r) = -\frac{G\,M}{\sqrt{r^2+\varepsilon^2}}, \tag{1}$$

[7] An AGN is a compact region at the centre of a galaxy which has a much higher than normal luminosity over some or all of the electromagnetic spectrum.

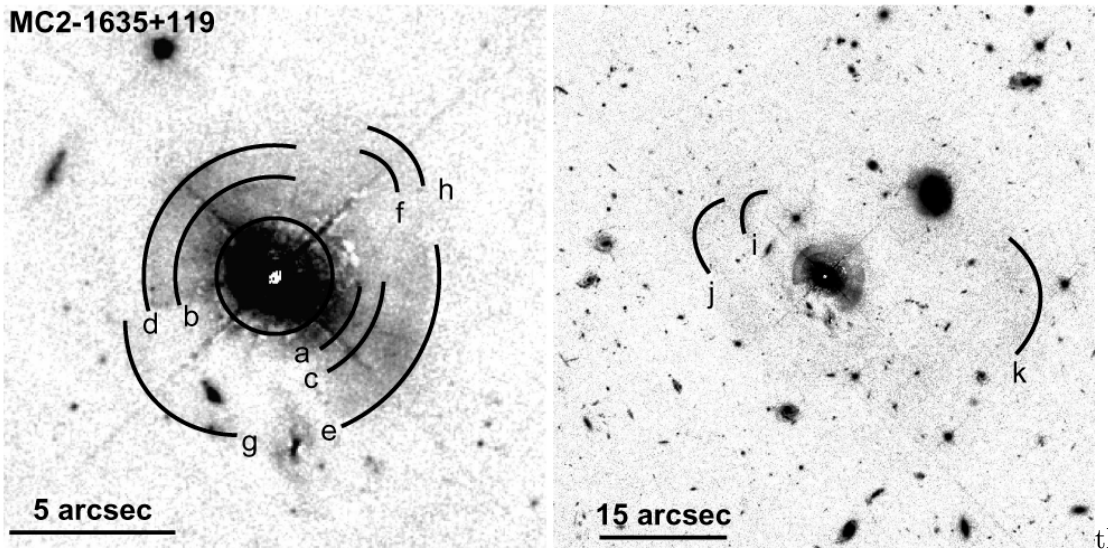

the same time

Figure 34: *Model subtracted HST/ACS images of the host galaxy of the quasar MC2 1635+119, where the most prominent fine-structure features are labelled, Canalizo et al. (2007).*

where G is the gravitational constant, M is the overall mass of the galaxy, r is the distance from the centre of the galaxy and ε is the Plummer radius, a scale parameter that determines the compactness of the galaxy. The lower the ε, the more compact the galaxy is. For $\varepsilon = 0$ the Eq. 1 represents a simple potential of a point mass.

While the Plummer model follows the profile of the real spherical galaxies only approximately (see a little more details in §9.3), we use it here – as was the case of numerous other studies of shell galaxies – because of its simple expressions of dynamical quantities. It was first used by Plummer (1911) to fit the observations of globular clusters and now is often used as a stellar distribution model in simulations.

From the Poisson equation $\triangle\Phi = 4\pi G\rho$, we can easily infer the radial density distribution ρ that acts as the source for the Plummer potential:

$$\rho(r) = \rho_0 \frac{1}{(1 + r^2/\varepsilon^2)^{5/2}}, \tag{2}$$

where $\rho_0 = 3M/(4\pi\varepsilon^3)$ is the central density. About $\sqrt{2}/4$ (approx. 35%) of the total mass of the galaxy is enclosed inside the $r = \varepsilon$ radius.

Fig. 35 shows the radial dependence of the Plummer potential (up to 100 kpc where the shells can still appear) and the corresponding mass density (for central 10 kpc) for various combinations of ε and M. The magenta and blue lines correspond to the same mass, but the blue one has four times larger ε (thus four times lower absolute value of the potential in the centre for the same M); whereas the magenta and red lines have the same ε, but the red one has half the mass than the magenta one (resulting in half the density for the same ε). The blue curve has 64 times lower central density, than the magenta one.

9.2 Velocity dispersion

In Part IV, we will need to know the velocity dispersion in the Plummer potential, so let's derive it briefly now. Applying the Jeans equations (see Binney and Tremaine

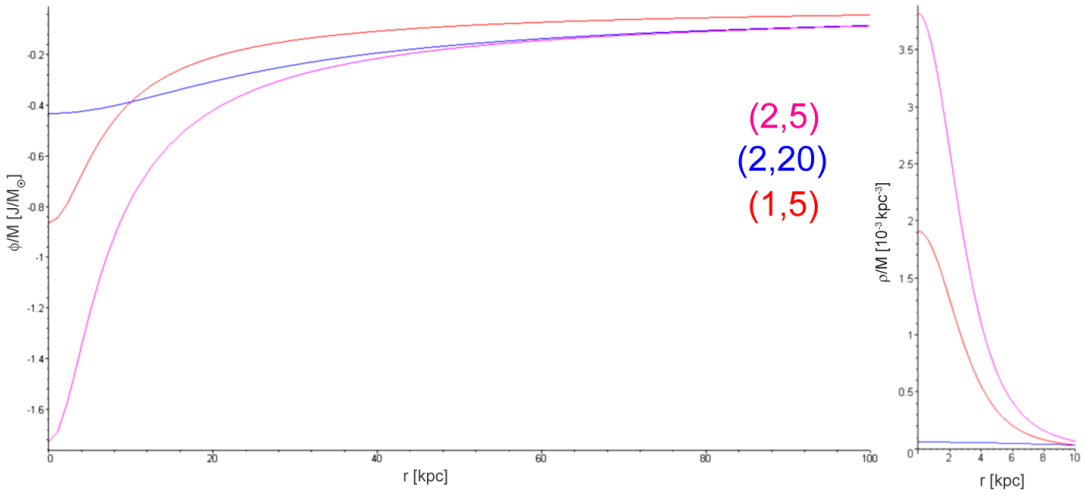

Figure 35: *The radial dependence of the potential and the density for the Plummer sphere. Both quantities are proportional to the mass, thus for an ordinary elliptical galaxy of 10^{11} $M_\odot$ mass, the y-axis gives the potential in Joules when multiplied by 10^{11}. By the same way, after a multiplication by 10^8 the other y-axis would show the density in $M_\odot/kpc^3$. Numbers in parentheses correspond to the parameters of curves with the same colour – the total mass in multiples of the solar mass (e.g. 10^{11} $M_\odot$) and the Plummer radius ε in kpc, respectively.*

1987, Ch. 4.2) to our spherically symmetric galaxy without any systematical movement, we get

$$\frac{\partial\left(\rho(r)\sigma^2(r)\right)}{\partial r} = -\rho(r)\frac{\partial\Phi(r)}{\partial r}, \tag{3}$$

where σ stands for the velocity dispersion, which is assumed isotropic at any given r. Applying the assumption $\sigma(\infty) = 0$ we get the solution:

$$\sigma^2(r) = \frac{1}{\rho(r)}\int_r^\infty \rho(r')\frac{\mathrm{d}\Phi(r')}{\mathrm{d}r'}\mathrm{d}r'. \tag{4}$$

The density ρ and potential Φ of the Plummer sphere are given by the Eqs. (2) and (1), respectively. The final formula for the velocity dispersion of the galaxy with mass M and Plummer radius ε is thus

$$\sigma^2(r) = \frac{G\,M}{6\sqrt{\varepsilon^2 + r^2}}. \tag{5}$$

For the galaxies in our model, we use the Eq. (5) in a slightly modified from, because in the previous derivation we considered an isolated Plummer sphere extending to the infinity. In reality, the size of a single galaxy is limited (by tidal forces) and so we assume that at some distance R it ends and here, $\sigma(R) = 0$. With this assumption we get:

$$\sigma^2(r) = \frac{G\,M}{6\,\varepsilon}(1 + r^2/\varepsilon^2)^{5/2}\left[\frac{1}{(1 + r^2/\varepsilon^2)^3} - \frac{1}{(1 + R^2/\varepsilon^2)^3}\right]. \tag{6}$$

The radial dependence of the velocity dispersion for the truncated and the infinite galaxy are compared in Fig. 36.

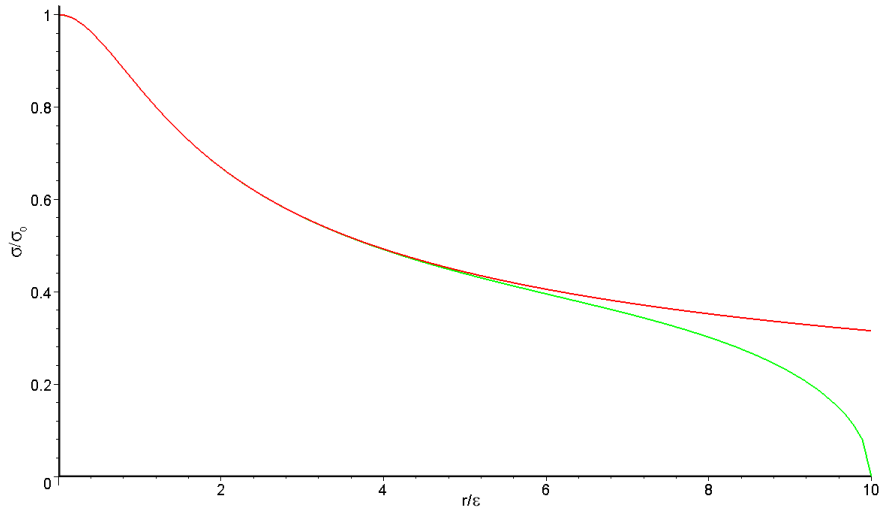

Figure 36: *The radial dependence of the velocity dispersion in a Plummer sphere galaxy extending to infinity (red line) and a galaxy having the same Plummer profile truncated in 10 times its scale radius (green line). The distance is in multiples of the scale and the velocity dispersion in the units of the dispersion in the centre* σ_0 *(*σ_0 *differs negligibly between the two cases).*

9.3 Period of radial oscillations

For further considerations, the period of radial oscillations in the Plummer potential will be important. Its radial dependence can be seen in Fig. 37 for the same combinations of parameters as in Fig. 35.

It is interesting to note that the period of radial oscillations does not tend to zero as $r \to 0$, instead it converges to some specific (non-negligible) value, as you can see in Fig. 37. On the first sight, this may seem a little counter-intuitive (when compared to the familiar case of a point mass), but it can be easily understood with the help of a simple model where we instead choose to compute the period of the circular motion around the centre at the same radius (which, however, happens to coincide with the period of the radial motion as $r \to 0$, for the Plummer potential). We start with the third Kepler's law (which, *for circular motion*, is valid in any potential with the spherical symmetry) in the form

$$\left(\frac{T}{2\pi}\right)^2 = \frac{r^3}{G\,M(r)}, \tag{7}$$

where T is the period, and $M(r)$ denotes the mass *inside* the radius r. For the Plummer sphere, this mass can be easily integrated from Eq. 2 and after simple manipulations we get

$$T = 2\pi\sqrt{\frac{\varepsilon^3}{G\,M}} \tag{8}$$

in the limit $r \to 0$ (where M without an argument is again the mass of the whole galaxy), what is anyway the same result as we would obtain for a homogeneous sphere with the density equal to $\rho_0 = 3M/(4\pi\varepsilon^3)$, the central density of the Plummer sphere – and is clearly a non-zero number, reflecting the fact that as $r \to 0$, the mass inside the orbit tends to zero and a test particle does not need much speed to overcome gravity.

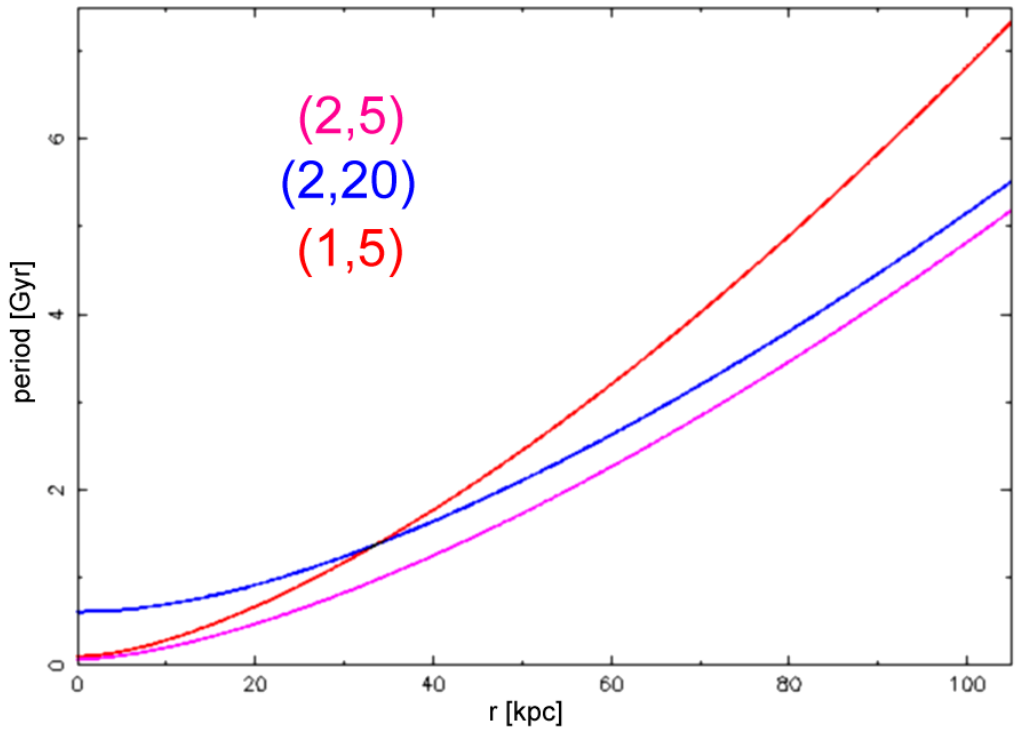

Figure 37: *The radial dependence of the period of radial oscillations in the Plummer potential. The meaning of numbers in parentheses is the same as in Fig. 35. The mass of the galaxy is either* 1×10^{11} *or* 2×10^{11} $M_\odot$.

The behaviour near the centre does not match observations of elliptical galaxies which show a density divergence all the way to the centre, at least down to the spatial resolution limit. But this divergence is very uncomfortable for the simulation and so we will assume that the influence of a small central part does not affect large-scale structures in the galaxy, as the shells certainly are.

10 One-dimensional shells

10.1 A tale of shells

For a better understanding of the shell formation mechanism we start gently, with a one-dimensional example. We evenly distribute 5,000 particles (that we will suggestively call stars) on the x-axis, between 1 and 5; the y-axis shows the linear density of particles. The time unit is just the time step, chosen just to be smooth enough. For the Plummer sphere with a total mass of 10^{11} $M_\odot$ and the Plummer radius $\varepsilon = 5$ kpc, the radial period on $r = \varepsilon$ is about 162 Myr. In our case, the period in the distance ε from the centre is about 860 time steps, what establishes the time step to be about 1.9×10^5 yr. The span of the displayed area is then from -30 kpc to 30 kpc.

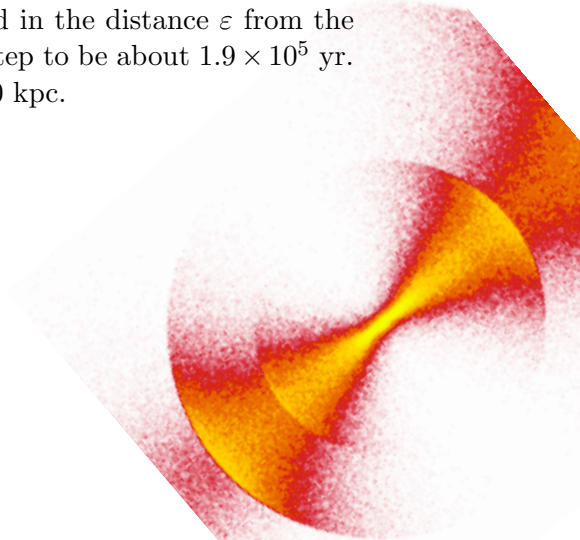

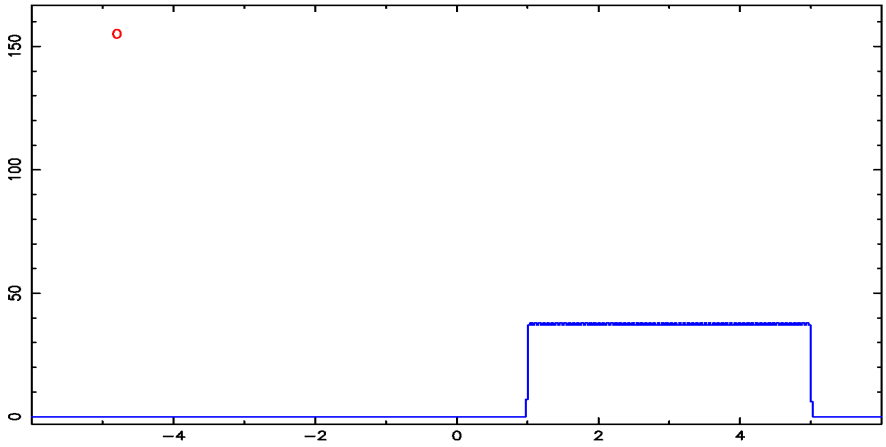

At $t = 0$ we see the stars at rest in a one-dimensional Plummer potential (Eq. 1), with the centre in 0 and the Plummer radius $\varepsilon = 1$. Turning the time on, stars begin to fall freely towards the centre of our imaginary one-dimensional galaxy.

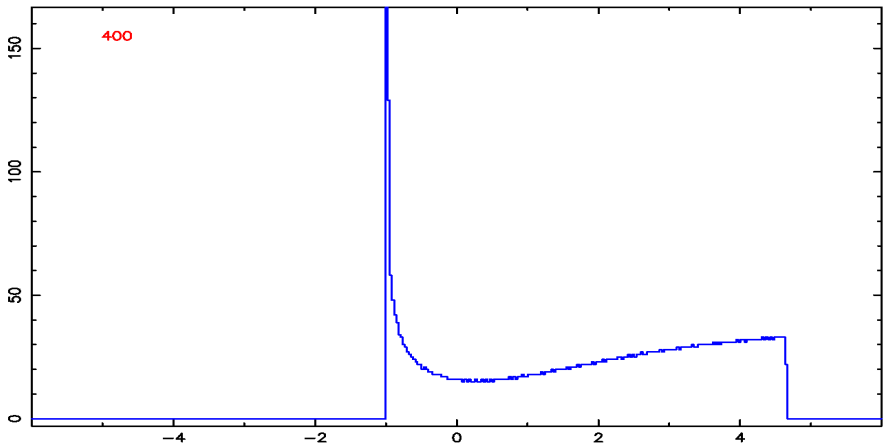

The stars that have originally been the closest to the centre (those that departed from the distance of 1) first reach their turning point (at -1), where their speed is obviously zero (around the 430th time step). Already sooner, their velocity that has been the largest in the centre, gets considerably lower and thus they will spend more time around their turning point and their density greatly increases – they form the first shell. (Strictly speaking it is not a shell, just a point of brightening in the one-dimensional case, when we stick to the story about the particles being stars, but we leave it with the proud name.)

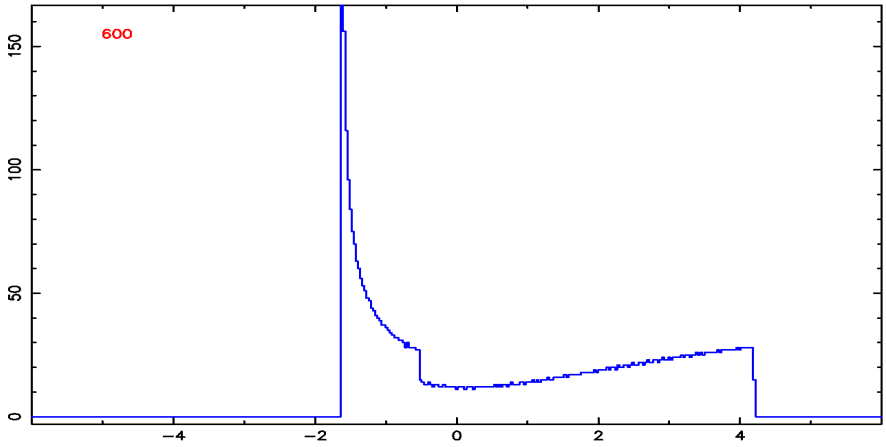

About 200 time steps later, the first stars are already on their course back (creating the step at -0.6) and as further and further stars reach their turning points, the first shell recedes to more distant radii. Now it passes the -1.7 position and it is composed of entirely different stars, than on the previous snapshot.

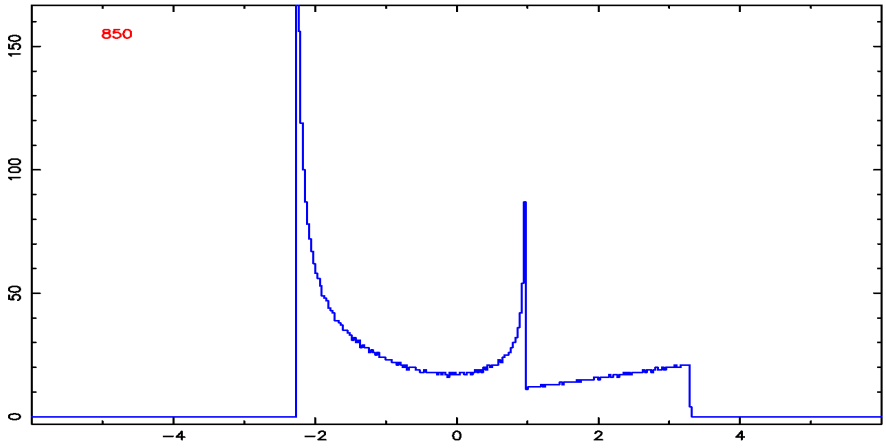

After 850 time steps, the first stars reach the point of their origin (their $t = 0$ position) and form the second shell. With this numbering, we will have the even shells to the right and odd to the left from the centre. The first shell has already gone more than 2 units to the left, whereas the outermost stars from the original setting did not get even 2 units from their starting points at 5.

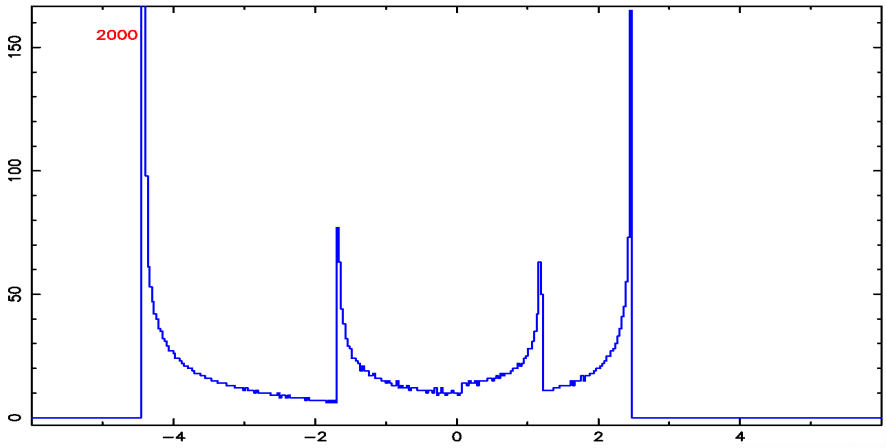

Now we have jumped forward a lot, into the 2,000th some step (377 Myr for $M =$

10^{11} $M_\odot$ and $\varepsilon = 5$ kpc), when our shell system already boasts about four pieces. The first shell is to reach its most distant point (-5), corresponding to the outermost starting position of the stars (5). But it means that the last stars are heading for their first turning points and the shell thus plunges towards its own destruction. In fact it does not plunge too much, as its progress gradually decreases, because the difference between periods of two adjacent stars increases with the distance from the centre (phrased more mathematically, the curves in Fig. 37 are convex).

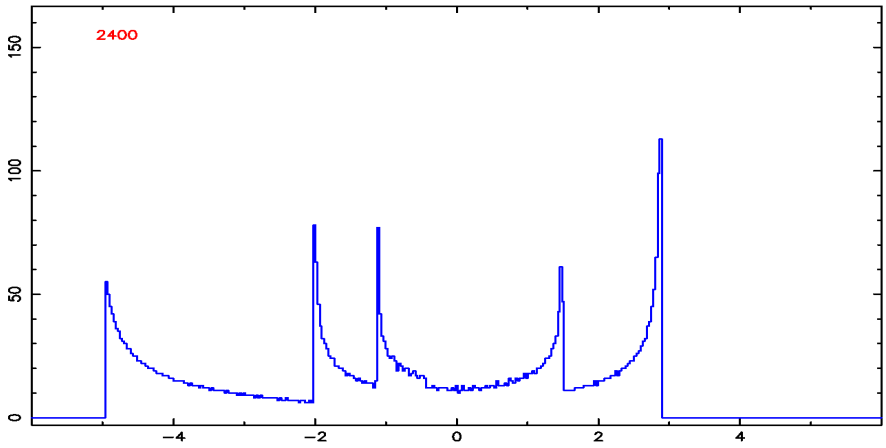

Nothing lasts forever, even in the universe and not even in our one-dimensional one. About 400 time steps later the first shell lives its last moments. After the last stars (starting form 5) turn around, there are no more to feed the shell. Its luminosity fades and while we regret it, we can note the fifth shell that has meanwhile appeared to the left from the centre.

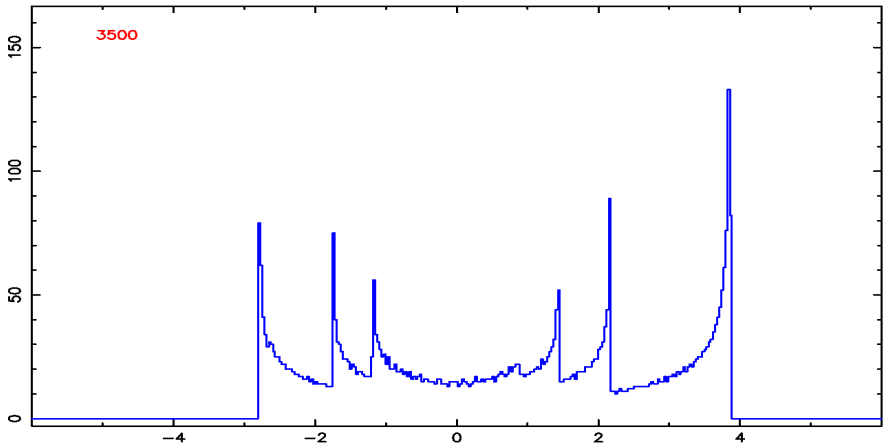

After more than a thousand time steps, there are no traces left from the first shell and the second one is at its greatest glare (so to say about an object composed entirely of stars). The 8th shell has just appeared (to the right) but for the already explained reasons, there are only 7 shells in the system.

10.2 Shell condensation

In the time step no. 4,900 (see pictures later in this chapter), it is clear that the distances between shells decrease. The reason follows from a simple thought – with each half-cycle of the innermost stars, one shell appears on one or the other side of the centre

and with each half-cycle of the outermost stars one shell disappears. The number of shells N in such a system at time t is given as

$$N = \frac{t}{T_{min}/2} - \frac{t}{T_{max}/2}, \tag{9}$$

where T_{min} is the period of stars with the shortest path (those starting from 1 in our case) and T_{max} the period of stars with the longest path (the stars from 5). The first term represents the amount of shells created and the second the amount of shells destroyed. As T_{min} is considerably smaller than T_{max}, the number of shells builds up with the time, but the range of their distances is strictly set by the range of energies of the stars (in our case they started between 1 and 5 and as such, they must turn there and between -1 and -5). Thus, the shells must be becoming denser.

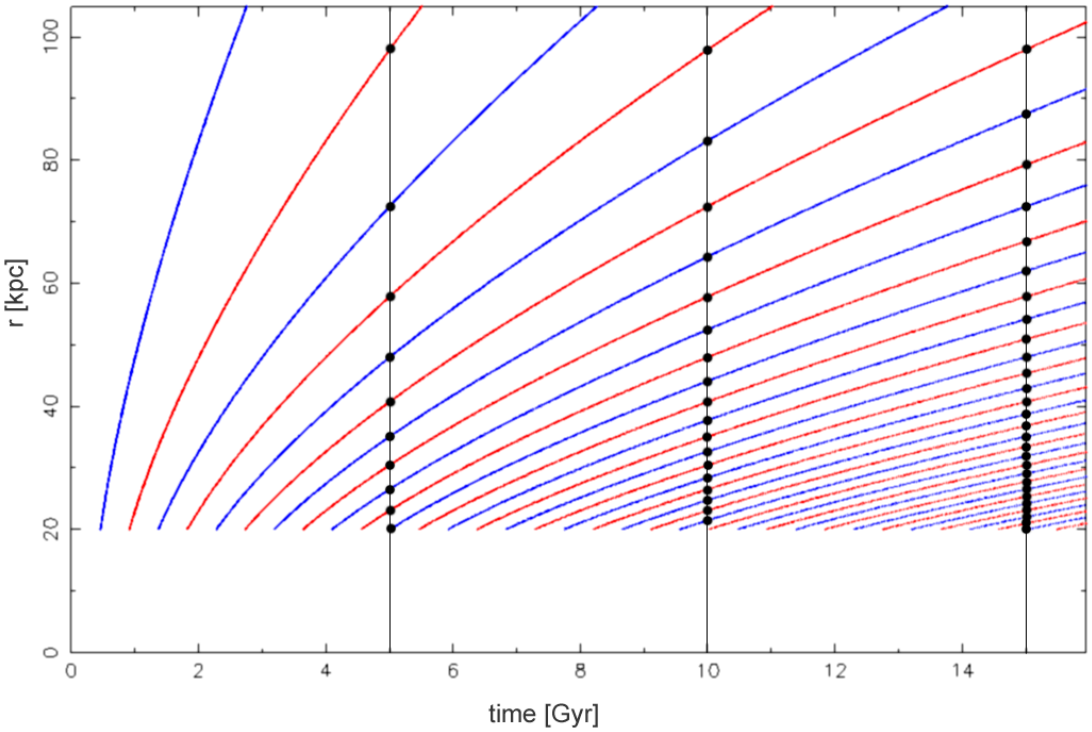

Figure 38: *The dependence of the position of the shells on the time in the Plummer potential of a galaxy with the mass of* 2×10^{11} $M_\odot$ *and* $\varepsilon = 20$ *kpc (the blue curve in Figs. 35 and 37). The shells to the left of the centre are shown in blue, the shells to the right in red. The shell distributions in 5, 10, and 15 Gyr, when the system contains 10, 18, and 27 shells between the radii of 20 and 100 kpc, respectively, are highlighted.*

Technically the reason is that the time difference between the points, when two neighbouring stars reach their turning points, is cumulative. If $\triangle t$ is the difference in periods between some two points A a B (imagine them to the right, with A closer to the centre), the shell no. 2 (first on the right side) moves from A to B in $\triangle t$. But in the second orbit, the stars from B will already have a lag of $\triangle t$ behind those from A and they are just getting a second one, so the shell no. 4 (second on the right side) reaches B from A in $2 \times \triangle t$. Every n-th shell on the right side then moves n times slower than the first one (the shell no. 2). The situation is similar on the left side and the shells are condensing.

The graph showing the dependence of position of the second shell on time is then

just the graph of period vs. radius inverted (so the first red curve in Fig. 38 is the inverse of the blue function from Fig. 37).

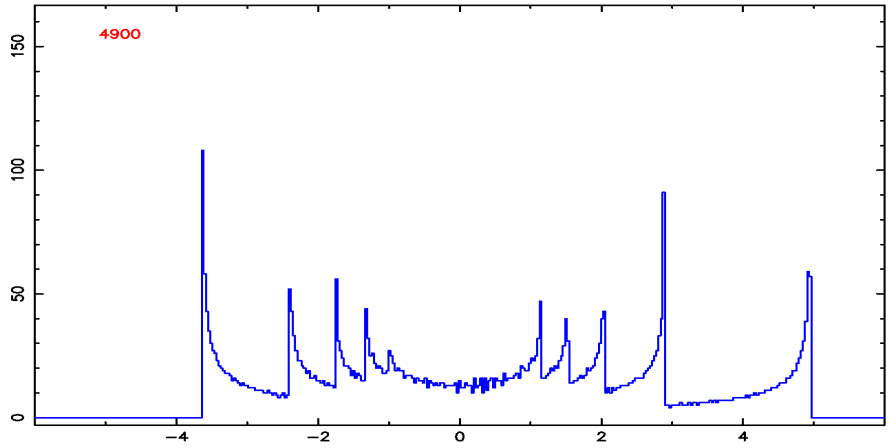

Back to the 4,900th time step: The innermost stars (with the period of about 860 time steps) have finished 5 cycles and a half and gave rise to eleven shells. Meanwhile the outermost stars did not finished a complete period and have put to an end only one shell – we can count 10 shells in the picture.

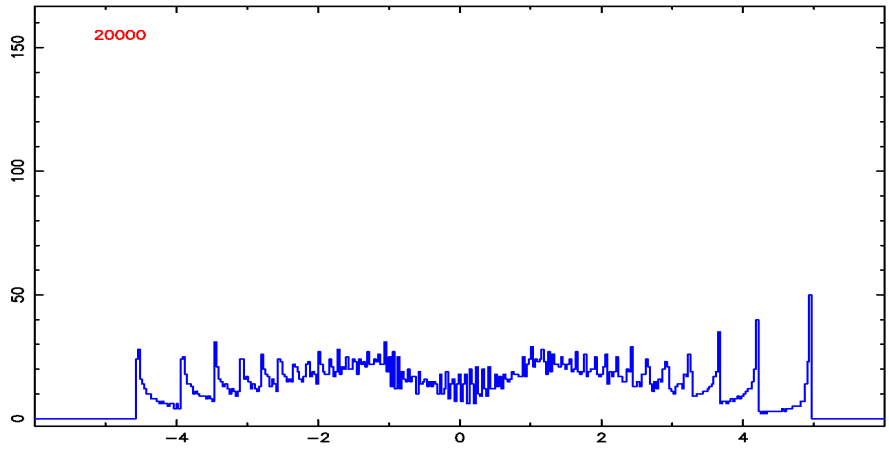

In the time step no. 20,000, already about 46 shells have appeared and 8 disappeared, so the system is to contain about 38 shells. But as the number of shells increases whilst the number of stars stays unchanged, their brightness (the amount of stars in one shell) decreases. Furthermore, the shells in the inner parts are too dense to be distinguished.

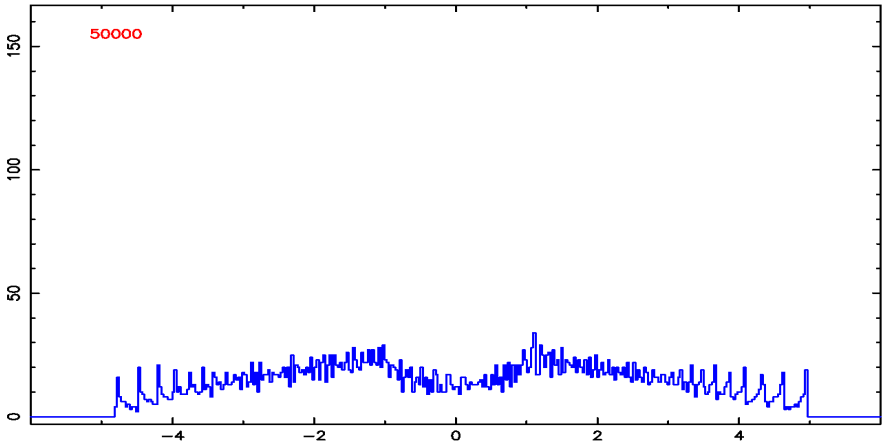

In about twice as much time we should have almost a hundred shells, but their discerning is practically impossible. For the system with the mass of $M = 10^{11}\ M_{\odot}$ and $\varepsilon = 5$ kpc, approximately 9.4 Gyr have elapsed. In real galaxies, shells are often observed on larger radii than the 25 kpc of this case (in the parallel to the above described system), and the time scale would so be longer.

10.3 A little reality

The true disruption of the secondary galaxy is a complex process, for which these simple considerations do not account. The three-dimensionality itself is not a big issue. But the stars are not dropped from rest, instead, the centre of mass of the secondary galaxy has some energy with respect to the primary galaxy which adds with the energy that the stars have with respect to the centre of mass of the secondary galaxy, thanks to its original velocity dispersion. In a simplified picture it means that the stars with the same energy start from different positions and reach the turning point (which is for them at the same distance from the centre of the host galaxy) at different times and the shell gets smeared.

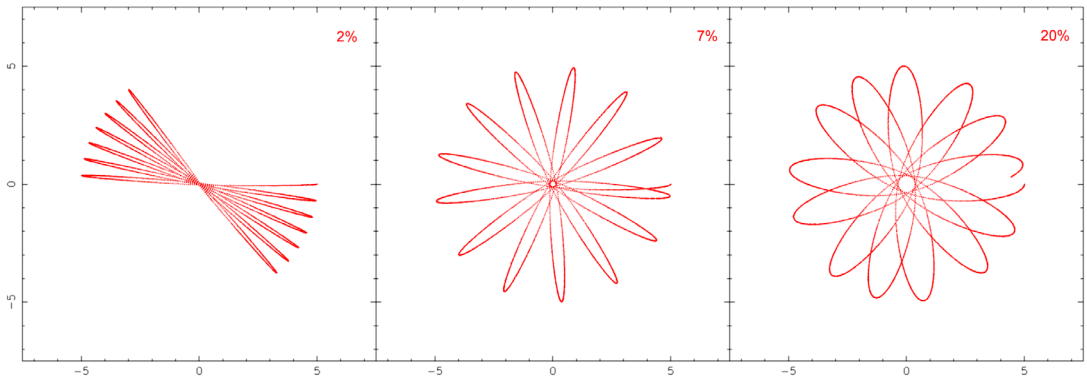

Figure 39: *The trajectory covered by a star in the Plummer potential in a given time for different initial velocities. The star departs from the x-axis (0;5) with zero velocity in the x-direction and with a corresponding fraction of the local circular velocity (2, 7 or 20%) in the y-direction, as indicated on the picture. The length units are multiples of the Plummer radius.*

Furthermore, even if the centre of mass of the secondary was on an exact radial trajectory (what we cannot expect anyway), the stars move with respect to it and so

they will almost always have some non-zero component of velocity perpendicular to the radial direction. Their path than will not be a straight line with forward-backward oscillations, but will form a more complex shape, see Fig. 39.

In reality the stars suffer also from the ellipticity and possible inhomogeneities of the primary galaxy, self-gravity of their own galaxy before it is completely disrupted, the dynamical friction (Part IV) and probably some another effects I have not thought of at the moment.

Even though this one-dimensional example is fairly detached from the reality, it serves well to understand the basic ideas of the principle of the shell formation with this mechanism.

11 Description of the model

At the beginning of our work we started from the source code of the MERGE 9 programme written by Bruno Jungwiert (2006, unpublished). The program is written in the FORTRAN language and the graphical output uses the PGPLOT, a graphics subroutine library written by Tim Pearson. My task was to improve this model by adding two new effects, namely the dynamical friction (Part IV) and the satellite mass loss (Part V).

11.1 Strategy

The strategy of the simulations is similar to that of Hernquist and Quinn (1988, 1989), see §6.4. The test (i.e. mass-less) particles of the secondary galaxy are generated (usually in counts from 10^4 to 10^6) so that they follow the density profile of a Plummer sphere (Eq. 2) with chosen parameters (the ratio of mass to the primary galaxy, Plummer radius, the position and relative speed of centres of masses of the galaxies). The particles then move according to a smooth gravitational potential (Eq. 1) of both galaxies in the centre-of-mass system of the masses of both galaxies. When the centres of the galaxies come closer to each other than some specific small distance, the potential of the secondary galaxy is suddenly switched off and the particles continue to move only in the fixed potential of the primary galaxy.

11.2 Leapfrog algorithm

For the numerical integration of motion of the test particles and the galaxies, the *Leapfrog* method was chosen. In this method, velocities derived for a time half step earlier (or later) than the current position are used to update the position. Conversely, to update the half-step velocity one step forward, the positions for the round position in between are used. In so doing the velocities can be seen to "leapfrog" over the current time step which is the origin of the algorithm's name.

Figure 40: *Leapfrogging frogs*

This simple enterprise improves the accuracy of the numerical computation by an order compared to when the position x and velocities v are taken simultaneously, as I am going to show now. The equations

$$x(t + \triangle t) = x(t) + \triangle t\, v(t + \triangle t/2), \tag{10}$$

$$v(t + \triangle t/2) = v(t - \triangle t/2) + \triangle t\, a(t) \tag{11}$$

show, how the position and velocity are updated in the *Leapfrog* algorithm, where t is time, Δt is the time step and $a(t)$ is the acceleration. Substituting from (11) to (10) and using the first two terms of the Taylor expansion of $v(t - \triangle t/2) \doteq v(t) - \frac{1}{2} \triangle t\, a(t)$ (what is consistent with the present orders of Δt), we get:

$$x(t + \triangle t) \doteq x(t) + \triangle t\, v(t) + \frac{1}{2}(\triangle t)^2\, a(t), \tag{12}$$

exactly the first three terms of the Taylor expansion for the position, what means that the error of Leapfrog is of the order of $(\triangle t)^3$. This is not so, when we evaluate the position and the speed at the same time:

$$x(t + \triangle t) = x(t) + \triangle t\, v(t), \tag{13}$$

$$v(t) = v(t - \triangle t) + \triangle t\, a(t - \triangle t). \tag{14}$$

Substituting now $v(t)$ to (13) from Eq. 14 (where we can put $a(t - \triangle t) \doteq a(t)$, as the error is at least of the order of $(\triangle t)^3$), using again the Taylor expansion to get rid of $v(t - \triangle t)$, we get (obviously) back (13), what is the Taylor expansion for the position only to the first order and thus the error is already at $(\triangle t)^2$. The higher accuracy together with low CPU time demand make the Leapfrog widely used.

For the time step commonly used in our simulations, the error for the trial circular motion was only 11 revolutions after 10,000 (compared to the simple analytical solution that is available in this case), what is only 1 per mile. Furthermore, the circular motion is bound to the systematic error of the particle moving on a regular polygon rather than a circle, as the path is always shorter.

11.3 The Force

The force $F(r)$ acting on a test particle (of a mass m) is calculated from the potential by the equation $F(r) = - \bigtriangledown \Phi(r)$, what reads in Plummer potential (Eq. 1) as:

$$F(r) = -G\, M\, m \frac{r}{(r^2 + \varepsilon^2)^{3/2}}. \tag{15}$$

The particles in our model then move according to an acceleration $\mathbf{a}(\mathbf{r})$ given by the potentials of both galaxies

$$\mathbf{a}(\mathbf{r}) = -G \left(M_p \frac{\mathbf{r_p}}{(r_p^2 + \varepsilon_p^2)^{3/2}} + M_s \frac{\mathbf{r_s}}{(r_s^2 + \varepsilon_s^2)^{3/2}} \right), \tag{16}$$

until the potential of secondary galaxy is switched off and the particles continue to move only in the fixed potential of the primary galaxy. The indexes p and s mark the quantities corresponding to the primary and the secondary galaxy, respectively ($\mathbf{r_p}$ or $\mathbf{r_s}$ is the vector of distance between the centre of the primary or secondary galaxy and the particle).

The action of two Plummer spheres on each other is a little more intricate. The non-zero radius reduces their attraction compared to two point masses. This interaction cannot be appropriately described by simple means, but we approximate the attraction by keeping the form of the Plummer potential and by defining a common softening parameter in order to fulfil the law of the action and reaction. The definition of the

common softening parameter is derived from both Plummer radii and then we use it in the equation of motion as:

$$F(r) = -G\, M_p M_s \frac{r}{(r^2 + \varepsilon_p^2 + \varepsilon_s^2)^{3/2}}, \tag{17}$$

where r is the relative distance of of centres of masses of galaxies. The common softening parameter is then $\varepsilon_{common} = \sqrt{\varepsilon_p^2 + \varepsilon_s^2}$.

11.4 Standard set of parameters

For the future reference, let us define **the standard set of parameters** for our simulations as the following set of values:

The mass of the primary galaxy: $M_p = 3.2 \times 10^{11}$ $M_\odot$
The secondary to primary mass ratio: 0.02
Plummer radius of the primary galaxy: $\varepsilon_p = 20$ kpc
The cut-off diameter for the primary galaxy: $R = 200$ kpc
Plummer radius of the secondary galaxy: $\varepsilon_s = 2$ kpc
The initial radial distance of the secondary galaxy: 180 kpc
The initial velocity of the secondary galaxy: the escape velocity for the initial distance

These values are used as the usual setup of the presented simulations and we will refer to them often, so we do not have to repeat them.

Let us only remark that the escape velocity is computed only approximately, on the same grounds as the force between the galaxy (see Eq. 17), i.e. we put

$$v_{esc} = \sqrt{\frac{2\, G\, (M_p + M_s)}{\sqrt{r^2 + \varepsilon_{common}^2}}}. \tag{18}$$

The results of our simulation show that, in the relevant range of radii, its difference from reality is negligible.

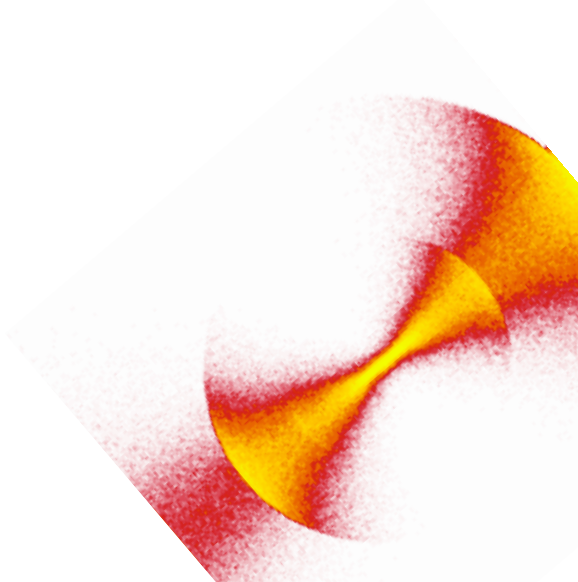

Part IV
Dynamical friction

12 A thermodynamic meditation

The dynamical friction is a braking force of gravitational origin, caused by the sole fact that the area, through which the secondary galaxy (or, in general, any object passing through a galaxy or another extended object) flies is not an empty space filled with a smooth potential, but a large sea of individual stars.

Thinking deeper, we can easily see that some slowdown of the secondary galaxy is inevitable. Every system, where energy transfer is possible tends to temperature equilibrium. In a system of at least three gravitating bodies such a transfer is indeed possible and frequently happens. The relatively fast and heavy secondary galaxy possesses a decent amount of kinetic energy and as such it is just a hot piece thrown into a colder sea of the stars of the primary galaxy. The slowdown of the intruder that cannot be accounted for in the fixed-potential model, is the way of levelling the temperatures. The kinetic energy transfers to the primary's stars – the same effect causes the heating of the cold disk population in the WIM, as mentioned in §5.2.

The reality of this process can be grasped from a complete different point of view. The relatively massive secondary galaxy attracts the primary's stars and thus creates an area of a higher density of stars behind itself. The passing galaxy is attracted backwards by this condensation, lowering its speed towards the primary.

13 The Chandrasekhar formula

13.1 Derivation of the Chandrasekhar formula

An analytical derivation of such a braking force is based on the following thought: In a distant encounter with just one star, the velocity of an object cannot be changed, instead it is only deflected from the original direction and thus enriched with a component of speed perpendicular to the original direction. For a very massive body, as our secondary galaxy is, the magnitude of this perpendicular component will not be large, neither will be the loss of the velocity in the original direction. But when it undergoes many such encounters, the contributions add. The contributions in the perpendicular directions will have randomly scattered azimuthal angles and thus add to zero (except for the overall action of the smooth potential). On the other hand, the contributions to the original direction of the velocity will always be opposite to it, resulting in the braking of the galaxy.

The Chandrasekhar formula was originally derived by Chandrasekhar (1943). Here I present a short version of the presentation of the chapter 7.1 in the bible of the galactic astronomy, "Galactic Dynamics" by Binney and Tremaine (1987).

To start, let us imagine the encounter of our object of interest with a single star. When two bodies meet, energy is not transferred, but the direction of velocity of our object changes. It is a matter of a simple mechanics and as a result, the change of the component of velocity parallel to its original direction, $\mid \triangle \mathbf{v}_{M\parallel} \mid$ between the times $t = -\infty$ and $t = \infty$ is given by (Eq. 7-10b in Binney and Tremaine 1987, see its derivation there):

$$\mid \triangle \mathbf{v}_{M\parallel} \mid = \frac{2\,m\,V_0}{M+m}\left[1+\frac{b^2 V_0^4}{G^2(M+m)^2}\right]^{-1}, \qquad (19)$$

where M is our object's (the secondary galaxy) mass, m is the mass of the star, b the impact parameter (the length of $\mathbf{b}$, the vector indicating the position of the star in a plane perpendicular to the original velocity of the galaxy) and $\mathbf{V}_0$ is the difference between the original velocity of the star $\mathbf{v}_m$ and velocity of our object $\mathbf{v}_M$, so $\mathbf{V}_0 = \mathbf{v}_m - \mathbf{v}_M$. The bold typeface indicates vectors, and their length is indicated by the same symbol in normal type.

For an object flying through a field of stars with the phase-space number density of stars $f(\mathbf{v}_m, \mathbf{b})$, the change in the parallel component of velocity $\mathrm{d}\mathbf{v}_{M\|}$ in an infinitesimal time $\mathrm{d}t$ will be given by the integration of Eq. 19 multiplied by the density $f(\mathbf{v}_m, \mathbf{b})$ over the plane of $\mathbf{b}$ and the space $\mathbf{v}_m$. For $\mathbf{b}$ is measured from a given point in a plane, it is advantageous to use the polar coordinates (b, φ):

$$\frac{\mathrm{d}\mathbf{v}_{M\|}}{\mathrm{d}t} = \int\int\int f(\mathbf{v}_m, b, \varphi) \frac{2m\, V_0(\mathbf{v}_m)\, \mathbf{V}_0(\mathbf{v}_m)}{(M+m)\left[1 + \frac{b^2 V_0^4(\mathbf{v}_m)}{G^2(M+m)^2}\right]} \mathrm{d}^3\mathbf{v}_m\, b\mathrm{d}b\, \mathrm{d}\varphi. \tag{20}$$

To derive the Chandrasekhar formula we further assume the homogeneity of the field of stars, so as the distribution function of the stars does not depend on $\mathbf{b}$. The remaining $\mathbf{b}$-dependent part is of the following form a can be easily integrated from 0 to some b_{max}:

$$\int_0^{b_{max}} \frac{b\mathrm{d}b}{1 + c^2 b^2} = \left[\frac{\ln(1 + c^2 b^2)}{2\, c^2}\right]_{b=0}^{b=b_{max}}, \tag{21}$$

where in our case $c = V_0^2/[G(M+m)]$. It is conventional to introduce the notation

$$\Lambda = \frac{b_{max} V_0^2}{G(M+m)}. \tag{22}$$

A typical value of Λ would be of the order of 10^3, thus we can neglect the one and put $\frac{1}{2}\ln(1+\Lambda^2) \cong \ln(\Lambda)$. This factor is often called the Coulomb logarithm. Furthermore we assume that we do not err too much when replacing V_0 in Λ by v_{typ}, a typical speed. Then the Coulomb logarithm does not depend on $\mathbf{v}_m$, and still $V_0 = \mid \mathbf{v}_m - \mathbf{v}_M \mid$ and the whole formula (20) goes to

$$\frac{\mathrm{d}\mathbf{v}_{M\|}}{\mathrm{d}t} = 4\pi \ln(\Lambda) G^2 m (M+m) \int f(\mathbf{v}_m) \frac{\mathbf{v}_m - \mathbf{v}_M}{\mid \mathbf{v}_m - \mathbf{v}_M \mid^3} \mathrm{d}^3\mathbf{v}_m. \tag{23}$$

The integral is of exactly the same form as in the Newton's law of gravity and if the stars move isotropically, the density distribution is spherical and by Newton's first theorem (see Binney and Tremaine 1987, chapter 2), the total acceleration of our object by dynamical friction is :

$$\frac{\mathrm{d}\mathbf{v}_{M\|}}{\mathrm{d}t} = -16\pi^2 \ln(\Lambda) G^2 m (M+m) \frac{\int_0^{v_M} f(v_m) v_m \mathrm{d}v_m}{v_M^3} \mathbf{v}_M \tag{24}$$

i.e., only stars moving slower then our object contribute to the force and this force always opposes the motion. Equation (24) is usually called the *Chandrasekhar dynamical friction formula*.

If $f(v_m)$ is Maxwellian with dispersion σ

$$f = \frac{n_0}{(2\pi\sigma^2)^{3/2}} \exp(-\frac{1}{2} v^2/\sigma^2), \tag{25}$$

we can integrate Eq. (24). The density of the stars is $\rho_0 = n_0\, m$ and for $M \gg m$, what happens to be our case, we can put $(M + m) \cong M$, and then Eq. (24) reads:

$$\frac{\mathrm{d}\mathbf{v}_{M\|}}{\mathrm{d}t} = -\frac{4\pi \ln(\Lambda) G^2 \rho_0 M}{v_M^3} \left[\mathrm{erf}(X) - \frac{2\,X}{\sqrt{\pi}} \mathrm{e}^{-X^2}\right] \mathbf{v}_M, \tag{26}$$

where Λ is given by the formula (22), $X \equiv v_M/(\sigma\sqrt{2})$ and $\mathrm{erf}(X)$ is the error function given by

$$\mathrm{erf}(X) \equiv \frac{2}{\sqrt{\pi}} \int_0^X \mathrm{e}^{-t^2} \mathrm{d}t \tag{27}$$

for which we can obtain tabulated values, or we can pre-generate them numerically with an arbitrary precision.

13.2 What a wonderful universe

Giving it a deeper thought, one can consider the validity of the *Chandrasekhar formula* almost a miracle. I have by the way disclosed that it works, at least approximately – the confrontation with numerical simulations of flybys through a galaxy or a cluster has been carried out by e.g. Lin and Tremaine (1983); Bontekoe and van Albada (1987), who proved that the analytical solution (given by the Chandrasekhar formula) is in a good agreement with the simulations in a relatively wide range of situations. The analytical solutions has some freedom in the Coulomb logarithm which is not completely well-defined. Its correct choice can help to better reproduce the numerical results and compensate other drawbacks of the formula – anyway, the freedom is small when we demand the Coulomb logarithm to stay constant.

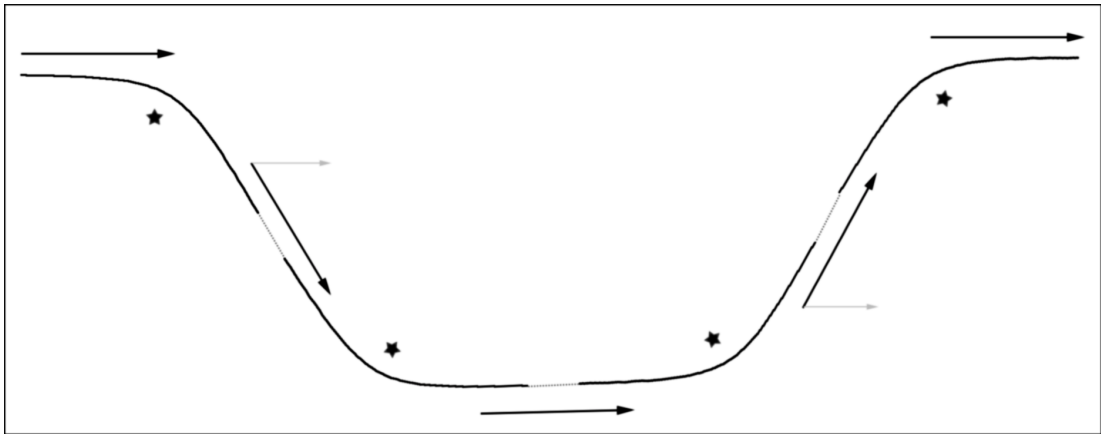

Figure 41: *The path and velocity changes of the objects undergoing encounters with individual stars. The absolute value of the velocity remains unchanged.*

But back to my astonishment. When our secondary galaxy deviates from its course, its speed in the original direction is reduced. But after meeting another star that compensates the deviation, it also gets back the original velocity in this direction, as is shown in Fig. 41.

The point is that the *Chandrasekhar formula* evaluates the change of the parallel component of the velocity after the flyby from infinity to infinity for every single star with the same initial conditions and then adds these changes and applies them to the secondary galaxy in one moment, the moment of the closest approach with these stars,

see Fig. 42. The change of the parallel component of the velocity and the compensation of the changes in the perpendicular direction then happen somehow at the same time, although the magnitude of their effect is calculated as if they happen consecutively – and by some wonder, it works.

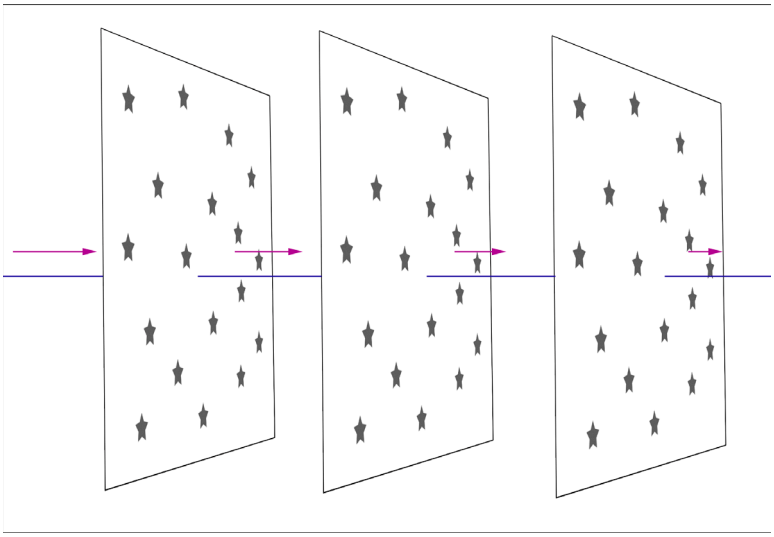

Figure 42: *A schematic depiction of the change of the velocity of the secondary galaxy after three steps. In every moment, only the influence of the stars lying in one plane perpendicular to the motion of the galaxy is taken into account.*

Let us just remark that the fact that we account for the influence of the stars in the moment of the closest approach is not so strong neglection. During an encounter of two bodies, roughly one half of the velocity change takes place around the point of the closest approach on the scale of the impact parameter. For the encounter of the galaxy with two stars, it is confirmed in the right panel of Fig. 43.

13.3 Why does it work?

We can see the mechanism of the dynamical friction in action even in a simple model of a "galaxy" interacting with two "stars", results of which are seen in Fig. 43. Although the model is a very simple one, it allows us to see in practice that yet in the system of three bodies (in contrary to two) the permanent energy and momentum transfer is possible. The symmetry of the configuration ensures that the galaxy will keep a straight line and thus any change of velocity it undergoes will be a change in the magnitude of the velocity. According to the idea of an infinite sea of stars, we take into account only the interaction between the stars and the galaxy, not mutually between the stars.

It is clear that due to the galaxy's gravity, the stars begin to move towards its track (meanwhile also moving towards the galaxy along the track, but let us not care for a moment). While the stars move towards the track, the attraction accumulates and they gather speed. When they cross the galaxy's track, the galaxy starts pulling them back (at least when we speak about the perpendicular component of the velocity) and they slow down. Anyway, thanks to the fact that they cross the track *after* the galaxy's passage, they spend more time in the phase where their perpendicular velocity component is increased than otherwise and finally they retain some speed in this direction. But it means they have gathered kinetic energy, what must be at the expense of the galaxy's kinetic energy and so the speed of the galaxy must have decreased (that is the dynamical friction) – even though it has moved much faster than before during the closest

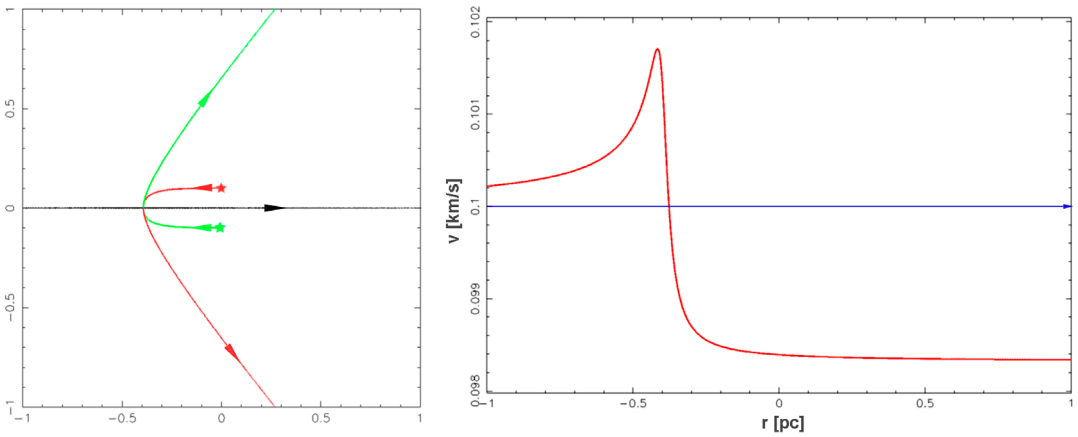

Figure 43: *The result of the simulation. A large body (with the mass of 200 $M_\odot$, straight black line) moves in the direction of the x-axis (with the velocity of only 100 m/s – this and the other unrealistic values have been chosen only to make the picture more illustrative in a linear and uniform scale) and encounters a pair of stars (2 $M_\odot$ each) that are initially place symmetrically with respect to its track (0.1 pc from the track). The mutual gravitational attraction of the stars is neglected. The right panel shows the development of the velocity of the large body during the closest approach. The blue line represents its original velocity, thus its path if the stars were not present.*

approach of the encounter. In reality, the situation is a little more complex, because apart from the energy, the momentum has to be also conserved – the momentum of the galaxy has decreased and so the stars must have also a non-zero parallel component of the velocity, to maintain this component of momentum.

In accordance with the derivation of the Chandrasekhar formula, we use the Eq. (19) just multiplied by two to derive the analytical formula for the change of the galaxy's velocity. For the impact parameter b we obviously put the original distance between the stars and the galaxy's track. Our numerical tests for various values of parameters (masses, initial velocity of the galaxy, impact parameter) show that the analytical results obtained this way tend to overestimate the decrease in the velocity, typically by about 15 per cent.

It could be anticipated that the numerical and analytical results will differ, as the analytical formula counts with two separated encounters from infinity to infinity. In such a case the galaxy follows a curved trajectory and thus its interaction with the star is slightly different than when both encounters happen at the same time and the galaxy is forced to stay on a straight line. (Let us remark that we have tested the model by removing one of the stars and then the results for the change of the parallel component of the velocity differ from the prediction in fractions of per mile.)

In reality, the situation is even more complex, there are many stars in the game and they also mutually interact and undergo the influence of all the surrounding stars that do not take part in the dynamical friction directly...

14 Beyond the Chandrasekhar formula

14.1 Avoiding the approximations

The Chandrasekhar formula contains two kinds of inaccuracies. The first of them is the principal one, namely the fact that the change in the parallel component of the

velocity from any individual star is added instantaneously at the point of the closest approach (of the secondary galaxy) to it. We have already shown that it is not too wrong, but what is worse, the influence of the star is taken to be such as if the galaxy passed it from infinity to infinity and there was nothing in the universe but the star and the galaxy. See §§13.1–13.3 for details.

The second source of inaccuracy lies in all the approximation that have been done when passing from Eq. (20) to Eq. (24). These will concern us in this section, leaving aside the assumptions of the Maxwellian velocity distribution and the negligence of the masses of the stars compared to that of the secondary galaxy, that led us from Eq. (24) to (26), which we use in the simulations and keeping the "principal inaccuracy" mentioned above.

The first approximations that allowed us to integrate Eq. (20) over the plane of the impact parameter was the assumed homogeneity of the star field, i.e. that the distribution function does not depend on position. Then we have taken the Coulomb logarithm to be independent of velocity of the stars $\mathbf{v}_m$ (it obviously isn't, but it varies slowly) and this has allowed us to simplify the $\mathbf{v}_m$-integral and given a suitable choice of the distribution function we could even carry out the integration (see §13.1). Both steps are only approximate even in the simple case of the spherical galaxy with the Plummer profile, as both the density (Eq. 2) and the velocity dispersion (Eq. 5) of the Plummer sphere do depend on the radius.

If we wish to avoid these simplification, we have to turn back to Eq. (20) and put in e.g. the Maxwellian distribution (Eq. 25) for $f(\mathbf{v}_m, b, \varphi)$, together with putting $n_0 m = \rho$, where ρ is the density of the primary at a given point – keeping in mind that the radius r (the distance of a point from the centre of the primary galaxy) on which the formulae depend is a function of b, φ and in fact also of the direction of motion of the braked body (the secondary galaxy). When dealing with the radial mergers, this direction points towards the centre of the primary galaxy and r becomes a particularly simple function of b:

$$r = \sqrt{d^2 + b^2}, \tag{28}$$

where d is (also in the following) the distance between the centres of the primary and the secondary galaxy. There is no φ-dependence in the radial case and the integration gives a trivial factor of 2π. For simplicity, we put the Eq. (5) for the velocity dispersion, as the friction is essentially negligible for both the simple and the cut-off dispersion in the areas where they significantly differ (see Fig. 36). Furthermore, during the multiple passages that occur in the simulations (where the friction becomes significant) the secondary galaxy does not reach these areas at all. Using Eq. (6) for the cut-off velocity dispersion would thus unnecessarily complicate the already complex formulae.

Putting all this together, we get

$$\frac{\mathrm{d}\mathbf{v}_{M\parallel}}{\mathrm{d}t} = \frac{3^{5/2}\varepsilon_p^2}{(\pi G)^{3/2} M_p^{1/2} M_s} \int\int \frac{\mid \mathbf{v}_m - \mathbf{v}_M \mid (\mathbf{v}_m - \mathbf{v}_M)}{(b^2 + d^2 + \varepsilon_p^2)^{7/4}} \times \tag{29}$$

$$\times \left[1 + \frac{b^2 (\mathbf{v}_m - \mathbf{v}_M)^4}{G^2 M_s^2}\right]^{-1} \exp\left[-\frac{3\mathbf{v}_\mathrm{m}^2}{GM_p}\sqrt{b^2 + d^2 + \varepsilon_p^2}\right] b\mathrm{d}b\,\mathrm{d}^3\mathbf{v}_m,$$

where the meaning of the variables is the same as when we derived the Chandrasekhar formula in §13.1. The indexes p and s again stand for the parameters of the primary and the secondary galaxy, respectively.

First, we shift the integration variable to $\mathbf{v}'_m = \mathbf{v}_m - \mathbf{v}_M$ and immediately rename it back $\mathbf{v}'_m \to \mathbf{v}_m$. We then perform the scalar product with the unit vector $\mathbf{v}_M/v_M$ on both sides, getting the projection of the friction acceleration to the direction of the velocity of the secondary galaxy. This is by symmetry its only nonzero component in the radial case and it will be advantageous to deal with a scalar-valued integral. The negative value means that the friction acts in the direction opposite to the motion of the braked body, what is the only feasible situation in any setup with an isotropic velocity distribution in the primary galaxy.

Transforming to the spherical coordinates (taking the z-axis parallel with the velocity of the secondary galaxy), we have $\mathbf{v}_m \cdot \mathbf{v}_M = v_m v_M \cos\theta$ and again no dependence on the azimuthal angle, leaving us with the obligatory factor of 2π. The θ-integral then can be carried out in the form that could be with some effort put on mere three lines:

$$\frac{\mathrm{d}\mathbf{v}_{M\parallel}}{\mathrm{d}t} \cdot \frac{\mathbf{v}_M}{v_M} = \frac{\sqrt{3\,M_p} G^{3/2} M_s \varepsilon_p^2}{2\sqrt{\pi} v_M^2} \int_0^{\sqrt{R^2-d^2}} \int_0^{\infty} \frac{b\mathrm{d}b\, v_m^2 \mathrm{d}v_m}{\left(\varepsilon_p^2 + d^2 + b^2\right)^{11/4} \left(G^2 M_s^2 + b^2 v_m^4\right)} \times \tag{30}$$

$$\times \left[e^{-3\frac{\sqrt{\varepsilon_p^2+d^2+b^2}(v_m - v_M)^2}{GM_p}} \left(GM_p - 6\, v_m v_M \sqrt{\varepsilon_p^2 + d^2 + b^2} \right) - \right.$$

$$\left. - e^{-3\frac{\sqrt{\varepsilon_p^2+d^2+b^2}(v_M + v_m)^2}{GM_p}} \left(GM_p + 6\, v_m v_M \sqrt{\varepsilon_p^2 + d^2 + b^2} \right) \right] ,$$

where R is the considered cut-off of the primary galaxy. We cannot proceed analytically with the integration (not even in one of the variables), instead we have solved it numerically in Maple for different values of the parameters (see §14.2).

We have come to a formula for the dynamical friction (30) that is more accurate than the Chandrasekhar formula, but it is valid only for a radially moving body in the Plummer sphere. It is also only more accurate in the sense of avoiding the approximation used between Eqs. (20) and (24) but it is still built atop the "principal inaccuracies" described above.

The reader who considers a formula to be the best figure can enjoy Eq. (30) and who considers a figure to be the best formula can explore Fig. 44, where the integrand of Eq. (30) is shown in dependence of both integration variables for a chosen set of parameters. It is clear that far most of the acceleration comes from a close neighbourhood of the braked body both in the plane of the impact parameter and the velocity space. However, the maximum of the integrand does not exactly coincide with the actual speed of the body, as there is no reason for it to be so, but it is very close.

The results of the numerical integration of Eq. (30), depending on the velocity and position of the braked body, for some sets of parameters, are shown in §§15.4 and 15.5 in Figs. 56 and 59.

14.2 The Coulomb logarithm (CL)

Using Eq. (30) and Maple, we tried to determine the proper value of the Coulomb logarithm (hereafter CL) to be used in the simulations. We used our FORTRAN code to generate a set of all the parameters of a chosen trajectory of the secondary galaxy (i.e. the position and velocity of the secondary galaxy for the chosen profile of the primary and masses of the galaxies). Then we had Maple recalculate the acceleration from the dynamical friction by numerically integrating Eq. (30). However at this stage, the values (e.g. the velocity and position) for the next step had been already calculated by the

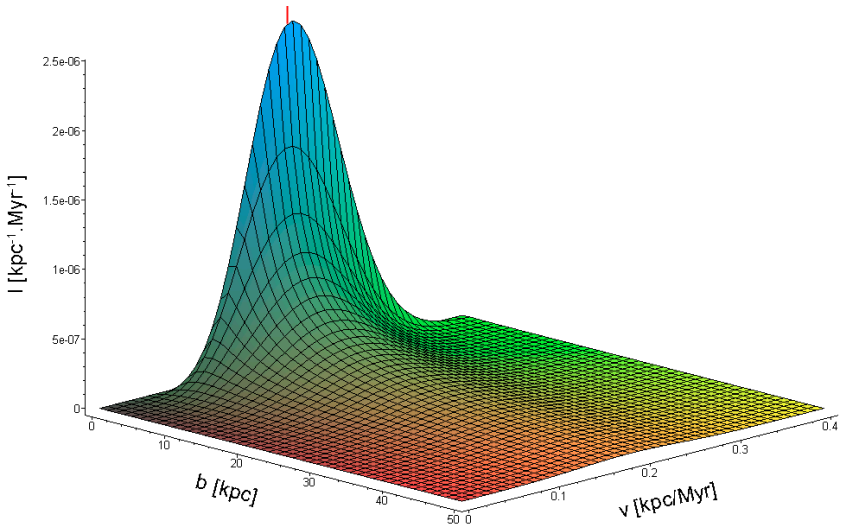

Figure 44: *The value of the integrand (including all the constants) from Eq. 30 in the dependence on the integration variables (the impact parameter and the relative velocity between the secondary galaxy and the stars) for the standard set of parameters (see §11.4) and the distance of the braked body (the secondary galaxy) from the centre of the primary of 70 kpc. The velocity of the body is taken to be 0.2 kpc/Myr (1 kpc/Myr ≐ 1000 km/s, see Appendix A). This value is also indicated in the graph by a red marker – it not surprising to find it near the peak, because there is a strong contribution from the stars that are in rest with respect to the centre of the primary galaxy, as the Maxwellian distribution peaks in zero.*

FORTRAN code using the Chandrasekhar formula in the way described in §15.1. The FORTRAN code was of course not aware of the new, presumably more correct value for the acceleration – thus in the following, the plots of the numerically integrated values do not represent a consistent trajectory of the secondary galaxy, instead they are merely meant for the comparison with the values calculated from the Chandrasekhar formula.

One possible strategy is to calculate the value of the CL in every step from the actual value of the velocity of the secondary galaxy. The V_0 in the definition Eq. (22) for Λ is the difference between the velocities of the stars and the secondary galaxy. As the stellar velocities are isotropic, the average value is just the velocity of the secondary galaxy with respect to the centre of the primary.

There is a uncertainty in the parameter b_{max} in the same equation – it should be theoretically equal to the distance between the centre of the secondary and the outer boundary of the primary measured in the plane perpendicular to the motion of the secondary. But the Eq. (26) assumes a homogeneous field of stars across all this distance, what is obviously not true. As the plane of the impact parameter is the plane perpendicular to the radial motion of the secondary galaxy, the density of the primary galaxy is always the highest in its centre and decreases outwards. Thus it may seem that the b_{max} should be smaller than the normal distance to the edge of the primary galaxy, but the approximation of the V_0 with the velocity of the galaxy and other circumstances make the situation more complex. The radial dependence of the CL in our model with a chosen fixed value b_{max} is shown in Fig. 45

Fig. 46 shows the comparison of of the values of the friction calculated with our model for two different values of b_{max} with the respective numerically computed values (in the sense described above). It seems that we get a smaller error using the lower

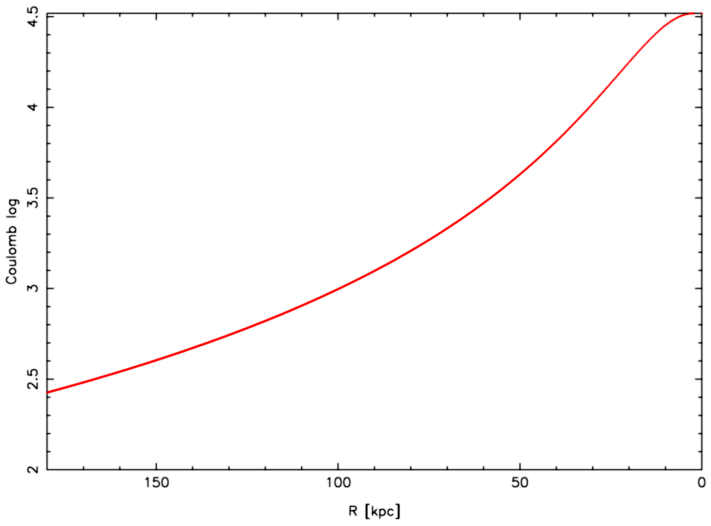

Figure 45: *The radial dependence of the CL for b_{max} = 20 kpc and the standard set of parameters (see §11.4).*

value of b_{max}. In the logarithmic plot, there is growing difference for this lower value in the outer region, but the absolute value of the friction here is very small – in the linear plot, both curves are completely identical in this region (from 60 kpc outwards) and virtually zero, so this part is not even shown.

Surprisingly, after all the best fit to the numerically integrated values is found with an appropriately chosen constant CL (see Fig. 47) – a method that is widely used and to which the previous strategy was originally meant as an improvement. It seems likely that it is a coincidence of the parameters and the radiallity of the merger that has lead to a cancellation among the various effects in the game – in the following chapters we will see that it is not a general feature and that our attempts for the improvement were not futile.

14.3 CL for multiple passages

We use the procedure described in §14.2 to get some clues about suitable values of CL in the situation where the secondary galaxy is not disrupted during the first passage across the centre of the primary. The best result from §14.2 (CL=4) was not satisfying in this case, see Fig. 48. The numerical values and values from the model fit nicely in the time before the first passage (that happens around 1000 Myr), but for the slow velocities that occur later, the CL=4 is a dramatic overestimate. For a smaller constant value the agreement is better for the slower velocities, but naturally worse for the faster part in the beginning.

We thus tried do derive the values of CL from the actual velocity of the secondary, as it is described in §14.2 using different values of b_{max}. This procedure shows different (but also unsatisfactory) behaviour: When it fits nicely for large velocities, it largely underestimates the friction for small velocities. Increasing the b_{max} increases values for the fast stage even beyond desirable level, still keeping the friction for the slow later stages underestimated, see Figs. 49 and 50.

Thus, the best results are achieved combining both approaches see Fig. 51. We used the adaptive version of CL with a suitable chosen b_{max} that fits nicely in the high velocity regime. When the value of CL decreases under a chosen limit, we put this limit

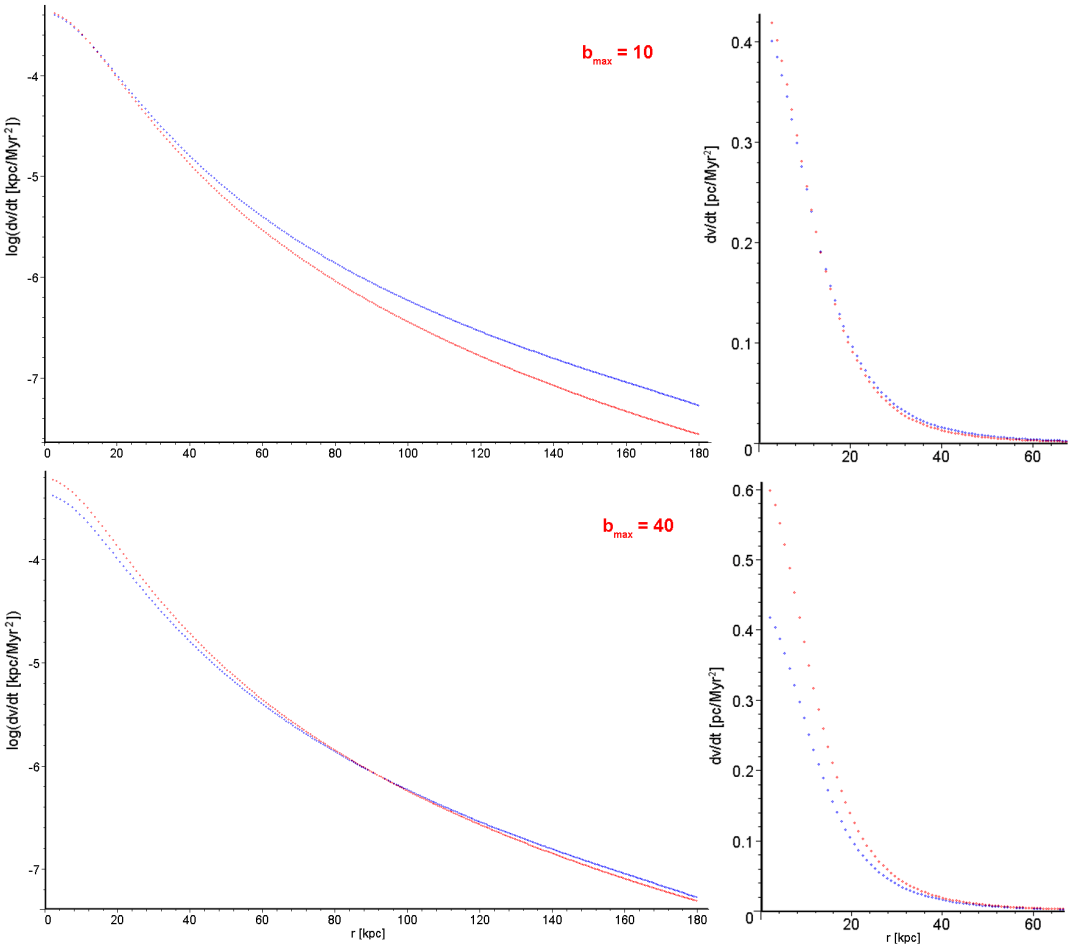

Figure 46: *The acceleration (deceleration) given by the dynamical friction to the secondary galaxy for the standard set of parameters (see §11.4). The red values are computed in the FORTRAN model, the blue ones numerically in Maple from Eq.* (30) *as explained in the text. In the top row, the model was run with* $b_{max} = 10$ *kpc, whereas in the lower one with 40 kpc. The plots in the first column are logarithmic, in the second linear.*

for the CL instead, dramatically improving the agreement for low velocities, if the limit is chosen wisely.

This procedure is rather cumbersome, but feasible. We use the potentially time-consuming numerical method only to adjust the parameters for the Chandrasekhar formula from the examination of the movement of a galaxy as a whole, as this does not require a lot of computation. Then we use the values to run the model based on the Chandrasekhar with a large amount of test particles for the secondary galaxy – a situation when the numerical integration for every individual test particle would be virtually impossible.

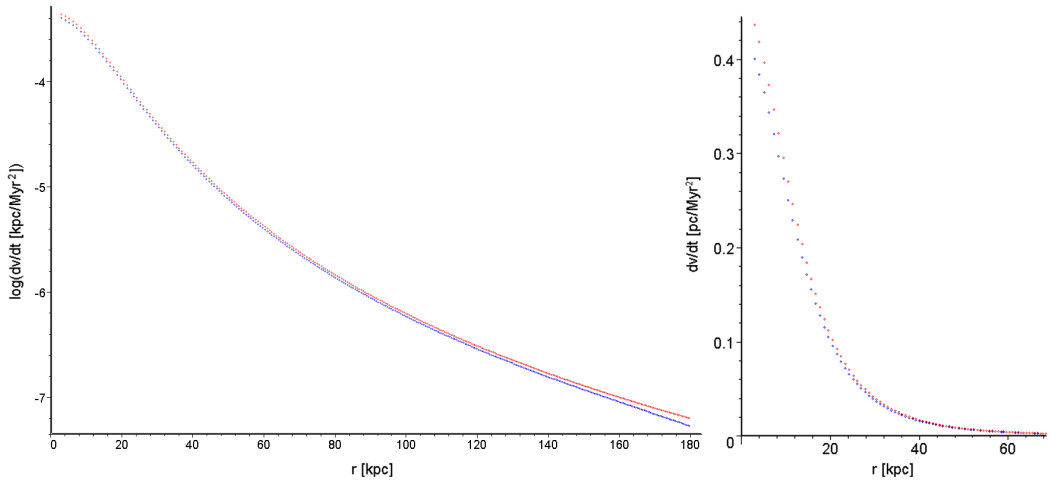

Figure 47: *The same as in Fig. 46 but for the constant value of the CL (equal to 4).*

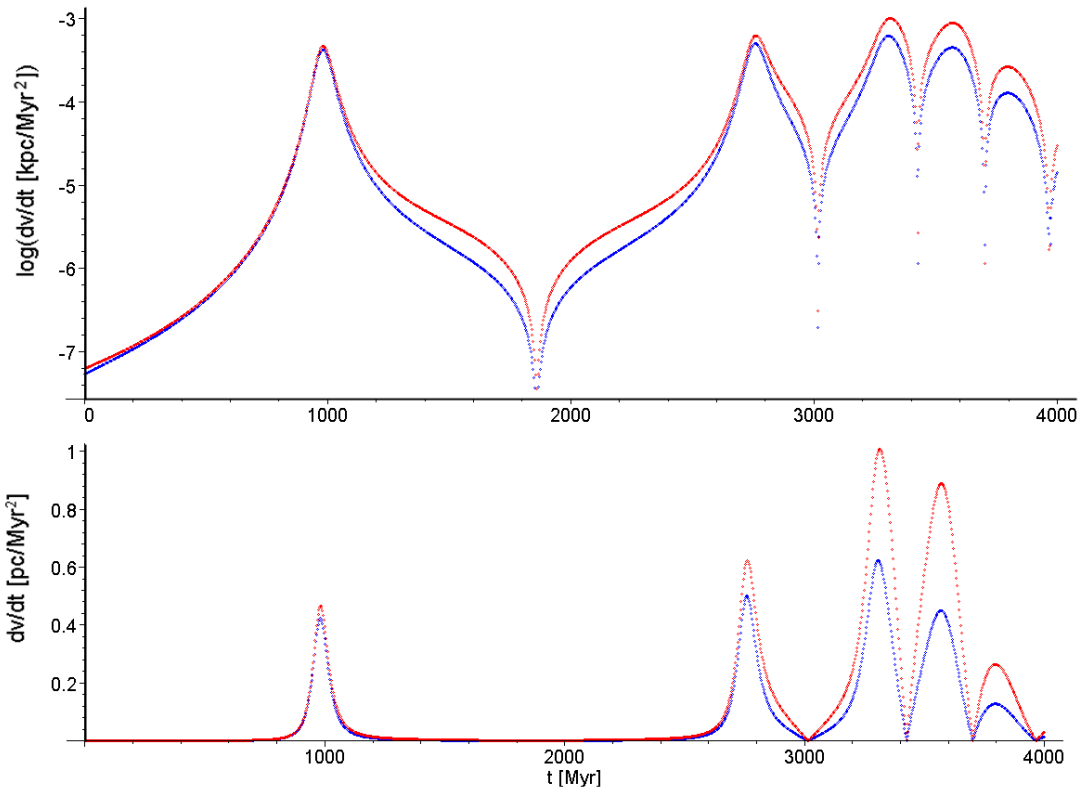

Figure 48: *The acceleration (deceleration) given by the dynamical friction to the secondary galaxy during multiple passes through the centre of the primary for the standard set of parameters (see §11.4) and for the constant value of the CL (equal to 4). The red values are computed in our model, the blue ones numerically in Maple. The upper graph is in the logarithmic scale, the lower is linear. Every peak corresponds to a passage through the centre, the drops in the logarithmic graph mark the turning points of the secondary.*

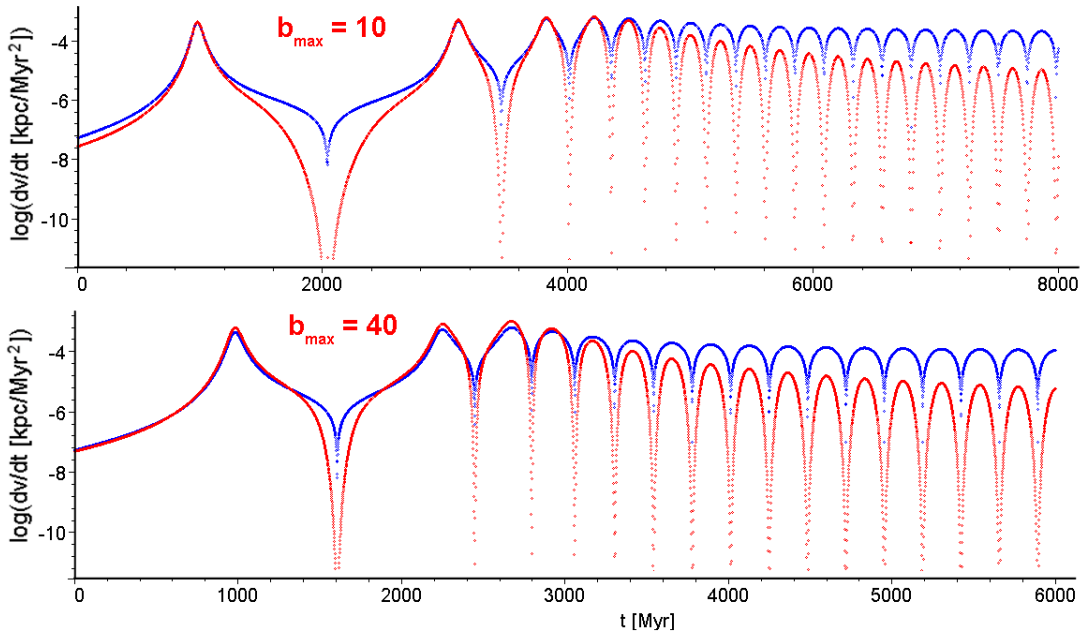

Figure 49: *The dynamical friction for the multiple passages of the secondary galaxy in the logarithmic scale. The red lines show the values from our model with CL computed from the actual velocity using* b_{max} *= 10 kpc (top) and* b_{max} *= 40 kpc (bottom). The blue lines represent the corresponding numerical values, see in text.*

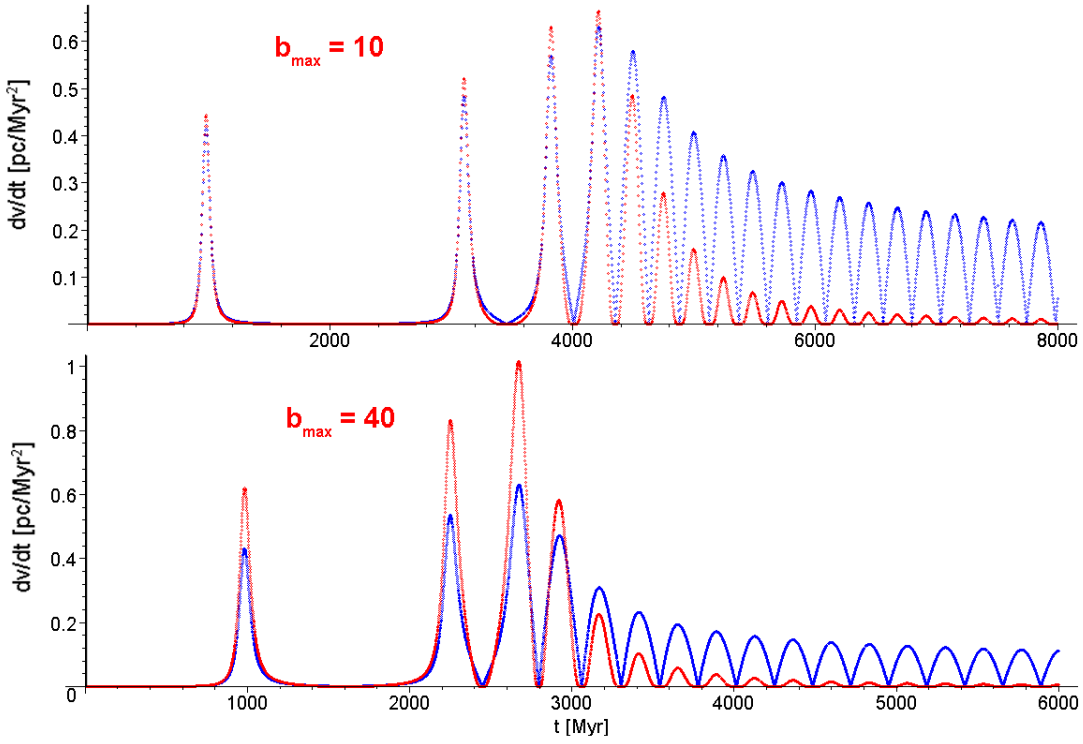

Figure 50: *The same as in Fig. 49, but in the linear scale.*

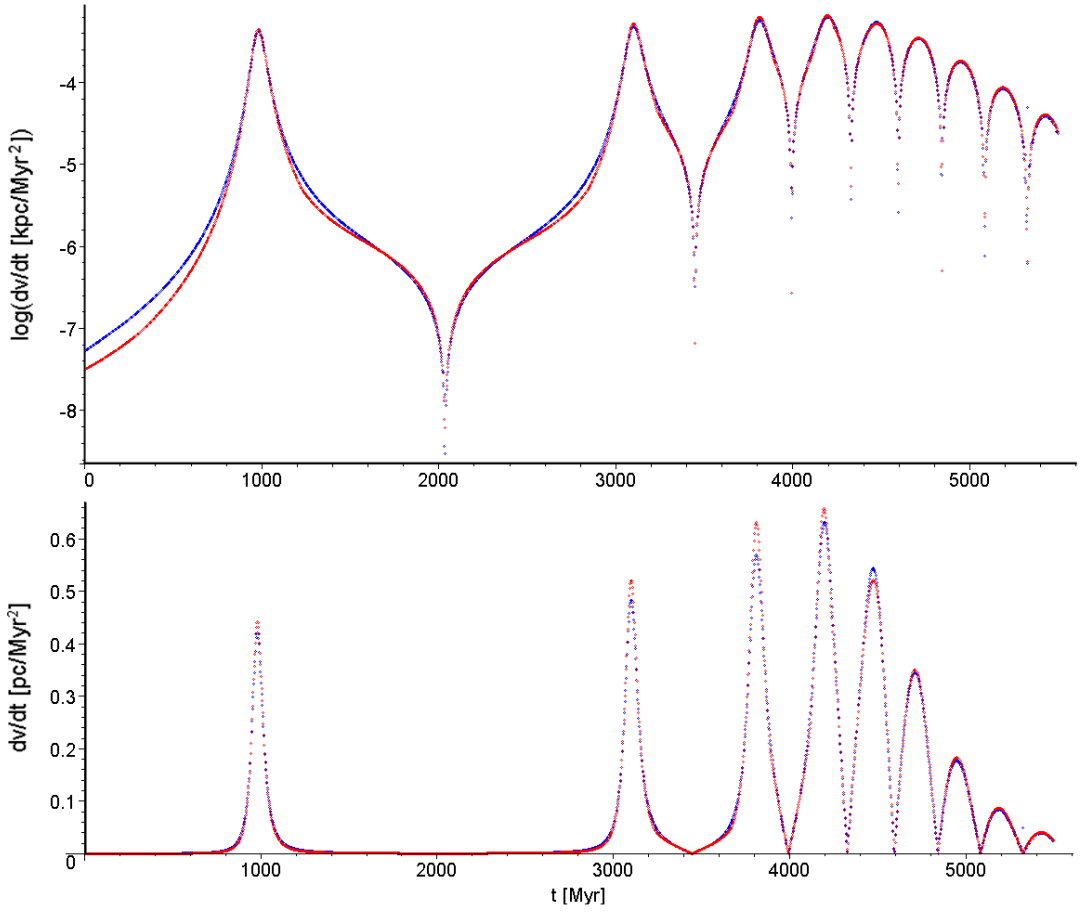

Figure 51: *The logarithmic and linear plots of the time dependence of the dynamical friction for multiple passages of the secondary galaxy, using* $b_{max} = 10$ *kpc together with the lower limit* $CL = 2$*. Red values are computed in the model, blue values are numerical, see in text.*

15 Dynamical friction and our model

A lot has been written and researched about the orbital motion of a dynamically braked body moving on a nearly circular orbit, as for this kind of motion, the dynamical friction is the fundamental effect influencing the shape of the orbit. It makes the body gradually spiral down to the centre of the galaxy it orbits, decreases the ellipticity of the orbit and so on.

The radial motion has not been much explored from this viewpoint. After one passage of the secondary galaxy through the primary, it is not a significant effect, as will be shown later. But when we wish to date the merger more accurately or generally to study the merger and the shells in detail, we have to consider considering this phenomenon.

15.1 Incorporation of the friction in the simulation

The question of incorporation of the dynamical friction in the simulations of the shell formation is tricky. In a fully self-consistent simulation, the dynamical friction would be automatically included, but such a simulation would be extremely demanding on resources – for the friction to be really well simulated, the number of particles of primary galaxy should not be several orders of magnitude smaller than the true amount of stars in the galaxies. Joining the stars in a smaller amount of more massive objects systematically overcounts the friction. Prugniel and Combes (1992); Wahde and Donner (1996), both cited in Peñarrubia et al. (2004), have indeed shown that the dynamical friction is artificially increased if the particle number is small. Using the analytical formula for the friction is not devoid of problems, but in some respects it could be more accurate than some of the self-consistent simulations.

On the other hand, the number of the particles of the secondary is an important quantity for the visibility of the shells in the simulations. And for the large number of required test particles ($\sim 10^6$) that represent just the secondary galaxy, even our "simple" simulations take hours of computation on a contemporary desktop computer. Furthermore, to explore the parameter space we have to run a lot of simulations, so we can really use a handy (semi-)analytical formula.

We can easily add the acceleration given by Eq. (26) into the equation of motion, where for ρ_0 we substitute the density of the primary galaxy in the position of the secondary galaxy. The density is given by (2), where we put the parameters of the primary galaxy for the mass and the Plummer radius. The velocity dispersion σ is also related to the primary galaxy in the given position and for its square we have Eq. (5), or better (6) that have been briefly derived in §9.2.

Using the Eq. (26) for the dynamical friction automatically assumes **Maxwell velocity distribution** (Eq. 25). This is not exactly true for the Plummer sphere, but the difference is small and the true velocity distribution in real galaxies is not known, so we cannot do much better, or say exactly how big mistake do we make.

The secondary galaxy is here treated as a **point mass** what artificially increases the friction, because as we have already seen (§11.3) the extended character of the galaxy softens the force. Specially the stars with a small impact parameter with respect to the centre of the secondary galaxy fly straight through it and their effect is significantly reduced compared to the Chandrasekhar formula for the point mass. The overestimation of the dynamical friction is not a crucial problem as we want to estimate how much the shell system is influenced by it – we can assume that the reality is not worse than our results and we get the upper bound on the effect.

The **Coulomb logarithm (CL)** is taken as a constant in the sense that we use

Eq. (26) which was derived with this assumption, however we allow it to vary in our simulations. We discuss the choice of the values of the CL in detail in §§14.2 and 14.3.

15.2 The comparison with the LMC

After inclusion of the Chandrasekhar formula in the code, as it is described in §15.1, we carried out a small test of its consistency. Our model is primary meant for radial encounters, but in this case we compared the motion of the secondary galaxy with friction on a rather circular orbit to the simulation of Růžička (2006) for the Magellanic Clouds.

Following this work, we integrate the motion of the galaxies 4 Gyr backwards. Both galaxies are again Plummer spheres, the secondary is supposed to be the Large Magellanic Cloud (LMC) and for the initialisation of its parameters we have used the data from Růžička (2006). The primary is the Milky Way galaxy with the mass of 10^{12} $M_\odot$ and the Plummer radius 40 kpc. The initial (today's, in fact) distance of the centres of the galaxies is 50 kpc, the mass ratio is 0.02 and the relative speed 270 km/s. The Plummer radius of the LMC is taken to be 3 kpc.

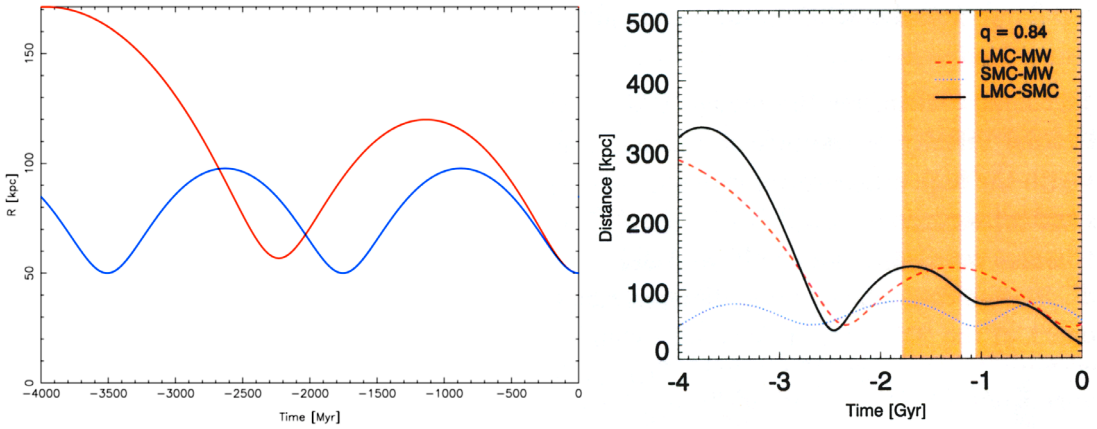

Figure 52: *Left panel: The red line shows the time dependence of the distance of "our LMC" and "our Milky Way" with friction, blue is the development without taking friction into account. Right panel: Results of the simulation by Růžička (2006), see also Růžička et al. (2007). For us, the red dashed line is relevant, as it also shows the time dependence of the LMC – Milky Way distance.*

The comparison is optimistic, see Fig. 52. We cannot expect a better agreement due to simplicity of our model of the LMC, as the real galaxies are quite different and for the Milky Way we model just the halo, and even the halo is only approximate. Adam Růžička's model is much more sophisticated and realistic. But given the simplicity of the model, we reached a reasonable agreement and so we conclude we have included the friction in the simulations successfully.

15.3 Dynamical friction in a radial merger

First, we look at the dynamical friction in the framework of the original model that assumes an immediate and complete disruption of the secondary galaxy at a distance very close to the centre for the primary galaxy.

We adopt our standard set of parameters (see §11.4) and we put the CL to be constantly 4 during the whole process – this choice is justified in §14.2. For this case the infall of the secondary is not much affected by the dynamical friction, see Fig. 53.

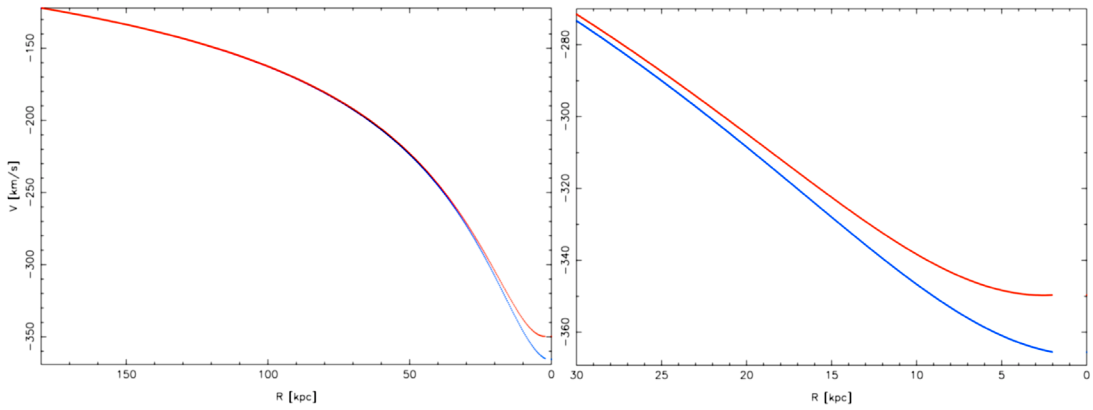

Figure 53: *The radial dependence of the velocity for the infall of the secondary galaxy with the standard set of parameters (see §11.4). The red line accounts for the friction, the blue line does not. The right panel zooms at the central 30 kpc.*

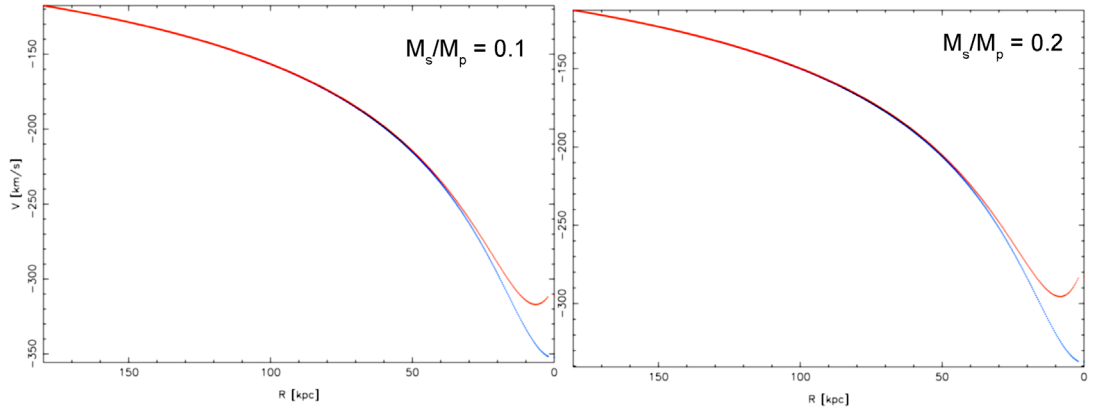

Figure 54: *The radial dependence of the velocity for the infall of the secondary galaxy with the standard set of parameters (see §11.4) except for the mass of the secondary galaxy, as the secondary-to-primary mass ratio is 0.1 in the left panel and 0.2 in the right panel. The red line accounts for the friction, the blue line does not.*

Ignoring the friction, the galaxy starting from 180 kpc reaches the centre of the primary in 972 Myr, with the friction the time is almost unchanged (974 Myr) and the effect on the velocity is also small.

We further increased the secondary-to-primary mass ratio in favour of the secondary galaxy to 0.1 and 0.2, respectively. Using the procedure described in §§14.2 and 14.3 we determined the most suitable choice of the Coulomb logarithm for those cases – it is derived from the velocity of the secondary with $b_{max} = 10$ kpc, but set to the fixed value of 0.8 if it would be smaller. The other parameters have been kept. The friction increases the time to the passage around the centre of the primary to 940 from 936 Myr for the ratio of 0.1 and to 902 from 896 Myr for 0.2. This is again not a big difference, but from Fig. 54 it is clear that in those cases the stars that we (up to the moment of the disruption) take to be bound to the secondary galaxy will have much smaller velocities at the end of the infall, when the friction is taken into account. This surely affects the possible future shell structure of the system. However, it remains questionable whether we can use this model for the mass ratio of 1:5. But obviously it was worthy to have a look on the faith of the dynamical friction for a more massive secondary galaxy.

15.4 Multiple passages

In this section we assume that the secondary galaxy is not disrupted during the first passage through the centre of the primary and we will investigate its further adventures in such a case.

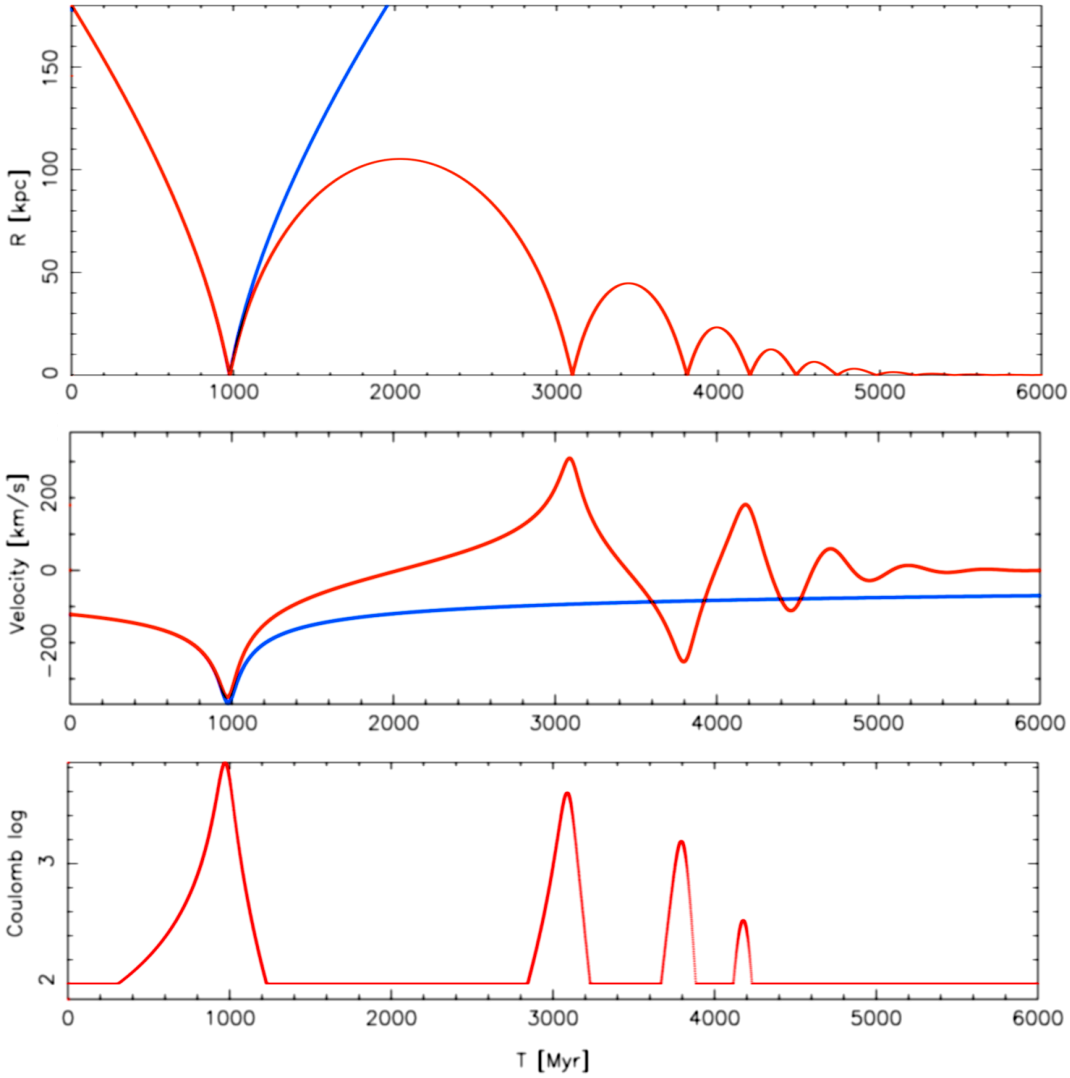

Figure 55: *The time development of the distance between the centres of the galaxies, their relative velocity and the CL for the merger with the standard set of parameters (see §11.4), including the multiple passages. The red lines account for the friction, the blue lines do not.*

We use again the standard set of parameters (see §11.4). In §§14.2 and 14.3, we derived that the best choice of the CL for the situation with multiple passes in our framework is either the adaptive CL with $b_{max} = 10$ kpc or the constant value of two, whichever is larger at a given point. Fig. 55 shows the result of this simulation. From there, it is obvious that the dynamical friction plays an essential role in the multiple passages. First of all the secondary galaxy was given an escape velocity at the beginning, so the dynamical friction is completely responsible for its capture, otherwise it would simply fly away to infinity. Furthermore, the amplitude of the oscillations is heavily damped and the secondary galaxy ends its voyage in the centre of the primary.

Keeping the rest of the standard set of parameters and varying the initial velocity, the time of the damping does not become comparable with the estimated lifetime of the universe (14 Gyr) until the velocity reaches about 1.4 times the escape velocity. On the other hand, lowering the initial speed of the secondary galaxy to 70% of the escape velocity (keeping other parameters fixed), the course of the merging looks similar. We even found out that when applying the procedure of §§14.2 and 14.3 we do not have to change the settings of the CL. However, the times of the passages have changed. The first encounter of the centres of the galaxies occurs about 0.2 Gyr later, but at the moment when the initially escaping galaxy would be paying the second visit to the centre of the primary, the $0.7v_{esc}$ galaxy makes already the third passage. Overall, the final damping of the oscillations to negligible amplitudes occurs almost 1 Gyr earlier.

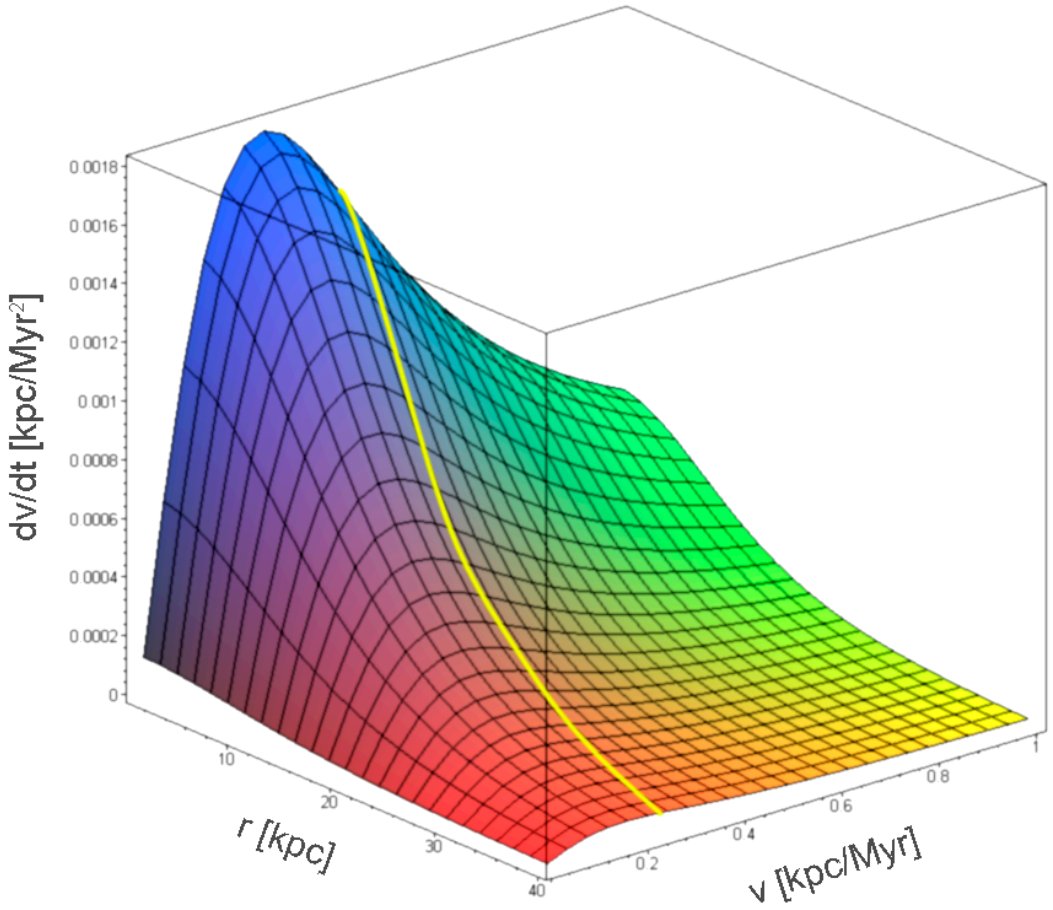

Figure 56: *The dependence of the friction according to Eq. 30 for a braked body with 0.02 of the mass of the primary galaxy on its velocity and position. The parameters of the primary follow the standard set of parameters (i.e.* $M_p = 3.2 \times 10^{11}\ M_\odot$ *and Plummer radius* $\varepsilon_p = 20$ *kpc). The yellow line corresponds to the first passage for the standard set of parameters (i.e. the braked body has the escape velocity in180 kpc, see §11.4).*

For the standard set of parameters, the choice of the escape velocity is rather favourable for the friction. During the first passage, the relative velocity of the galaxies is close to the value where the friction is maximal for the given primary galaxy, see Fig. 56. As the velocity is lowered, the situation gets even more favourable for friction, but

after further braking the efficiency of the friction falls of steeply. From the figure and figures in §14.3, it can be seen that most of the friction on the secondary galaxy occurs in the close proximity of the centre of the primary galaxy.

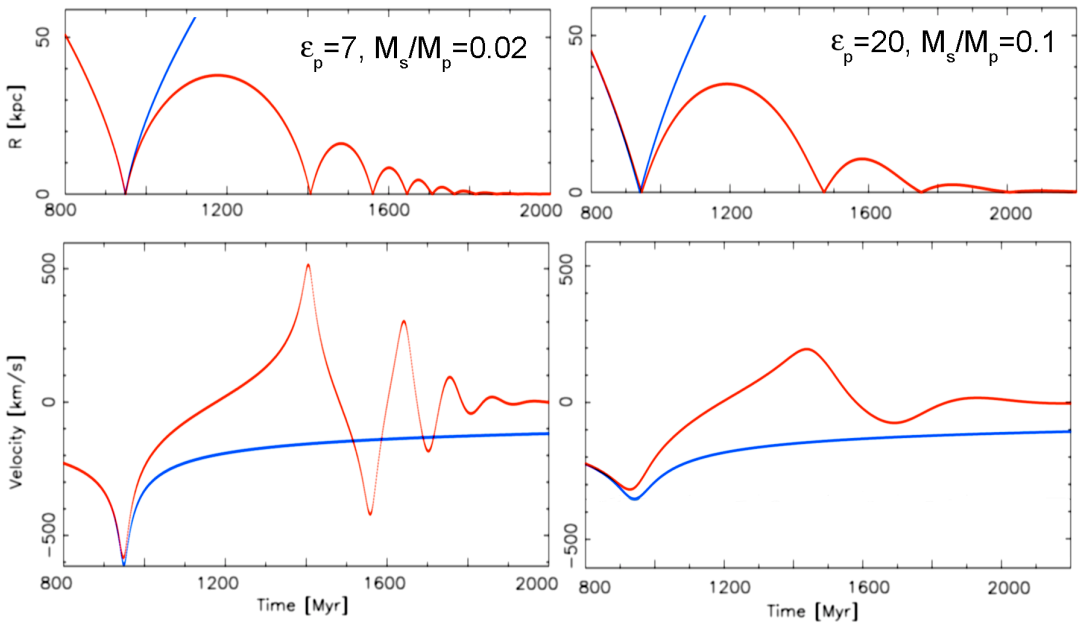

Figure 57: *The time development of the relative distance and velocity of the galaxies for two different mergers, including multiple passages . In both of the mergers the standard set of parameters (see §11.4) has been used with one exception. In the left column, the primary galaxy is more compact (ε_p = 7 kpc), in the right column the secondary is more massive (mass ratio 0.1). The red lines account for the friction, the blue lines do not.*

A big influence on the magnitude of the friction comes from the compactness of the primary galaxy and the mass of the secondary. First, we have changed the Plummer radius of primary (from 20 kpc) to 7 kpc and kept the rest of the standard set of parameters see Fig. 57 (left column). We have used the usual procedure to seek a suitable value of CL. A good fit is obtained using b_{max} = 3 kpc but CL not smaller than 2. In this case, the secondary galaxy is braked to almost still before it would reach the first turning point with ε = 20 kpc.

Increasing the mass of the secondary five times, the choice of the right CL is a little more subtle matter, but we finally reached a good agreement for b_{max} = 9 kpc and CL not lower than 0.75. The damping is a little slower than in the previous case, but needs much less passages, see Fig. 57 (right column). In Fig. 58 it is shown, how the efficiency of the friction varies with the changing secondary-to-primary mass ratio for different velocities. For very light secondary galaxies, the friction is small and the peak in its efficiency is in lower velocities. As the mass of the secondary increases, the efficiency of the friction increases as well and its maximum value moves quickly to 0.2 kpc/Myr (≅200 km/s) for the chosen fixed parameters of the primary galaxy. Increasing further the mass of the secondary, the friction increases at a slower pace and also the position of the peak moves slowly to almost 0.3 kpc/Myr for the mass ratio of 0.3.

15.5 Two-component model

Till this moment we have modelled the potential of the primary galaxy by one component which we have taken to be the luminous mass. In this section we will inspect

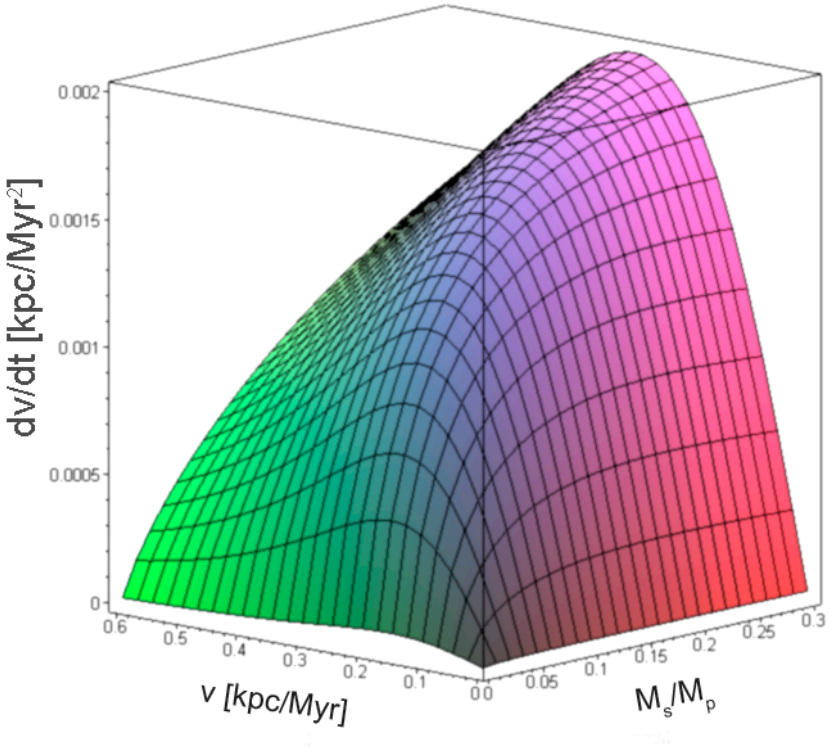

Figure 58: *The dependence of the friction in the centre of the primary galaxy according to Eq. 30 on the velocity and relative mass of the braked body. The primary galaxy conforms with the standard set of parameters (i.e.. $M_p = 3.2 \times 10^{11}$ $M_\odot$ and Plummer radius $\varepsilon_p = 20$ kpc).*

the effect of a dark matter halo added to the primary galaxy. Choosing the parameters for the halo, we sought inspiration inHumphrey et al. (2006). Although according to them the halo does not possess a Plummer profile, we adopt it again for simplicity. We have chosen the halo to be 20× heavier than the luminous component and to have the Plummer radius $\varepsilon_h = 60$ kpc. The luminous component has been chosen to be more compact with $\varepsilon_p = 7$ kpc while keeping its original mass $M_p = 3.2 \times 10^{11}$ $M_\odot$.

First, we again started the secondary galaxy in 180 kpc from the centre of the primary (the braking further out from the centre is at the level of the uncertainty of the simulation) with the escape velocity, which is now more than four times larger than in previous cases. With the usual procedure (see §§14.2 and 14.3) we found out that keeping simply $b_{max} = 20$ kpc is a suitable choice for the CL for the entire course of the merger. However the merger is not much glorious in this case – whole 6 Gyr after first passing by the centre (with a velocity of roughly 1,300 km/s) the galaxy reaches its first turning point, some 900 kpc away. It is unlikely that the object would reach such a distance without being captured by another galaxy and even if it was not the case, it returns back to the centre for the primary in a time too long for such a case to be interesting. The velocity in this setup is simply too high and the secondary moves to the area in the configuration space, where the dynamical friction is too inefficient, even though it is now due to a much larger mass, see Fig. 59.

For the comparison we have given the secondary galaxy (still in 180 kpc from the primary) the same velocity as it has in the standard set of parameters (roughly 130

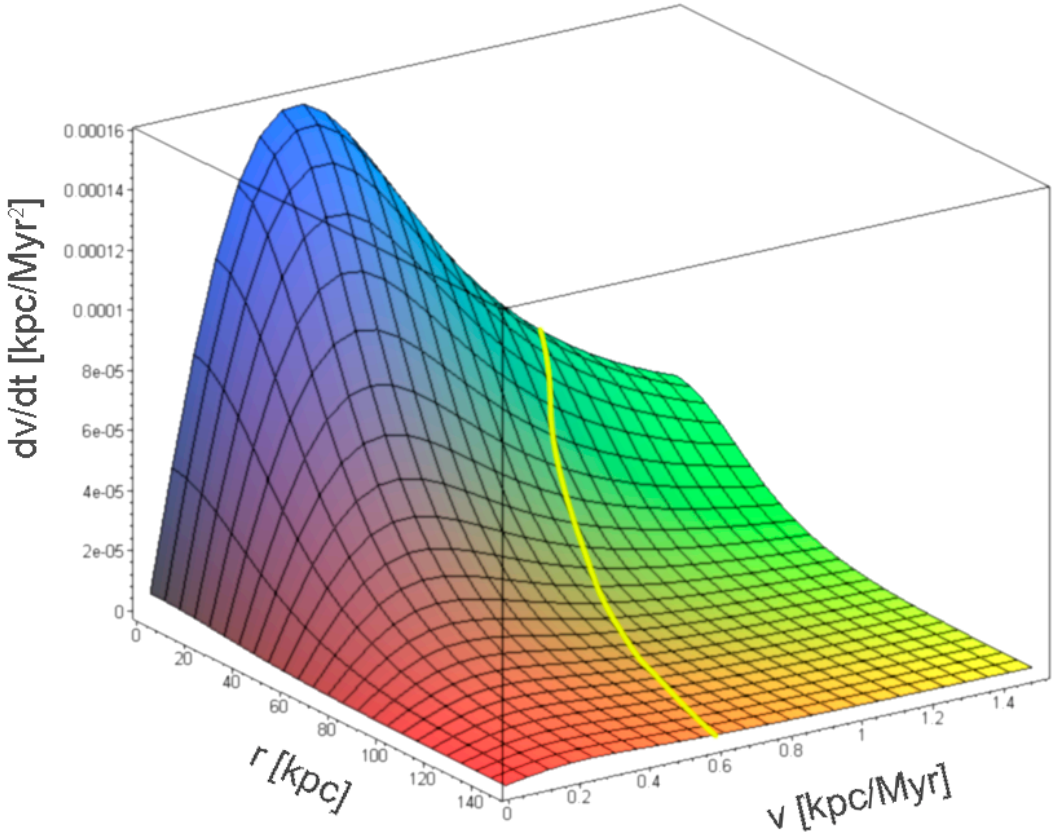

Figure 59: *The dependence of the friction from the halo (from Eq. 30) for a braked body with 0.001 mass of the halo on its position and velocity. The mass of the halo is* $M_h = 6.4 \times 10^{12}\ M_\odot$ *and Plummer radius* $\varepsilon_h = 60$ *kpc. The yellow line corresponds to the first passage of the body starting from 180 kpc with the escape velocity.*

km/s). The parameters for the halo and the luminous component of the primary have been kept. The CL was computed with $b_{max} = 5$ kpc but no lower than 1.1 for the luminous component, the friction form the halo is computed just with $b_{max} = 20$. Anyway, the secondary galaxy is accelerated to more than 1,000 km/s, again interfering with the efficiency of the braking. In the left column Fig. 60 it can be seen that the velocity is decreased only slightly during the first couple of passages. As the dynamical friction increases with the lowering velocity, the secondary galaxy gets braked more efficiently.

A dramatic braking can be achieved increasing the mass of the secondary 10 times, even when starting it from the full escape velocity with respect to the halo, see the right column of Fig. 60. The parameters of the primary galaxy are again kept, the CL for the luminous component is computed with $b_{max} = 4$ kpc but CL not lower than 0.7, for the halo we use $b_{max} = 20$ but keep CL not lower than 2.

Increasing again the mass of the secondary to 0.02 of the mass of the halo itself, its oscillations are damped as soon as in 1.2 Gyr from the first passage through the centre of the primary. In this case (not shown) it was again necessary to adjust the CL parameters – for the luminous mass we have $b_{max} = 3.5$ kpc but CL not lower than 0.2, for the halo $b_{max} = 23$ kpc but CL now lower than CL = 2.

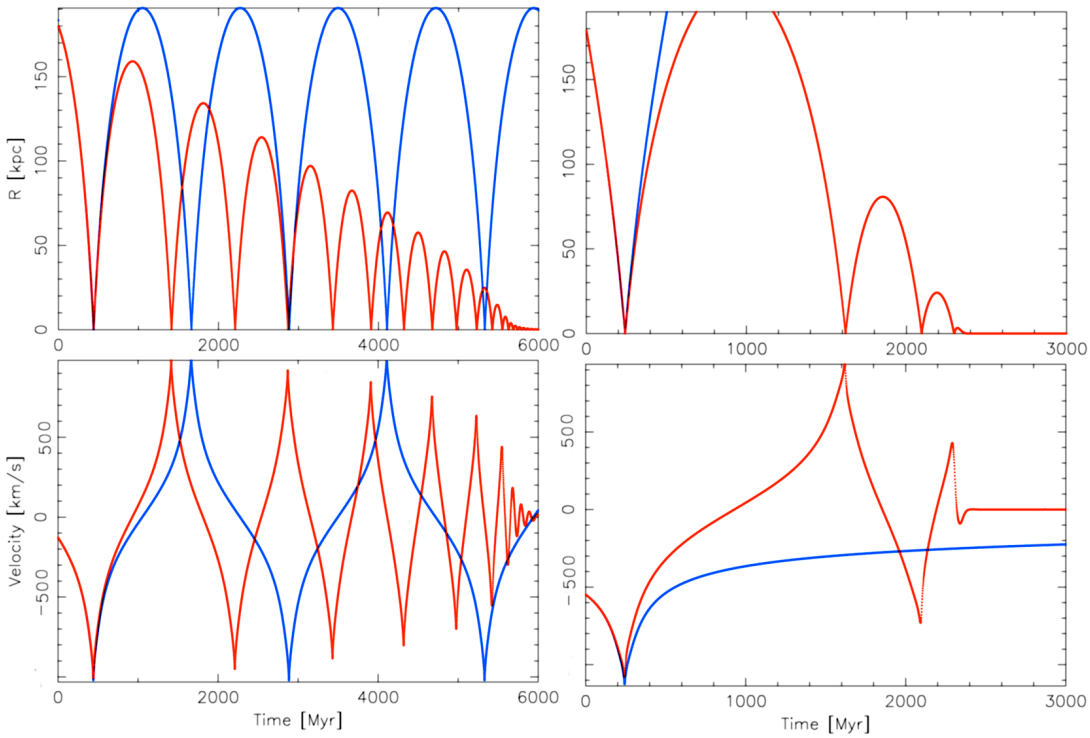

Figure 60: *The time development of the relative distance and velocity of the galaxies for two different mergers. The primary galaxy has a luminous component with the mass* $M_p = 3.2 \times 10^{11}\ M_\odot$ *and Plummer radius* $\varepsilon_p = 7$ *kpc and a 20× more massive dark matter halo with* $\varepsilon_h = 60$ *kpc. In the left column, the secondary galaxy (wighting 0.02 times the mas of the luminous component) started with the escape velocity only with respect to the luminous component. In the right column it started with the full escape velocity with respect to the halo, but it has a mass ratio to the luminous component of 0.2. The red lines account for the friction, the blue lines do not.*

Part V
Tidal stripping

In the whole Part IV we assumed that the mass of the secondary galaxy is always equal to a chosen constant. This is obviously not true in reality – as the secondary galaxy passes through the primary, the tidal forces strip its stars off and so we can expect the mass of the stars that stay bound to the secondary to gradually decrease. In this part we investigate this effect.

16 Tidal radius

The tidal forces acting on an object are often derived using the following picture: A massive body (secondary galaxy) as a whole follows the force acting on it in its centre of mass. But the force acting on outer parts of the body is different, as it is at different distances of the source (the primary galaxy). If this difference is larger than the binding force with the secondary for a given star, it is stripped off.

The tidal radius r_{tidal} is then defined as the distance (from the centre of the secondary), where the difference of the force of the primary from its force in the centre of mass of the secondary is just equal to the force from the secondary:

$$F_p(d - r_{tidal}) - F_p(d) = F_s(r_{tidal}), \tag{31}$$

where d is the separation between the centres of the galaxies and $F_p(r)$ and $F_s(r)$ is the force from the primary and the secondary for a given test particle (its mass is immediately cancelled out from the equation).

16.1 Tidal radius for point masses

Given the two bodies are point-like (with masses M_p and M_s), we can write Eq. (31) as:

$$\frac{G\,M_p}{d^2(1 - r_{tidal}/d)^2} - \frac{G\,M_p}{d^2} = \frac{G\,M_s}{r_{tidal}^2}. \tag{32}$$

Assuming further $r_{tidal} \ll d$ we can use the Taylor expansion $(1 - x)^{-2} \cong 1 + 2x$ for $x = r_{tidal}/d$ as it is then a small quantity. under this assumption we get a simple formula for the tidal radius:

$$r_{tidal} = d \sqrt[3]{\frac{M_s}{2\,M_p}}. \tag{33}$$

However, for two point masses we can get an exact result for the tidal radius. Not making any approximation in (32) we can cast it as a fourth-order polynomial

$$X^4 - 2\,X^3 + q\,X^2 - 2\,q\,X + q = 0, \tag{34}$$

where $X = r_{tidal}/d$ and $q = M_s/M_p$. A polynomial with an order less than five can be always solved. In our case, where q is positive, there are two real roots, from which we take the one that gives $r_{tidal} < d$ and thus $X < 1$. The second real root corresponds to a point of the other side of the primary galaxy that is not of interest for us. The expression for this root does not give much insight, but an interested reader can find it in Appendix B.

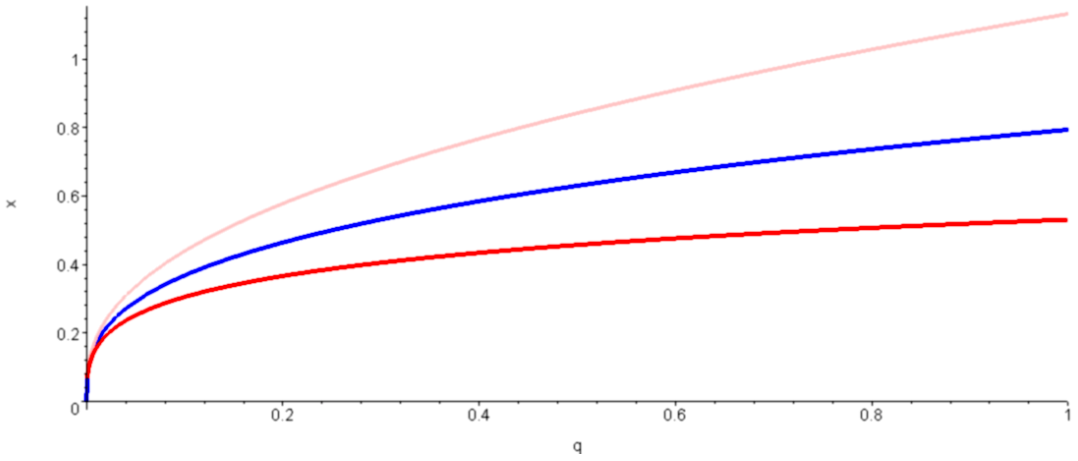

Figure 61: *Tidal radius for two point masses: the approximate solution (Eq. 33) is shown in blue, the exact solutions in red (the outer one in light red, the inner in dark red). The shows y-axis* $X = r_{tidal}/d$*, the x-axis shows the secondary-to-primary mass ratio.*

Eq. (31) gives the tidal radius for the particles on the line connecting the centres of the two bodies – we call it the inner tidal radius. Similarly we can write an equation for the particles on the other side of the secondary than the centre of primary lies:

$$F_p(d) - F_p(d + r_{tidal}) = F_s(r_{tidal}). \tag{35}$$

It again leads to a fourth-order polynomial for which we can obtain the root that we call the outer tidal radius. The approximate solution (33) is the same for both equations (31 and 35). Let us remark that the tidal radius is in any case just proportional to d as there is no other scale in the problem. Fig. (61) shows the dependence of the three radii on the mass ratio of the bodies. We can see that for all relevant ratios the approximate formula is just between the inner and the outer tidal radius.

16.2 Tidal radius for spatially extended bodies

The tidal radius for a point mass is in some sense an oxymoron, as these object have zero proportions by definition. For spherically symmetric bodies we can write Eq. 32 as

$$\frac{G\,M_p(d - r_{tidal})}{(d - r_{tidal})^2} - \frac{G\,M_p(d)}{d^2} = \frac{G\,M_s(r_{tidal})}{r_{tidal}^2}, \tag{36}$$

where $M(r)$ is the mass enclosed in the radius r. Particularly for the Plummer sphere we get this value integrating Eq. 2 over the sphere with the radius r:

$$M(r) = \frac{M}{(1 + \varepsilon^2/r^2)^{3/2}}, \tag{37}$$

where M is the overall mass of the body and ε is the Plummer radius (see §9). Unfortunately this makes the equation too complex to be easily solved. Let us compare graphically the tidal radii for point masses and Plummer spheres of the same overall masses just for one particular case – Fig. 62.

The figure (or a simple thought) shows that the notion of the tidal radius in a general potential makes sense only when the force grows with the distance. Otherwise

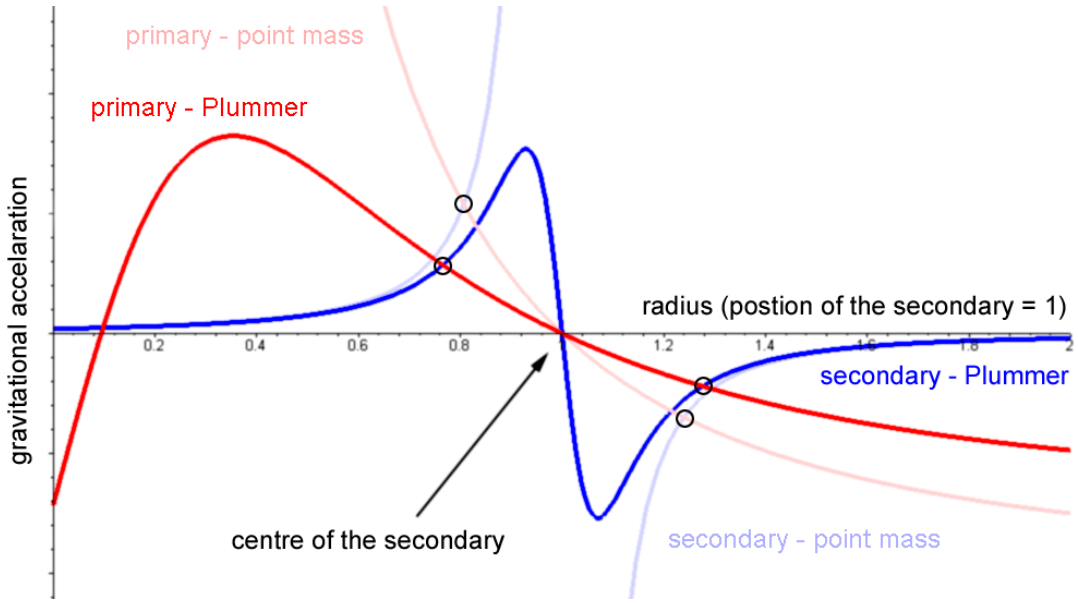

Figure 62: *The outer and inner tidal radii (marked with circles) for the point masses and Plummer spheres with the secondary-to-primary mass ratio of 0.02. In the Plummer case, the Plummer radius of the primary is 0.5 of the distance between the bodies and the Plummer radius of the secondary is 0.1 of the same quantity. Blue lines (light blue for the point mass, dark blue for the Plummer sphere) show the gravitational force of the primary in arbitrary units, red lines (light red for the point mass, dark red for the Plummer sphere) show the difference between the gravitational force of the primary in a given point and its value in 1, where the centre of the secondary is. The tidal radii are the points of intersection of corresponding curves.*

the tidal force acts in the same direction as the gravitation of the secondary and thus cannot strip off any mass. In the Plummer potential the force reaches its maximum in $\sqrt{2}\,\varepsilon/2$, so the tidal radius is not defined under this radius, whereas for the point masses it is defined everywhere.

17 Tidal stripping and our model

The idea of the tidal radius is just an approximation to the complex processes during encounters of two extended bodies. It also does not define a sphere around the centre of the secondary galaxy, but as we have seen, it is different for various locations, with the lowest value towards the centre of the primary galaxy and the highest on the opposite side. For these reasons it is not really useful to improve its evaluation and so we have used the approximate formula (33) that as we have seen gives the values somewhere in the middle between the two extreme values of the tidal radius. For M_p we put the mass of the primary galaxy enclosed within the radius equal to the actual separation between the centres of the galaxies. Because the tidal radius does not evolve dramatically during the encounter, we put for M_s the mass of the secondary derived in the previous time step.

The mass of the secondary decreases until the moment when it comes to the point of the the maximum of the force of the primary in $\sqrt{2}\,\varepsilon_p/2$ (i.e. about 14 kpc from the centre of the primary for the standard set of parameters). From this point we do not compute the tidal radius any more and the mass of the secondary remains fixed, see

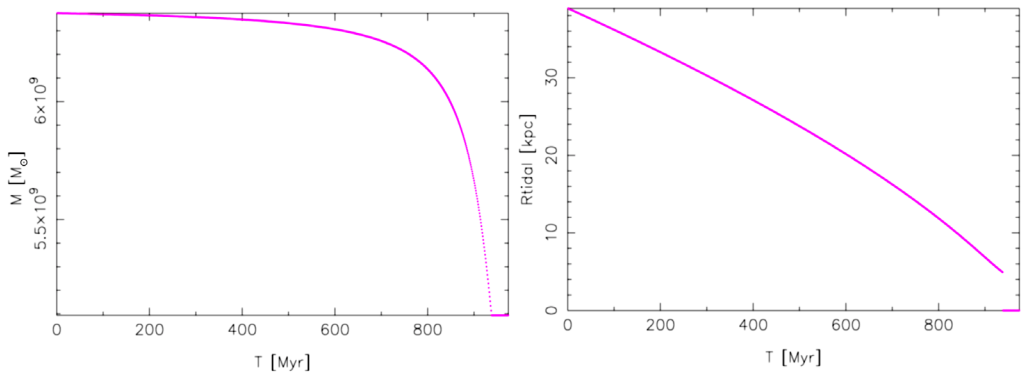

Figure 63: *The time dependence of the mass of the secondary galaxy and its tidal radius for the standard set of parameters (§11.4).*

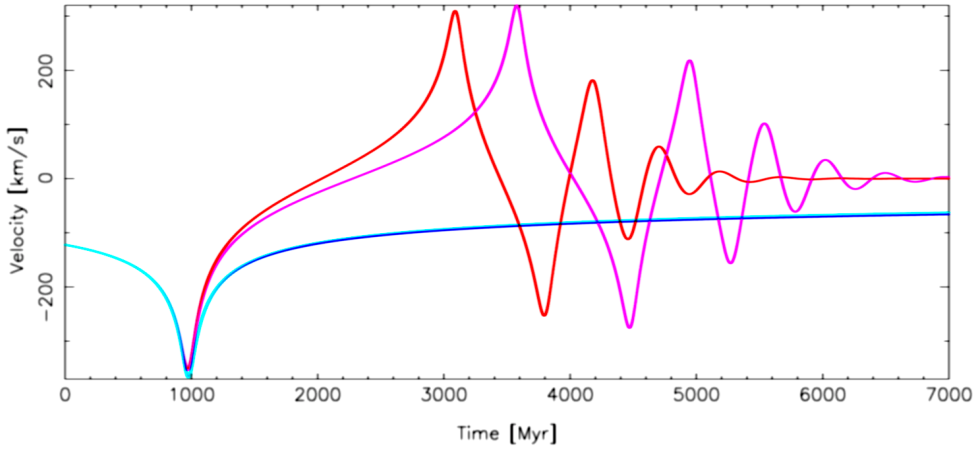

Figure 64: *The time dependence of the velocity for multiple passages of the secondary galaxy with the standard set of parameters. (§11.4). Dark blue: no friction nor tidal stripping; light blue: tidal strapping, no friction; red: friction, no tidal stripping; pink: tidal stripping and friction.*

Fig. 63. The figure includes the friction, but as the mass is decreased only during the first passage by the centre (when the influence of the friction is small) it does not make much difference.

For our standard set of parameters (see §11.4) we carried out the simulation of the merging with all the possible combinations of the friction and tidal stripping being on or off, see Fig. 64. Without the friction the effect of the mass loss is not significant. With the dynamical friction, we see how the tidal stripping decreases the efficiency of the friction, but it does not change its overall effect of slowing down the galaxy to almost rest, it only occurs later – even lowered by the tidal stripping the friction radically changes the course of the merger.

In reality, the secondary galaxy would start to expand after its outer layers were stripped off. Thus more and more stars would be stripped during the following encounters with the centre – the speed and magnitude of this expansion is not known and so our model does not take this effect into account as the mass of the secondary is changed only during the first passage. This is one of the points to be explored in the future.

Part VI
Conclusions and future plans

As described in Part II, most of the simulations of the shell formation have been carried out more than 15 years ago. Motivated by the discovery of the shells in the host galaxy of a quasar (see §8) we came back to the old problem with the new possibilities offered by the now widely available advanced computer technology. We have investigated the effect of the dynamical friction during the presumed shell-forming mergers. For this purpose we have developed a semi-analytical procedure (§§14.2 and 14.3) based on the Chandrasekhar formula (see §13.1) which improves the computation of the magnitude of the friction.

Given the large uncertainty in the initial conditions for the merger we would like to explore a large portion of the parameter space. However the fully self-consistent simulations are heavily demanding on the CPU time and for them to be realistic and useful (concerning the contrast of the shells) they have to include a large number of particles. Thus we are trying to develop a model that would utilise test particles and at the same time at least to some extent reflect the real processes that occur during galactic mergers.

From the results shown in §15 it is clear that the dynamical friction can have a significant effect during the shell formation process and should not be neglected in their exploration. We tried to increase the accuracy of the dynamical friction given by the Chandrasekhar formula via the numerical evaluation of the integral in Eq. (30) that describes the inhomogeneous distribution of stars in the Plummer sphere and the derivation of which was allowed by the assumed radiality of the merger. We have shown that the Coulomb logarithm does not represent the less approximate formula (Eq. 30) well and we have found a procedure to adjust the value of the Coulomb logarithm so that we can achieve a better agreement.

However, we must always keep in mind that even those "better" values are subject to the same "principal inaccuracies" (as we have called them in §14.1 and described in §13) as does the Chandrasekhar formula, thus the real values of the dynamical friction can be still different. Still, our simulation can help establishing a better estimate for dating the shell structures in the galaxies. Furthermore they show that the dynamical friction can bring the stars of the secondary galaxy into tightly bound orbits in the primary.

The approach used in Part IV has an important flaw, namely keeping the mass of the secondary galaxy constant throughout the simulation. During a realistic merger, a gradual stripping of the mass from the secondary galaxy and thus the decrease in its mass inevitably occurs. This effect obviously decreases the efficiency of the dynamical friction and we give a simple discussion of it in Part V. The results of this Part show that the tidal forces probably leave a large portion of the mass of the secondary in a bound system during the first passage across the centre of the primary. The dynamical friction can bind this remnant of the secondary galaxy to the primary even when the initial velocities are large (e.g. tens of per cent beyond the escape velocity) so a new generation of more tightly bound shells can be created during the following passages.

On the other hand, this declining efficiency of the dynamical friction by mass loss can be compensated by the decrease of the orbital energy via the asymmetric mass loss. This effect has been demonstrated by Heisler and White (1990) in their self-consistent simulation of the secondary galaxy, where the apocentre of the satellite has moved about a quarter of its original value towards the centre of the primary, while

still not taking into account any energy transfer between the galaxies, thus also not the dynamical friction. Their discovery is briefly described in §6.5 and our simulation is momentarily unable to reproduce it.

In §15.5 we introduced the second component of the primary galaxy as a dark matter halo. The mass of the halo increases the dynamical friction, but at the same time increases the velocity of the infalling secondary and for high velocities the friction is inefficient. When we increase the mass of the secondary to regain the original (before the addition of the halo) secondary-to-primary mass ratio, the efficiency of the friction rapidly increases.

In the future we wold like to improve our time-efficient model to be even closer to reality. It is necessary to enrich the simulations of the gradual expansion of the tidally stripped secondary galaxy. For this purpose we have to first investigate the details of process. At least for some chosen simulations we would like to obtain the comparison with a self-consistent simulations – for this we obviously need first to develop a viable self-consistent model. Another big issue is the behaviour of the gas during the shell formation, as it can give us some clues on the connection with the AGN. The deep investigation of this shall be the topic of our further work.

Appendix

A Units and conversions

When dealing with galaxies, we need to describe objects and time spans incommensurable with our daily experience that defines the standard sets of units, such as SI. Throughout the text we thus use a set of units adapted for this task – we measure the mass in $M_\odot$ the length in kpc and the time in Myr. Although their meaning is clear, they sometimes give rise to rather awkward derived units. We will briefly list the most prominent of them (together with the basic ones) and give their relation to the SI and cgs units.

Time: 1 Myr $= 10^6$ yr $= 3.156 \times 10^{13}$ s

Distance: 1 kpc = 3 262 ly $= 3.086 \times 10^{19}$ m $= 3.086 \times 10^{21}$ cm

Mass: 1 $M_\odot = 1.989 \times 10^{30}$ kg $= 1.989 \times 10^{33}$ g

Velocity: 1 kpc/Myr = 977,8 km/s $= 9.778 \times 10^7$ cm/s (the roundness of this value allows for an easy conversion for most of our plots)

Acceleration: 1 kpc/Myr^2= 3.098×10^{-8} m/s^2 $= 3.098 \times 10^{-6}$ cm/s^2

Density: 1 $M_\odot$/kpc^3= 6.768×10^{-29} kg/m^3 =6.768×10^{-32} g/cm^3

Grav. unit: 1 kpc^3/Myr^2/$M_\odot$ = 14,83 m^3/s^2/kg = 14 830 cm^3/s^2/g –
thus G = 6.674×10^{-11} m^3/s^2/kg = 4.500×10^{-12} 1 kpc^3/Myr^2/$M_\odot$

B Expressions for the tidal radius

Here we give the analytical formulae for the tidal radii in the system of two point masses as discussed in §16.1. For the inner tidal radius we have:

$$\frac{r}{d} = \frac{1}{2} + \frac{\sqrt{3}}{6}\left(\frac{\sqrt{y}}{\sqrt[6]{z}} - \sqrt{6 - 4\,q - \sqrt[3]{qz} - \sqrt[3]{\frac{q^5}{z}} + 6\,\sqrt[6]{z}\sqrt{\frac{3}{y}}(q+1)}\right),$$

where

$$y = (3 - 2\,q)\sqrt[3]{z} + \sqrt[3]{qz^2} + q^{5/3}$$

$$z = 54 + q^2 + 6\sqrt{81 + 3\,q^2}$$

and for the outer tidal radius we get similar expressions:

$$\frac{r}{d} = \frac{1}{2} + \frac{\sqrt{3}}{6}\left(\frac{\sqrt{u}}{\sqrt[6]{v}} + \sqrt{6 + 4\,q - \sqrt[3]{qv} - \sqrt[3]{\frac{q^5}{v}} + 6\,\sqrt[6]{v}\sqrt{\frac{3}{u}}(q-1)}\right),$$

where

$$u = (3 + 2\,q)\sqrt[3]{v} + \sqrt[3]{qv^2} + q^{5/3}$$

$$v = -54 - q^2 + 6\sqrt{81 + 3\,q^2}$$

and in all the expressions we use

$$q = \frac{M_s}{M_p}.$$

References

Arp, H.: 1966a, *Atlas of peculiar galaxies*. Pasadena: California Inst. Technology, 1966.

Arp, H.: 1966b, 'Atlas of Peculiar Galaxies'. ApJS **14**, 1–+.

Athanassoula, E. and A. Bosma: 1985, 'Shells and rings around galaxies'. ARA&A **23**, 147–168.

Balcells, M.: 1997, 'Two Tails in NGC 3656 and the Major Merger Origin of Shell and Minor-Axis Dust Lane Elliptical Galaxies'. ApJ **486**, L87+.

Balcells, M. and D. Carter: 1993, 'High-resolution rotation curves of NGC 7626: Dynamics of a young kinematically peculiar core'. A&A **279**, 376–384.

Balcells, M. and P. J. Quinn: 1990, 'The formation of counterrotating cores in elliptical galaxies'. ApJ **361**, 381–393.

Balcells, M. and R. Sancisi: 1996, 'Gas Accretion in NGC 3656 (ARP 155)'. AJ **111**, 1053–+.

Balcells, M., J. H. van Gorkom, R. Sancisi, and C. del Burgo: 2001, 'H I in the Shell Elliptical Galaxy NGC 3656'. AJ **122**, 1758–1769.

Barnes, J. E.: 1989, 'Evolution of compact groups and the formation of elliptical galaxies'. Nature **338**, 123–126.

Bennert, N., G. Canalizo, B. Jungwiert, A. Stockton, F. Schweizer, M. Lacy, and C. Peng: 2007, 'Spectacular Shells in the Host Galaxy of the QSO MC2 1635+119'. In: *American Astronomical Society Meeting Abstracts*, Vol. 209 of *American Astronomical Society Meeting Abstracts*. pp. 251.04–+.

Bertschinger, E.: 1985, 'Self-similar secondary infall and accretion in an Einstein-de Sitter universe'. ApJS **58**, 39–65.

Binney, J. and S. Tremaine: 1987, *Galactic dynamics*. Princeton, NJ, Princeton University Press, 1987, 747 p.

Bontekoe, T. R. and T. S. van Albada: 1987, 'Decay of galaxy satellite orbits by dynamical friction'. MNRAS **224**, 349–366.

Bosma, A., R. M. Smith, and K. J. Wellington: 1985, 'Rotation and velocity dispersion in the stellar component of NGC 1316 (Fornax A)'. MNRAS **212**, 301–307.

Canalizo, G., N. Bennert, B. Jungwiert, A. Stockton, F. Schweizer, M. Lacy, and C. Peng: 2007, 'Spectacular Shells in the Host Galaxy of the QSO MC2 1635+119'. *ArXiv e-prints* **707**.

Carter, D., D. A. Allen, and D. F. Malin: 1982, 'Nature of the shells of NGC1344'. Nature **295**, 126–128.

Carter, D., J. L. Prieur, A. Wilkinson, W. B. Sparks, and D. F. Malin: 1988, 'Spectra of shell ellipticals - Redshifts, velocity dispersions and evidence for recent nuclear star formation'. MNRAS **235**, 813–825.

Carter, D., R. C. Thomson, and G. K. T. Hau: 1998, 'Minor axis rotation and the intrinsic shape of the shell elliptical NGC 3923'. MNRAS **294**, 182–+.

Chandrasekhar, S.: 1943, 'Dynamical Friction. I. General Considerations: the Coefficient of Dynamical Friction.'. ApJ **97**, 255–+.

Charmandaris, V. and F. Combes: 2000, 'Minor Mergers and the Formation of Shell Galaxies'. In: M. J. Valtonen and C. Flynn (eds.): *IAU Colloq. 174: Small Galaxy Groups*, Vol. 209 of *Astronomical Society of the Pacific Conference Series*. pp. 273–+.

Charmandaris, V., F. Combes, and J. M. van der Hulst: 2000, 'First detection of molecular gas in the shells of CenA'. A&A **356**, L1–L4.

Colbert, J. W., J. S. Mulchaey, and A. I. Zabludoff: 2001, 'The Optical and Near-Infrared Morphologies of Isolated Early-Type Galaxies'. AJ **121**, 808–819.

Combes, F. and V. Charmandaris: 1999, 'The Gas Dynamics of Shell Galaxies'. In: D. R. Merritt, M. Valluri, and J. A. Sellwood (eds.): *Galaxy Dynamics - A Rutgers Symposium*, Vol. 182 of *Astronomical Society of the Pacific Conference Series*. pp. 489–+.

Combes, F. and V. Charmandaris: 2000, 'Formation of Gaseous Shells'. In: F. Combes, G. A. Mamon, and V. Charmandaris (eds.): *Dynamics of Galaxies: from the Early Universe to the Present*, Vol. 197 of *Astronomical Society of the Pacific Conference Series*. pp. 339–+.

Dunlop, J. S., R. J. McLure, M. J. Kukula, S. A. Baum, C. P. O'Dea, and D. H. Hughes: 2003, 'Quasars, their host galaxies and their central black holes'. MNRAS **340**, 1095–1135.

Dupraz, C. and F. Combes: 1986, 'Shells around galaxies - Testing the mass distribution and the 3-D shape of ellipticals'. A&A **166**, 53–74.

Dupraz, C. and F. Combes: 1987, 'Dynamical friction and shells around elliptical galaxies'. A&A **185**, L1–L4.

Efstathiou, G., R. S. Ellis, and D. Carter: 1982, 'Further observations of the elliptical galaxy NGC 5813'. MNRAS **201**, 975–990.

Fabian, A. C., P. E. J. Nulsen, and G. C. Stewart: 1980, 'Star formation in a galactic wind'. Nature **287**, 613–+.

Forbes, D. A.: 1992. Ph.D. thesis, PhD thesis University of Cambridge , (1992).

Forbes, D. A., D. B. Reitzel, and G. M. Williger: 1995, 'Shell colors in the peculiar elliptical galaxy IC 1459'. AJ **109**, 1576–1581.

Forbes, D. A. and R. C. Thomson: 1992, 'Shells and isophotal distortions in elliptical galaxies'. MNRAS **254**, 723–728.

Forbes, D. A., R. C. Thomson, W. Groom, and G. M. Williger: 1994, 'A search for secondary nuclei in shell galaxies'. AJ **107**, 1713–1716.

Fort, B. P., J.-L. Prieur, D. Carter, S. J. Meatheringham, and L. Vigroux: 1986, 'Surface photometry of shell galaxies'. ApJ **306**, 110–121.

González-García, A. C. and M. Balcells: 2005, 'Elliptical galaxies from mergers of discs'. MNRAS **357**, 753–772.

González-García, A. C. and T. S. van Albada: 2005a, 'Encounters between spherical galaxies - I. Systems without a dark halo'. MNRAS **361**, 1030–1042.

González-García, A. C. and T. S. van Albada: 2005b, 'Encounters between spherical galaxies - II. Systems with a dark halo'. MNRAS **361**, 1043–1054.

Goudfrooij, P., J. Mack, M. Kissler-Patig, G. Meylan, and D. Minniti: 2001, 'Kinematics, ages and metallicities of star clusters in NGC 1316: a 3-Gyr-old merger remnant'. MNRAS **322**, 643–657.

Hau, G. K. T., D. Carter, and M. Balcells: 1999, 'The shell elliptical galaxy NGC 2865: evolutionary population synthesis of a kinematically distinct core'. MNRAS **306**, 437–460.

Hau, G. K. T. and R. C. Thomson: 1994, 'A New Model for the Formation of Kinematically Decoupled Cores in Elliptical Galaxies'. MNRAS **270**, L23+.

Heisler, J. and S. D. M. White: 1990, 'Satellite disruption and shell formation in galaxies'. MNRAS **243**, 199–208.

Hernquist, L. and J. E. Barnes: 1991, 'Origin of kinematic subsystems in elliptical galaxies'. Nature **354**, 210–212.

Hernquist, L. and P. J. Quinn: 1987a, 'Shell galaxies and alternatives to the dark matter hypothesis'. ApJ **312**, 17–21.

Hernquist, L. and P. J. Quinn: 1987b, 'Shells and dark matter in elliptical galaxies'. ApJ **312**, 1–16.

Hernquist, L. and P. J. Quinn: 1988, 'Formation of shell galaxies. I - Spherical potentials'. ApJ **331**, 682–698.

Hernquist, L. and P. J. Quinn: 1989, 'Formation of shell galaxies. II - Nonspherical potentials'. ApJ **342**, 1–16.

Hernquist, L. and D. N. Spergel: 1992, 'Formation of shells in major mergers'. ApJ **399**, L117–L120.

Hernquist, L. and M. L. Weil: 1992, 'Starbursts in the nuclei of shell galaxies'. Nature **358**, 734–736.

Hibbard, J. E. and A. E. Sansom: 2003, 'A Search for H I in Five Elliptical Galaxies with Fine Structure'. AJ **125**, 667–683.

Horellou, C., J. H. Black, J. H. van Gorkom, F. Combes, J. M. van der Hulst, and V. Charmandaris: 2001, 'Atomic and molecular gas in the merger galaxy NGC 1316 (Fornax A) and its environment'. A&A **376**, 837–852.

Humphrey, P. J., D. A. Buote, F. Gastaldello, L. Zappacosta, J. S. Bullock, F. Brighenti, and W. G. Mathews: 2006, 'A Chandra View of Dark Matter in Early-Type Galaxies'. ApJ **646**, 899–918.

James, R. A. and A. Wilkinson: 1987, 'Initial Tidal Effects of Shell Formation'. In: P. T. de Zeeuw (ed.): *Structure and Dynamics of Elliptical Galaxies*, Vol. 127 of *IAU Symposium*. pp. 471–+.

Kojima, M. and M. Noguchi: 1997, 'Sinking Satellite Disk Galaxies. I. Shell Formation Preceded by Cessation of Star Formation'. ApJ **481**, 132–+.

Kormendy, J.: 1984, 'Recognizing merger remnants among normal elliptical galaxies NGC 5813'. ApJ **287**, 577–585.

Kundt, W. and M. Krause: 1985, 'The nature of the IGM'. A&A **142**, 150–156.

Lauer, T. R., S. M. Faber, K. Gebhardt, D. Richstone, S. Tremaine, E. A. Ajhar, M. C. Aller, R. Bender, A. Dressler, A. V. Filippenko, R. Green, C. J. Grillmair, L. C. Ho, J. Kormendy, J. Magorrian, J. Pinkney, and C. Siopis: 2005, 'The Centers of Early-Type Galaxies with Hubble Space Telescope. V. New WFPC2 Photometry'. AJ **129**, 2138–2185.

Lin, D. N. C. and S. Tremaine: 1983, 'Numerical simulations of the decay of satellite galaxy orbits'. ApJ **264**, 364–372.

Liu, C. T., J. H. van Gorkom, J. E. Hibbard, D. Schiminovich, and A. Fujita: 1999, 'Deep Optical Imaging and Photometry of Shell Galaxies'. In: *Bulletin of the American Astronomical Society*, Vol. 31 of *Bulletin of the American Astronomical Society*. pp. 833–+.

Loewenstein, M., A. C. Fabian, and P. E. J. Nulsen: 1987, 'Formation of shells in elliptical galaxies from interstellar gas'. MNRAS **229**, 129–141.

Longhetti, M., A. Bressan, C. Chiosi, and R. Rampazzo: 1999, 'Star formation history of early-type galaxies in low density environments. V. Blue line-strength indices for the nuclear region'. A&A **345**, 419–429.

Longhetti, M., A. Bressan, C. Chiosi, and R. Rampazzo: 2000, 'Star formation history of early-type galaxies in low density environments. IV. What do we learn from nuclear line-strength indices?'. A&A **353**, 917–929.

Longhetti, M., R. Rampazzo, A. Bressan, and C. Chiosi: 1998a, 'Star formation history of early-type galaxies in low density environments. I. Nuclear line-strength indices'. A&AS **130**, 251–265.

Longhetti, M., R. Rampazzo, A. Bressan, and C. Chiosi: 1998b, 'Star formation history of early-type galaxies in low density environments. II. Kinematics'. A&AS **130**, 267–283.

Lynden-Bell, D.: 1967, 'Statistical mechanics of violent relaxation in stellar systems'. MNRAS **136**, 101–+.

Lynds, R. and A. Toomre: 1976, 'On the interpretation of ring galaxies: the binary ring system II Hz 4.'. ApJ **209**, 382–388.

Malin, D. F.: 1977, 'Unsharp masking.'. In: *AAS Photo Bulletin*, Vol. 16 of *AAS Photo Bulletin*. pp. 10–13.

Malin, D. F.: 1978, 'Photographic amplification of faint astronomical images'. Nature **276**, 591–593.

Malin, D. F.: 1979, 'A jet associated with M89'. Nature **277**, 279–+.

Malin, D. F. and D. Carter: 1980, 'Giant shells around normal elliptical galaxies'. Nature **285**, 643–645.

Malin, D. F. and D. Carter: 1983, 'A catalog of elliptical galaxies with shells'. ApJ **274**, 534–540.

Malin, D. F., P. J. Quinn, and J. A. Graham: 1983, 'Shell structure in NGC 5128'. ApJ **272**, L5–L7.

Marcum, P. M., C. E. Aars, and M. N. Fanelli: 2004, 'Early-Type Galaxies in Extremely Isolated Environments: Typical Ellipticals?'. AJ **127**, 3213–3234.

McGaugh, S. S. and G. D. Bothun: 1990, 'Stellar populations in shell galaxies'. AJ **100**, 1073–1085.

Merrifield, M. R. and K. Kuijken: 1998, 'Measuring galaxy potentials using shell kinematics'. MNRAS **297**, 1292–1296.

Peñarrubia, J., A. Just, and P. Kroupa: 2004, 'Dynamical friction in flattened systems: a numerical test of Binney's approach'. MNRAS **349**, 747–756.

Pellegrini, S.: 1999, 'BeppoSAX observation of NGC 3923, and the problem of the X-ray emission in E/S0 galaxies of low and medium L_X/L_B'. A&A **343**, 23–32.

Pence, W. D.: 1986, 'Spectrophotometry of shell galaxies'. ApJ **310**, 597–604.

Peng, C. Y., L. C. Ho, C. D. Impey, and H.-W. Rix: 2002, 'Detailed Structural Decomposition of Galaxy Images'. AJ **124**, 266–293.

Petric, A., D. Schiminovich, J. van Gorkom, J. M. van der Hulst, and M. Weil: 1997, 'HI imaging of the shell galaxy NGC 1210'. In: *Bulletin of the American Astronomical Society*, Vol. 29 of *Bulletin of the American Astronomical Society*. pp. 1344–+.

Pierfederici, F. and R. Rampazzo: 2004, 'BV photometry of five shell galaxies'. *Astronomische Nachrichten* **325**, 359–375.

Piran, T. and J. V. Villumsen: 1987, 'Shells and Encounters of Disk Galaxies with Ellipticals'. In: P. T. de Zeeuw (ed.): *Structure and Dynamics of Elliptical Galaxies*, Vol. 127 of *IAU Symposium*. pp. 473–+.

Plummer, H. C.: 1911, 'On the problem of distribution in globular star clusters'. MNRAS **71**, 460–470.

Pogge, R. W. and P. Martini: 2002, 'Hubble Space Telescope Imaging of the Circumnuclear Environments of the CfA Seyfert Galaxies: Nuclear Spirals and Fueling'. ApJ **569**, 624–640.

Prieur, J.-L.: 1988, 'The shell system around NGC 3923 and its implications for the potential of the galaxy'. ApJ **326**, 596–615.

Prieur, J.-L.: 1990, *Dynamics and Interactions of Galaxies*. Ed. R. Wielen (Springer-Verlag), 72.

Prugniel, P. and F. Combes: 1992, 'Dynamical friction between two elliptical galaxies'. A&A **259**, 25–38.

Quinn, P. J.: 1982. Ph.D. thesis, PhD thesis Australian National University , (1982).

Quinn, P. J.: 1983, 'On the formation and dynamics of shells around elliptical galaxies'. In: E. Athanassoula (ed.): *Internal Kinematics and Dynamics of Galaxies*, Vol. 100 of *IAU Symposium*. pp. 347–+.

Quinn, P. J.: 1984, 'On the formation and dynamics of shells around elliptical galaxies'. ApJ **279**, 596–609.

Rampazzo, R., P. Alexander, C. Carignan, M. S. Clemens, H. Cullen, O. Garrido, M. Marcelin, K. Sheth, and G. Trinchieri: 2006, 'The hot, warm and cold gas in Arp 227 - an evolving poor group'. MNRAS **368**, 851–863.

Rampazzo, R., M. D'Onofrio, P. Bonfanti, M. Longhetti, and L. Reduzzi: 1999, 'Star formation history of early-type galaxies in low density environments. III. The isophote shape parameter and nuclear line-strength indices'. A&A **341**, 357–360.

Rampazzo, R., A. Marino, R. Tantalo, D. Bettoni, L. M. Buson, C. Chiosi, G. Galletta, R. Grueztbauch, and R. M. Rich: 2007, 'The GALEX UV emission in shell galaxies: tracing galaxy "rejuvenation" episodes'. *ArXiv e-prints* **707**.

Rampazzo, R., H. Plana, M. Longhetti, P. Amram, J. Boulesteix, J.-L. Gach, and O. Hernandez: 2003, 'Warm gas kinematics in shell galaxies'. MNRAS **343**, 819–830.

Reduzzi, L., M. Longhetti, and R. Rampazzo: 1996, 'Comparative study of fine structure in samples of isolated and paired early-type galaxies'. MNRAS **282**, 149–156.

Reduzzi, L., M. Longhetti, and R. Rampazzo: 1997, '2D Colour Maps of Galaxies with Shells'. In: M. Arnaboldi, G. S. Da Costa, and P. Saha (eds.): *The Nature of Elliptical Galaxies; 2nd Stromlo Symposium*, Vol. 116 of *Astronomical Society of the Pacific Conference Series*. pp. 233–+.

Richardson, W. H.: 1972, 'Bayesian-based iterative method of image restoration'. *Journal of the Optical Society of America (1917-1983)* **62**, 55–59.

Růžička, A.: 2006. Ph.D. thesis, PhD thesis Charles University Prague, (2006).

Růžička, A., J. Palouš, and C. Theis: 2007, 'Is the dark matter halo of the Milky Way flattened?'. A&A **461**, 155–169.

Sadler, E. M.: 1984, 'Radio and optical observations of a complete sample of E and SO galaxies. III. A radio continuum survey at 2.7 and 5.0 GHz.'. AJ **89**, 53–63.

Sahu, D. K., S. K. Pandey, D. K. Chakraborty, A. Kembhavi, and V. Mohan: 1996, 'Nuclear dust and outer shells in the elliptical galaxy NGC 7562.'. A&A **314**, 721–728.

Schiminovich, D., J. van Gorkom, T. van der Hulst, T. Oosterloo, and A. Wilkinson: 1997, 'Imaging and Kinematics of Neutral Hydrogen in and around "Shell Galaxies"'. In: M. Arnaboldi, G. S. Da Costa, and P. Saha (eds.): *The Nature of Elliptical Galaxies; 2nd Stromlo Symposium*, Vol. 116 of *Astronomical Society of the Pacific Conference Series*. pp. 362–+.

Schiminovich, D., J. H. van Gorkom, J. M. van der Hulst, and S. Kasow: 1994, 'Discovery of Neutral Hydrogen Associated with the Diffuse Shells of NGC 5128 (Centaurus A)'. ApJ **423**, L101+.

Schiminovich, D., J. H. van Gorkom, J. M. van der Hulst, and D. F. Malin: 1995, 'Neutral hydrogen associated with shells and other fine structure in NGC 2865: A dynamically young elliptical?'. ApJ **444**, L77–L80.

Schombert, J. M. and J. F. Wallin: 1987, 'ARP 227 - A case for shells without mergers?'. AJ **94**, 300–305.

Schweizer, F.: 1980, 'An optical study of the giant radio galaxy NGC 1316 /Fornax A/'. ApJ **237**, 303–318.

Schweizer, F.: 1982, 'Colliding and merging galaxies. I - Evidence for the recent merging of two disk galaxies in NGC 7252'. ApJ **252**, 455–460.

Schweizer, F.: 1983, 'Observational evidence for mergers'. In: E. Athanassoula (ed.): *Internal Kinematics and Dynamics of Galaxies*, Vol. 100 of *IAU Symposium*. pp. 319–326.

Schweizer, F. and W. K. Ford, Jr.: 1985, 'Fine Structure in Elliptical Galaxies'. In: J.-L. Nieto (ed.): *New Aspects of Galaxy Photometry*, Vol. 232 of *Lecture Notes in Physics, Berlin Springer Verlag*. pp. 145–+.

Schweizer, F. and P. Seitzer: 1988, 'Ripples in disk galaxies'. ApJ **328**, 88–92.

Serra, P., S. C. Trager, J. M. van der Hulst, T. A. Oosterloo, and R. Morganti: 2006, 'IC 4200: a gas-rich early-type galaxy formed via a major merger'. A&A **453**, 493–506.

Sikkema, G., D. Carter, R. F. Peletier, M. Balcells, C. Del Burgo, and E. A. Valentijn: 2007, 'HST/ACS observations of shell galaxies: inner shells, shell colours and dust'. A&A **467**, 1011–1024.

Silva, D. R. and G. D. Bothun: 1998, 'The Ages of Disturbed Field Elliptical Galaxies. II. Central Properties'. AJ **116**, 2793–2804.

Stickel, M., J. M. van der Hulst, J. H. van Gorkom, D. Schiminovich, and C. L. Carilli: 2004, 'First detection of cold dust in the northern shell of NGC 5128 (Centaurus A)'. A&A **415**, 95–102.

Thomson, R. C.: 1991, 'Shell formation in elliptical galaxies'. MNRAS **253**, 256–278.

Thomson, R. C. and A. E. Wright: 1990, 'A Weak Interaction Model for Shell Galaxies'. MNRAS **247**, 122–+.

Thronson, Jr., H. A., J. Bally, and P. Hacking: 1989, 'The components of mid- and far-infrared emission from S0 and early-type shell galaxies'. AJ **97**, 363–374.

Toomre, A.: 1978, 'Interacting systems'. In: M. S. Longair and J. Einasto (eds.): *Large Scale Structures in the Universe*, Vol. 79 of *IAU Symposium*. pp. 109–116.

Toomre, A. and J. Toomre: 1972, 'Galactic Bridges and Tails'. ApJ **178**, 623–666.

Turnbull, A. J., T. J. Bridges, and D. Carter: 1999, 'Imaging of the shell galaxies NGC 474 and 7600, and implications for their formation'. MNRAS **307**, 967–976.

Umemura, M. and S. Ikeuchi: 1987, 'Formation of stellar shells and X-ray coronae around elliptical galaxies'. ApJ **319**, 601–613.

Wahde, M. and K. J. Donner: 1996, 'Influence of the disc on the orbital decay of satellite galaxies.'. A&A **312**, 431–438.

Weil, M. L. and L. Hernquist: 1993a, 'Nuclear Distribution of Gas in Shell Galaxies'. In: G. H. Smith and J. P. Brodie (eds.): *The Globular Cluster-Galaxy Connection*, Vol. 48 of *Astronomical Society of the Pacific Conference Series*. pp. 629–+.

Weil, M. L. and L. Hernquist: 1993b, 'Segregation of gas and stars in shell galaxies'. ApJ **405**, 142–152.

Wilkinson, A., I. W. A. Browne, C. Kotanyi, W. A. Christiansen, R. Williams, and W. B. Sparks: 1987a, 'Radio emission from shell elliptical galaxies'. MNRAS **224**, 895–910.

Wilkinson, A., I. W. A. Browne, and R. D. Wolstencroft: 1987b, 'Shell galaxies detected with IRAS'. MNRAS **228**, 933–940.

Wilkinson, A., J.-L. Prieur, R. Lemoine, D. Carter, D. Malin, and W. B. Sparks: 2000, '0422-476: a shell galaxy with azimuthally distributed shells'. MNRAS **319**, 977–990.

Wilkinson, A., R. M. Sharples, R. A. E. Fosbury, and P. T. Wallace: 1986a, 'Stellar dynamics of CEN A'. MNRAS **218**, 297–329.

Wilkinson, A., W. B. Sparks, D. Carter, and D. A. Malin: 1987c, 'Two Colour CCD Photometry of Malin / Carter Shell Galaxies'. In: P. T. de Zeeuw (ed.): *Structure and Dynamics of Elliptical Galaxies*, Vol. 127 of *IAU Symposium*. pp. 465–+.

Wilkinson, A., W. B. Sparks, D. Carter, and D. F. Malin: 1986b, ''. In: *IAU Symposium*, Vol. 127 of *IAU Symposium*. pp. 465–+.

Williams, R. E. and W. A. Christiansen: 1985, 'Blast wave formation of the extended stellar shells surrounding elliptical galaxies'. ApJ **291**, 80–87.

Wright, A. E.: 1972, 'Computational models of gravitationally interacting galaxies'. MNRAS **157**, 309–+.

Wright, M. C. H.: 1974, 'An Interferometer Study of H i Absorption in Centaurus A'. A&A **31**, 283–+.